Summer 7-18-2014

Utilizing Liquid Crystal Phases to Obtain Highly Ordered Thin Films for Organic Electronics

Mike T. Springer
University of Colorado Boulder, michael.springer@colorado.edu

Utilizing Liquid Crystal Phases to Obtain Highly Ordered Thin Films for Organic Electronics

by

Mike T. Springer

B.A., University of Nevada Reno, 2005

B.S., University of Nevada Reno, 2008

B.S., University of Nevada Reno, 2009

A thesis submitted to the

Faculty of the Graduate School of the

University of Colorado in partial fulfillment

of the requirements for the degree of

Doctor of Philosophy

Department of Chemistry and Biochemistry

2014

This thesis entitled:

Utilizing Liquid Crystal Phases to Obtain Highly Ordered Thin Films for Organic Electronics

written by Mike T. Springer

has been approved for the Department of Chemistry and Biochemistry by

_____

David M. Walba

_____

Wei Zhang

Date: _____

The final copy of this thesis has been examined by the signatories, and we find that both the content and the form meet acceptable presentation standards of scholarly work in the above mentioned discipline.

Springer, Mike T. (Ph.D. Organic Chemistry)

Utilizing Liquid Crystal Phases to Obtain Highly Ordered Thin Films for Organic Electronics

Thesis directed by Professor David M. Walba

Organic electronic materials offer several advantages when compared to inorganic materials, but they suffer from low charge carrier mobility. Two major factors hindering effective charge transport in organic materials are: 1) effective wavefunction overlap in organic crystals and 2) the domain morphology of thin films. Charge transport in organic materials occurs via a *hopping* mechanism along the conjugated π system. Often, rigid, aromatic organic materials crystallize in a herringbone, edge-to-face orientation, limiting π-π stacking and decreasing charge carrier mobility. Face-to-face orientation of aromatic rings decreases intermolecular π-π distances and increases wavefunction overlap. Control of the crystal structure can be achieved to some extent by tuning structural features of the molecule, like increasing the ratio of carbon atoms to hydrogen atoms in the aromatic rings; this is often achieved by introducing heteroatoms like sulfur and oxygen into the aromatic ring structure.

Thin films of organic materials often contain many unaligned domains; this is caused by rapid crystallization. Control of the domain morphology of thin films has been shown to increase charge carrier mobility by 6 orders of magnitude for thin films of the same material. Liquid crystal phases allow a slow process of crystallization, whereby the molecules in a thin film can be slowly aligned into a monodomain before crystallization. The crystal-smectic phases, like smectic E, are particularly attractive for this strategy due to their high degree of intermolecular order.

This project describes the synthesis and characterization of organic semiconductors designed to exhibit short π-π distances and highly ordered crystal-smectic phases to obtain thin films with high charge carrier mobility. The n,2-OBTTT series contains 15 newly designed and synthesized mesogens. The liquid crystal and solid crystal structures of these mesogens are examined and deposition conditions are optimized for the production of highly ordered, monodomain thin films.

This dissertation is dedicated to my wife, Milly, for her never-ending support during late nights and early mornings.

Acknowledgements

I would first like to acknowledge my advisor, Dave Walba, for his support during my time in graduate school. Whether it was a graduate certificate in science and technology policy or serving as the lead graduate teacher for the department of chemistry and biochemistry, Dave always encouraged me to follow my interests. Also, my lab mates in the Walba lab were always sources of inspiration when I was feeling deflated.

I would also like to thank my undergraduate advisor, Ben King, for truly being someone I could look up to; your work ethic and creativity were always a beacon whenever I questioned whether I really wanted to do this!

Of course, I couldn't have done any of this without my parents. There was no way that my dad was going to let me drop out of school! My mom was always willing to help pay for rent and tuition, even when I opted to go back to school for a third degree! I will make certain to provide the same opportunities to my children.

Table of Contents

List of Tables

List of Figures

Chapter I: Introduction

1.1 Motivation

Organic materials offer several advantages when compared to inorganic materials for electronic applications: 1) less expensive to manufacture, 2) potential for rapid, large area production using high-throughput methods, 3) tuning and tailoring of material properties, 4) lower environmental impact, and 5) decreasing foreign dependence on imports of rare-Earth metals. However, organic materials suffer from low charge carrier mobilities and short device lifetimes.

Charge carrier mobility is affected by the intermolecular arrangement within the crystal structure of organic semiconductors, as well as the degree of disorder within the morphology of thin films. Both of these obstacles can be overcome by careful molecular design. Although by no means completely understood, organic molecular structure / material property relationships have been widely established for many properties. It is possible to control the intermolecular π-stacking distance within crystals, as well as control the morphology of thin films by utilizing focused molecular design.

In this work, a bottom-up approach is employed to achieve this nanoscale control. A bottom-up approach to materials engineering begins with designing molecules that will self-assemble to induce certain bulk phase features of the material. This is opposed to a top-down approach, wherein the surface of a material can be manipulated by utilizing photolithography or other microfabrication techniques. A bottom-up approach relies on the self-assembly of molecules into larger macrostructures. Liquid crystal phases provide a mechanism for this molecular self-assembly. This study describes the design and synthesis of a series of molecules exhibiting liquid crystal phases to achieve nanoscale

ordering in thin-films organic electronics applications. The liquid crystal behavior, crystal morphology, thin film morphology, and charge carrier mobilities of thin-films of the newly synthesized semiconductors are examined.

1.2 Overview of Dissertation

This dissertation is organized into two parts: 1) progress toward the design of liquid crystalline materials for highly ordered thin films and 2) research involving the incorporation of computer models into the undergraduate organic chemistry lecture. Part 1 begins with an introduction to liquid crystals for organic electronics and the prior work done in this area (chapter 2). Also included, in partial fulfillment of a Graduate Certificate in Science and Technology Policy from the Center for Science and Technology Policy Research at the University of Colorado at Boulder, is a discussion of the socioeconomic impacts and political issues surrounding organic electronics (chapter 3). Chapter 4 describes the design and synthesis of a series of liquid crystal mesogens for organic electronic materials, the n,2-OBTTT series. It has previously been shown that charge mobility varies in different liquid crystal (LC) phases and that the "soft crystal/liquid crystal" phases have charge mobilities comparable to crystal phases. Further, thin films processed from materials that exhibit the soft-crystal liquid crystal phases can be aligned to avoid the formation of grain boundaries. A series of mesogens was designed to induce these soft-crystal phases with varied tail lengths to study the factors that affect formation of these soft-crystal LC phases, the n,2-OBTTT series. Synthesizing the target molecule required the development of a novel procedure for obtaining 2-alkoxythiophenes, a species that until recently was not described in the

literature. Chapters 5 describes the characterization of the liquid crystalline behavior of the n,2-OBTTT series. Only short chain and long chain members of the series exhibited the soft-crystal smectic phases, not the medium chain members, indicating an effect of alkoxy chain length on liquid crystal phase formation. Further, all but one member of the series (4,2-OBTTT) exhibited paramorphic phase transitions, ideal for creating highly ordered thin films. Chapter 6 presents the solid-state material properties of the n,2-OBTTT series, including crystal structure and thin-film morphology. Part 2 describes work performed in the area of chemistry education. Chapter 7 presents the results of a study designed, performed, and published solely by the author of the present work, investigating the incorporation of computer models into the undergraduate organic chemistry lecture. A significant improvement in students' scores was observed as a result of the experimental treatment, suggesting an economical method of achieving significant gains in students' conceptual understanding of molecular structure.

Chapter II: Liquid Crystals for Organic Electronics

2.1 Introduction: Organic Materials

Organic chemistry is a mature discipline. It is now possible to synthesize and characterize nearly any organic molecule that can be imagined. Computational strategies have aided in the design of molecules with new and unique properties. New catalysts, synthetic procedures, and purification techniques have afforded access to a wide variety of functionally unique and ultra-pure organic materials. Ubiquitous access to powerful molecular characterization techniques like NMR and high-resolution mass spectrometry has become routine. Many structure/property relationships have been established, enabling precise tailoring of molecular features to maximize or minimize material properties at will. Organic materials are typically much cheaper, more flexible, and take less energy to process than inorganic materials. Organic materials are essential components of next-generation applications in nanotechnology and biotechnology. The modern versatility of organic synthesis and the virtually infinite variations of organic compounds surely indicate that organic materials will soon replace many inorganic materials and infiltrate nearly every facet of human existence. The 2000 Nobel Prize in Chemistry was awarded to Alan Heeger, Alan MacDiarmid, and Hideki Shirakawa for their discovery of intrinsically conductive polymers. With distinctly appropriate timing, the 21st century has given birth to the organic electronics industry.

2.2 Organic Materials for Electronics

Organic materials for electronics offer several advantages: 1) they are inexpensive to manufacture, 2) there is potential for rapid, large area production using high-throughput methods[1], 3) tuning and tailoring of material properties by utilizing organic synthesis[2], 4) a lower environmental impact[3], and 5) a potential decrease in foreign dependence on imports of rare-Earth metals.[4] However, organic materials currently suffer from much lower values of charge carrier mobility than inorganic materials.[5] Inorganic materials have a much larger dielectric constant than organic materials, which facilitates efficient charge transfer. The relatively weak intermolecular forces that exist in solid organic materials hinder the movement of charges. Further, the chemical bonds of organic materials are weaker than inorganic crystalline lattices, so devices constructed from organic materials often have much shorter lifetimes and are subject to degradation under environmental conditions.[5] Environmental degradation of organic materials is a double-edged sword, since it decreases effective device lifetime, but presents opportunities for recycling. Low charge carrier mobility and short device lifetimes are two of the major obstacles to overcome before organic electronics can become a commercially competitive industry.

2.3 Charge Transport in Organic Materials

Charge transport is the movement of electrons and holes across a material. Two of the most important factors affecting charge transport in organic materials are: 1) intermolecular distance between and alignment of the conjugated π-systems and 2) the degree of order in the morphology of the thin film.[6] Charge transport in organic materials

is often described as having contributions from a *tunneling* mechanism, as well as a *hopping* mechanism.[6,7] The extent to which each mechanism contributes to the overall mobility is a function of temperature, electron-phonon coupling, electronic and phonon bandwidths, and phonon energy. In organic materials, electron-phonon couplings have been shown to be comparable to, or even greater than, electron-electron interactions.[5]

An electron on a molecule has some probability of *tunneling* through the space between 2 molecules to "appear" on the other molecule. Quantum mechanical tunneling occurs as a coherent process, where there is no energy transfer out of the electron system and all phase information is retained upon the transfer.[7] Electron tunneling is highly dependent on intermolecular distance and temperature; when the temperature is low, the charge mobility in organic materials is dominated by the tunneling mechanism.[8,9] However, for most device applications, the temperature is likely to be much higher, decreasing the tunneling contribution to the overall charge mobility in organic materials. In the temperature range of most practical applications, charge mobility in organic materials is dominated by the *hopping* mechanism.[8] This is certainly true for materials that operate in a liquid crystal phase, as well, since these phases seldom occur below room temperature.

In addition to *tunneling*, electrons may *hop* from molecule to molecule along overlapping π-systems. Though both processes move an electron from one molecule to the next, the physical mechanisms are significantly different. The tunneling mechanism is a coherent process, during which phase information is retained and occurring without the transfer of energy. Tunneling often involves the delocalization of eigenstates over an entire system, spreading every atom or molecular in the material.[10] The hopping

mechanism, conversely, is incoherent, requires the transfer of energy either to or from the electron, and is highly localized. The hopping mechanism is thought to involve Frenkel excitons that typically exhibit a maximum radius of only about 10 Å. Consequently, the charge is typically localized within 1-2 molecular radii. The *phonon* system supplies the energy required or absorbs the energy emitted upon electron transfer.[6] A phonon is a particle-like, quantized mode of vibrational energy arising from the collective oscillations of atoms within a material. These electron-phonon interactions dominate charge transport in organic materials and induce the formation of quasi-particles called *polarons*. A polaron is a system of electron-phonon interactions: when an electron moves through a material, the atoms or molecules shift from their equilibrium positions to screen the charge, creating a lattice vibration. Charge mobility in organic materials is often limited by the dynamic disorder arising from polaron formation.[11,12]

In materials, charge carrier mobility is affected by several factors including molecular packing, molecular disorder, and temperature.[6,11,12] Conjugated molecules often exhibit the highest charge mobilities because of the delocalized nature of the π-system. In many cases, conjugated molecules with rigid aromatic cores crystallize into a layered herringbone structure (figure 2-2a). Such packing gives rise to 2D charge transport within the layers, while transport between layers is less efficient.[13] This makes sense, as the π-system extends orthogonally to the plane of the aromatic rings, in which the long axis of the molecule often lies and this distance is often much shorter than the distance between π-systems interlayer. Depending on the arrangement of the electrodes (for photovoltaic or transistor applications), the anisotropic character of charge transport in most organic materials requires molecules to orient appropriately to facilitate the

hopping of electrons between molecules. Figure 2-1 shows two device architectures: a) an organic field-effect transistor (OFET) and b) a thin-film organic photovoltaic (OPV) device. Charge moves between electrodes (or from source to drain in an OFET). Different devices require different molecular orientations to facilitate charge transport: the molecules either must align parallel or perpendicular to the electrode surface.

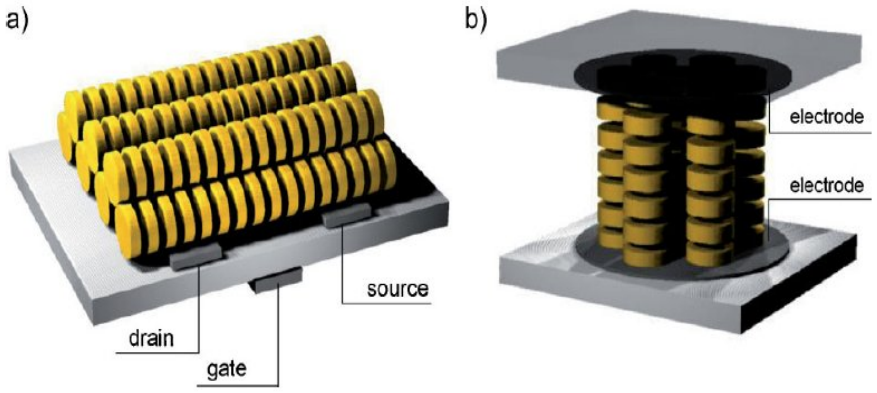

Figure 2-1. (a) The device architecture for an organic field-effect transistor (OFET); (b) the device architecture for an organic photovoltaic device (OPV). The anisotropic nature of charge transport through organic materials necessitates different molecular orientations for different devices. [Source: Macromol. Rapid Commun. 2009, 30, 1179–1202]

Electron-electron coupling can change by a factor of 3-4 between 3.4 and 4.0 Å, intermolecular distances typically found in organic conjugated crystals and thin films.[14] The herringbone orientation of the aromatic rings does not seem to provide the most efficient path for electron transport since the π-system is *rolled* off of the stacking axis. Face-to-face (cofacial) contacts would seem to facilitate charge transport and increase charge carrier mobility (figure 2-2b). It is possible to alter molecular structure to induce these co-facial orientations: this approach has been investigated for pentacene derivatives[15] and for tetrathiafulvalene (TTF) derivatives.[16] One strategy is to maximize the ratio of carbon atoms to hydrogen atoms in the conjugated π-system since hydrogen

atoms often align with the electron density of an aromatic ring, inducing edge-to-face orientations. In practice, this is often achieved by the addition of heteroatoms into the aromatic ring structure like sulfur and oxygen, since they do not have open valences to accommodate hydrogen atoms. However, despite the fact that a more cofacial orientation would seem to increase π-overlap, there is no evidence that achieving a more cofacial orientation in thin films can actually improve charge carrier mobility.[6]

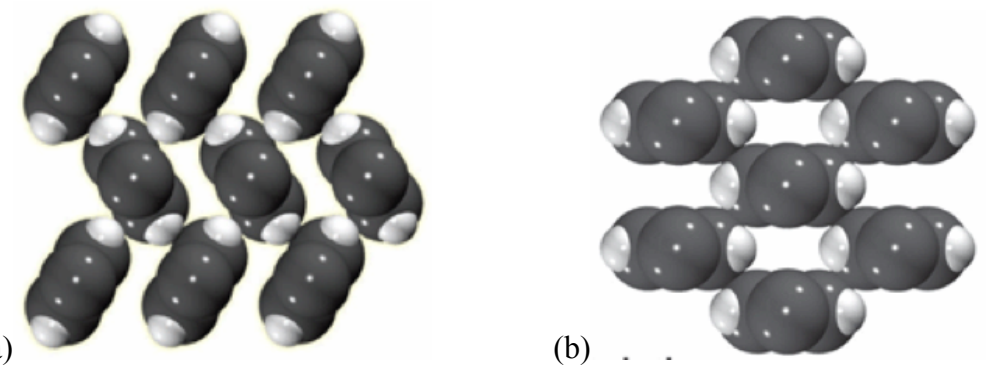

(a) (b)

Figure 2-2. (a) Herringbone structure of aromatic rings; (b) face-to-face structure of aromatic rings.

One possible explanation for the observation that increasing the degree of cofacial arrangment doesn't improve charge carrier mobility is that perfect face-to-face alignment of aromatic rings is energetically unfavorable, as this arrangement maximizes electrostatic repulsion between the rings. This is precisely why the cofacial arrangement is not typically seen in organic crystals. Further, it is not necessarily spatial alignment of the aromatic rings that maximizes electronic coupling; it is the degree of *wavefunction* overlap. Crystal packing certainly does affect charge carrier mobility[16], but to maximize wavefunction overlap, the pattern of the bonding-antibonding orbitals on adjacent

molecules must be complimentary.[17] This is not necessarily as simple as maximizing spatial overlap, since asymmetric molecules can often have asymmetric frontier orbitals.

To improve charge carrier mobility, it is important that the local molecular interactions within a thin film be favorable, like the molecule-to-molecule orientation of the π-systems just discussed. It is also important that the bulk structure of the film be ordered, on a global scale, throughout the entirety of the material.[6] When an organic material is deposited onto a substrate to create a thin film, crystallization is typically nucleated at several sites simultaneously, leading to the formation of several domains separated by grain boundaries. Although the molecules in each grain may be well-ordered, the grains themselves are randomly aligned. Charge transport is severely affected by these grain boundaries (figure 2-3).[18] Materials that exhibit universal molecular alignment are said to contain only one domain, a *monodomain*, like the morphology seen in figure 2-3a. Conversely, materials that crystallize very quickly often form thin films with grain boundaries (figure 2-3b).

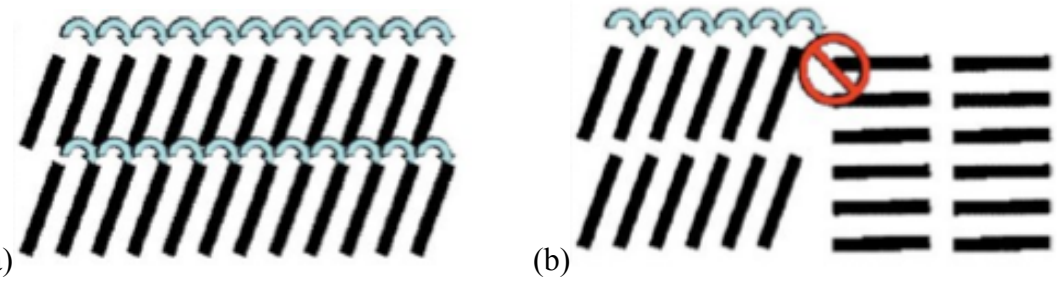

Figure 2-3. (a) Charge transport via a hopping mechanism is uninterrupted in a material without grain boundaries; (b) charge transport in a material with grain boundaries limits charge carrier mobility. [Source: Macromol. Rapid Commun. 2009, 30, 1179–1202]

Avoiding the creation of grain boundaries has enormous implications for charge carrier mobility, improving the mobility in pentacene films by 6 orders of magnitude.[19] Thus,

even molecules designed to yield a crystal structure perfectly suited for charge mobility (maximum wavefunction overlap) still need to be deposited into thin films that lack grain boundaries, a process that is not straightforward. The rate of crystallization upon film deposition is enormously important.

2.4 Liquid Crystal Phases for Highly Ordered Thin Films

Two of the major obstacles facing organic electronic materials are low charge carrier mobilities and short device lifetimes resulting from environmental degradation. A major factor affecting the charge carrier mobility of organic electronic materials is the difficulty associated with achieving highly ordered thin films free of grain boundaries. Controlling crystal growth and morphology is incredibly difficult. Liquid crystal phases offer a route a control the morphology of thin films, achieving films free of grain boundaries. Further, because they self-assemble, defects in liquid crystal structures usually self-heal, presenting an opportunity to increase the useful lifetime of organic electronic materials by simply heating into a mesophase and cooling back into a solid phase.

Liquid crystal phases exist in some materials as intermediate phases between crystalline solids and isotropic liquids. Some typical liquid crystal phases for different shapes of molecules are depicted in figure 2-4.

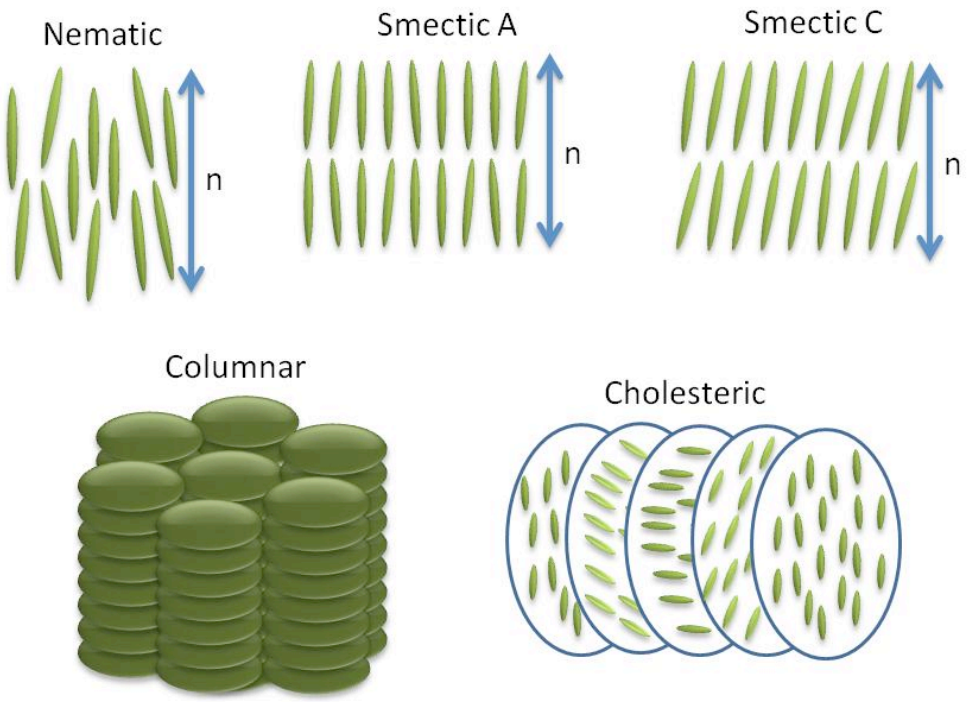

Figure 2-4. Some typical liquid crystal phases; cholesteric and smectic phases of calamitic mesogens and a columnar phase of discotic liquid crystals. [source: http://cnx.org/content/m46154/1.2/]

Though liquid crystals are intermediate between liquid and solid phases, their properties do not necessarily follow this same trend. For example, an electric field of about 100 mV/m is enough to align the molecules in a liquid crystal phase, but fields 5 orders of magnitude larger are unable to affect the molecules in a liquid or solid phase.[20] One benefit of liquid crystal phases is that their properties are often unique: they can be aligned and, in some cases, that order can be maintained throughout cooling and crystallization, creating thin films free of defects.

Although charge carrier mobility in liquid crystal phases can be considerably higher than in amorphous organic materials, it is not typically as high as in ordered, single organic crystals (figure 2-5).

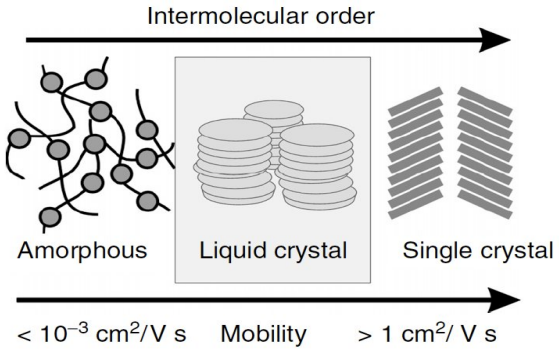

Figure 2-5. Charge carrier mobility as a function of intermolecular order. [Source: Macromol. Rapid Commun. 2009, 30, 1179–1202]

This same trend is followed within the liquid crystal regime: charge carrier mobility is improved as intermolecular order within the phase increases, from fluid-smectic phases (like SmA and SmC) to crystal-smectic phases (like SmE and SmG). The molecular distance intra-smectic layer is typically between 3.5 to 6 Å[20], whereas the intermolecular distances in crystals (and thin films) are typically between 3.4 to 4 Å.[15] Charge carrier mobility is a function of intermolecular distance and these relatively small differences can have drastic effects.[16] For this reason, although liquid crystal phases are useful to align thin films, organic crystals are still the end goal to maximize charge carrier mobility. Even though a material will not be operated in a liquid crystal phase, it is still desirable for a material to exhibit liquid crystal phases, especially the highly ordered crystal-smectic phases. This is because the order conferred upon the material during self-assembly in a liquid crystal phase can be maintained upon cooling into a crystal phase. In summary, the structure of the *crystal* is important to maximize charge carrier mobility by maximizing π-overlap. Similarly, the structure of the *liquid crystal* phases of a material are an important design consideration, as well, to maximize processability and order in thin films.

The strategy employed in the present dissertation to address the shortcomings associated with organic electronic materials utilizes liquid crystal phases to obtain highly ordered thin films. Charge mobility is affected by: 1) intermolecular π-stacking distance and 2) domain morphology of thin films. Intermolecular π-stacking distance can be minimized by designing a molecule with specific functionalities and a high C/H ratio and the domain morphology of thin films can be controlled by utilizing highly ordered, crystal-smectic, liquid crystal phases. This project contains several separate parts:

- The design of molecules exhibiting close intermolecular pi-stacking and liquid crystal phases to maximize charge carrier mobility,
- The characterization of liquid crystalline behavior of the synthesized mesogens,
- The deposition and alignment of thin films utilizing liquid crystal phases,
- The measurement of charge carrier mobility in highly aligned thin films.

Chapter III: Organic Electronics for U.S. Energy Independence

[*submitted in partial fulfillment of a certificate in Science and Technology Policy*]

3.1 Introduction: Material Dependence of the Modern US Economy

Today, society is very dependent on different materials and elements to enable our vast array of technologies.[21] Fossil fuels are essential to power our economy. A modern computer is made of more than 60 elements.[22]

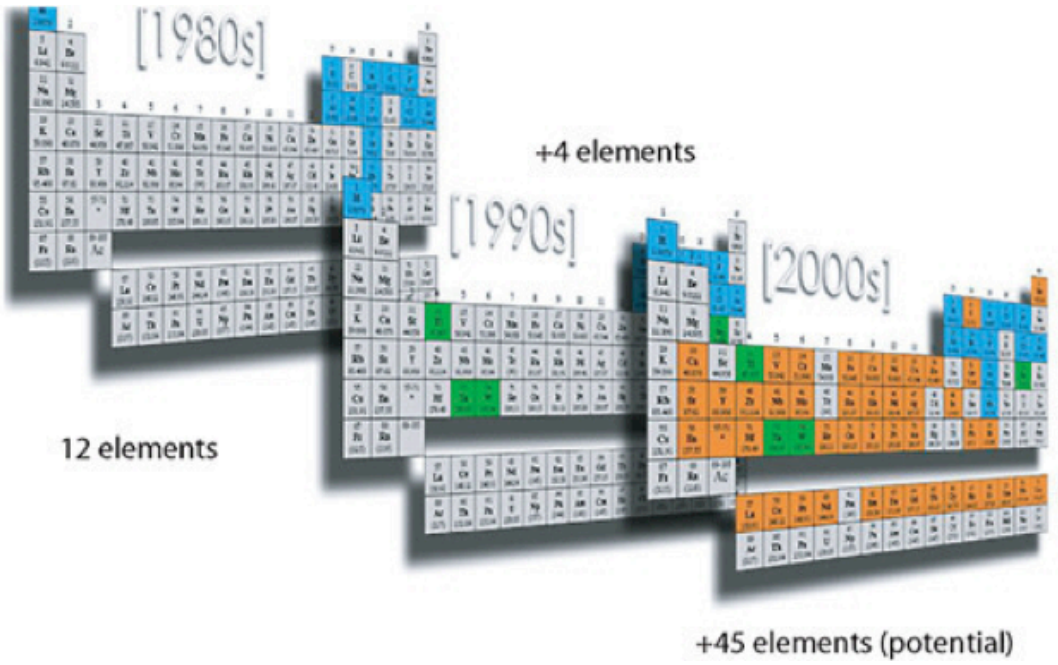

Figure 3-1. Historical evolution of the elements necessary to make a computer chip. [Source: Intel.com]

The availability of the materials necessary for our modern society can't always be ensured. Some of the materials are quite scarce and there is only a limited supply on Earth. Other materials necessary for important technologies are more abundant, but they are not mined domestically and the countries that control these essential resources may or may not have a political or trade relationship with the United States.

3.1.1 U.S. Dependence on Foreign Oil

The U.S. is the world's largest petroleum consumer, at 18.6 million barrels per day.[23] The U.S. imported about 40% of the oil it consumed in 2012 and although more than half of these imports were from the Western Hemisphere (53%), the remaining sources of imported oil products into the U.S. were the Persian Gulf (28%) and Africa (16%). The top five sources of imported crude oil and petroleum products in 2012 were: Canada (28%), Saudi Arabia (13%), Mexico (10%), and Venezuela (9%), and Russia (5%).

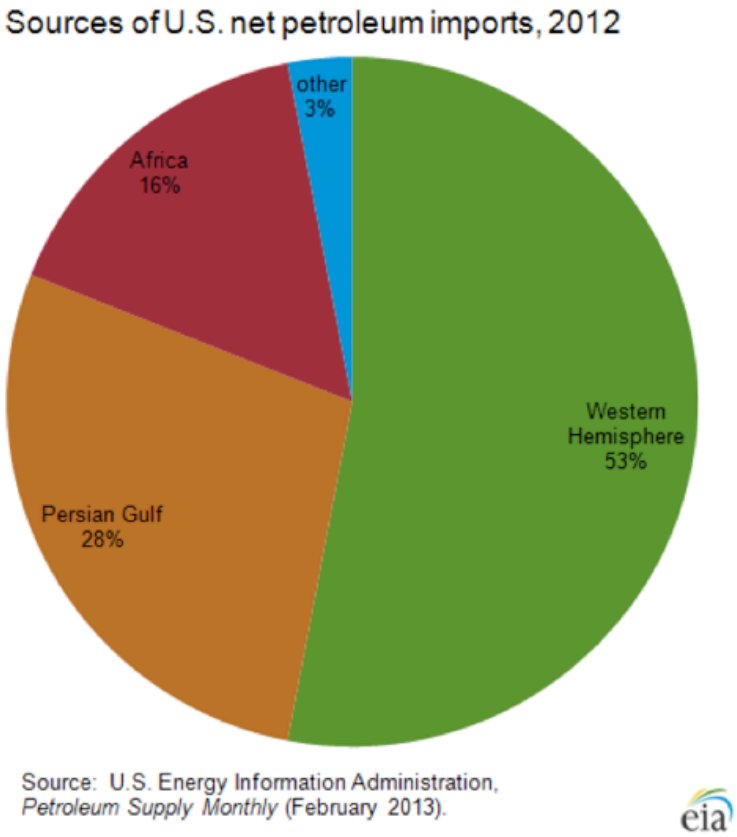

Figure 3-2. Sources of U.S. net petroleum imports for 2012. [Source: U.S. Energy Information Administration]

Our dependence on importing foreign petroleum has declined since peaking in 2005. The U.S. is currently the world's third largest produced of crude oil and petroleum products and is predicted to surpass Saudi Arabia is production by 2015. Although much of the decline is from increases in domestic production of crude oil and natural gas, a decline in consumer consumption resulting from economic downturn after the 2008 financial crisis is also a major factor.

Much of the crude oil and petroleum products imported by the U.S. are from unstable or dangerous countries.[24] A recent report from the Center for American Progress states that the in 2012, the U.S. imported 4 million barrels of oil a day from the State Department's list of "dangerous or unstable" countries. That is nearly 22% of the oil consumed every day in the U.S. is from politically unstable regions. 10 of the countries are on the State Department's Travel Warning List: Algeria, Chad, Colombia, the Democratic Republic of the Congo, Iraq, Mauritania, Nigeria, Pakistan, Saudi Arabia, and Syria. Further, the 22% figure doesn't even include the imports that come from Venezuela, which although not on the State Department's list, has maintained a strong anti-American political stance. This reliance on unstable nations has been said to be compromising our national security and tethering us to hostile regimes.[25]

3.1.2 U.S. Dependence on Foreign Rare Earth Minerals

Many electronic devices, including many advanced photovoltaic devices, are composed of materials and elements that are not found domestically and the U.S. must rely on foreign imports. For example, China currently enjoys a near-monopoly on rare Earth materials, necessary components of most modern electronic devices.[26] The United

States receives nearly all of its supply of rare Earth metals from China. The United States does not have a strong relationship with China and the future availability of this resource is not guaranteed. In fact, in 2010, China briefly halted exportation of rare Earth minerals to Japan resulting from an unrelated international dispute. This episode has forced the U.S. to assess its dependence on China for importation of rare Earth minerals since it seems that China may use its control of rare Earth materials to attain its political and economic goals.

Rare Earth elements are essential components of many of today's electronic devices like cell phones and computers. Further, rare Earth elements are essential components of many military weapons systems. Although the U.S. used to be the major producer of these materials, China is currently the only exporter of commercial quantities of rare Earth elements. In 2010, the U.S. Government Accountability Office (GAO) reported on the world's production of rare Earth minerals and stated that China produced 97% of rare Earth ore, 97% of rare Earth oxides, 89% of rare Earth alloys, 75% of neodymium iron boron magnets (NdFeB), and 60% of samarium cobalt magnets (SmCo). In fact, the U.S. currently lacks the refining, fabricating, and manufacturing capacity to process rare Earth elements. So even if U.S. production of rare Earth minerals was to increase, most of the processing and metal fabrication would have to occur in China. Many members of the U.S. congress have expressed concern that the complete reliance of the U.S. on China for importing rare Earth elements could pose a national security risk.

3.2 Photovoltaics for Energy Production

Worldwide energy consumption is currently estimated to be 15 terawatts (TW) per year and is expected to double by 2050 and more than triple by 2100.[27] The burning of fossil fuels releases greenhouse gases that are largely responsible for global climate change, including an increase in average surface temperatures, increasing frequency of extreme floods and droughts, and more powerful storms. Although fossil fuel reserves are finite, many suggest that the devastating effects of climate change will prompt a pivot to clean energy long before we deplete our reserves.[28] Further, many regions that supply fossil fuel resources are mired in conflict and political instability. As a result, it is necessary for the U.S. to begin researching alternative sources of energy.

More than 120,000 TW of energy from the sun strikes the surface of the Earth every year (nearly 10,000 times more energy than we currently use) and its utilization by photovoltaic devices is emission free.[29] Energy from the sun is abundant, likely lasting for tens to hundreds of thousands of future years, and is found everywhere on Earth, precluding the need to secure the resource from politically instable regions. This makes solar energy an attractive alternative to fossil fuels.

3.2.1 Obstacles to Further Deployment of PV

Despite the natural abundance of solar energy and the availability of the several technologies designed to capture this energy, in 2011, solar power only accounted for 0.2% of energy generated in the U.S. and 0.5% of global electricity demand.[30] Why is the U.S. so slow to adopt a virtually unlimited and free source of energy? There are

several obstacles to further development and deployment of solar power in the U.S. including the cost, intermittency, and transmission of the electricity generated.

Certainly, cost is one of the most important factors affecting the further development and deployment of PV. Electricity generated from solar technologies is still more expensive than many other forms of electricity. In 2012, the cost of electricity generated from PV in the U.S. was $4.44 per installed watt compared to $2.10 per installed watt of coal-generated electricity.[31] The price/installed watt has certainly decreased substantially in recent years; in 2011, the price of silicon wafer panels decreased from $1.85/watt to $0.97/watt. As such, although cost has been and continues to be an obstacle to PV, it is likely that the reaching parity with conventional fossil fuels will occur in the very near future. By some estimates, solar power will be able to compete against fossil fuels without subsidies in half of the world by 2015.[32,33]

Another potential issue with power generated from PV is intermittency issues. Factors like unpredictable weather and limited daylight hours affect how electricity from PV is utilized in the U.S. Further, solar energy is not evenly distributed in the U.S., making it difficult to fully rely on solar energy for our needs. These issues are being addressed by developing storage technologies that allow energy produced during peak daylight hours to be stored for use during low-production hours. Energy could also potentially be stored in the form of chemical bonds by using the PV-generated electricity to reduce carbon dioxide into methanol or other chemical fuels.[34]

Lastly, there is a lack of transmission infrastructure. Solar energy must be collected in sunny areas and transported to areas where it is needed. Often the areas that have the most potential for solar energy collection, like deserts, are very isolated and

remote, with no nearby infrastructure. Thus, not only would large-scale solar collection facilities need to be built, but so too would the transmission infrastructure to connect the solar power systems to the grid. One potential solution to this issue is to generate the solar electricity where it will ultimately be used, obviating the need for transmission lines. Rather than using large solar farms in the desert to collect solar energy and subsequently transmit the energy to where it is needed, the electricity could be generated on-site. Although it is true that more electricity would be produced in sunnier areas, it is also true that much of that energy would be wasted as heat during the transmission.[35]

3.2.2 Policy Options to Help Promote Solar Power

Although some of the obstacles to further deployment of PV are technical, many more are political. It has been mentioned that the cost of PV is still much more than the cost of fossil fuel generated power. However, the end cost of fossil fuel generated power is decreased through several political mechanisms. The global subsidies of fossil fuels total nearly $523 billion per year.[36] That is six times the amount of money spent on renewable energy.(http://www.odi.org.uk/subsidies-change-the-game) In the U.S. alone, it is estimated that as much as $52 billion per year is spent on fossil fuel subsidies.[37] It is much more difficult for PV-generated electricity to reach grid parity when the cost of fossil fuels is artificially deflated. One potential political solution to promote solar power is to spend the estimated $52 billion per year that is currently spent on fossil fuel subsidies on renewable energy subsidies instead.

Another way in which the cost of fossil fuel generated electricity is artificially deflated is that there is no economic accountability for the greenhouse gases that are

generated. The damage from climate change is estimated to be $150 billion per year in the U.S. alone.[38] Who is to pay for this annual damage? It certainly makes sense that the producers of the greenhouse gases responsible for climate change should pay for the damage. Two potential political mechanisms that could hold companies financially accountable for the greenhouse gases that they emit are carbon taxes or cap-and-trade programs. Both of these mechanisms would make energy generated from fossil fuels more expensive and more illustrative of the true cost of this type of electricity. As a case in point, voters in Boulder, Colorado in 2006 approved the first municipal carbon tax. The Boulder Climate Action Plan tax generated $1.8 million in 2010.[39]

Renewable energy portfolio standards are regulations that require a certain portion of a utility's power plant capacity or power generation to come from renewable energy sources like wind, biomass, solar, and geothermal. 16 U.S. states and the District of Colombia have adopted mandatory renewable energy portfolio standards (RPS).[40] The RPS mechanism has been very successful in promoting investment in renewable energy investment and deployment of renewable energy resources in the U.S. In a report released by the Lawrence Berkeley National Laboratories (LBNL), the benefits generated from RPS policies range from $28-$103/MWh compared to costs ranging from a savings of $4/MWh to costs of $48/MWh. Though, in some cases utilities have seen an extra cost for compliance with RPS regulations, others have seen a decrease in cost. Further, the human health benefits calculated in the study ranged from $28-103/MWh, fair outweighing any additional costs imposed by compliance.[41]

As seen from the previous examples, the development and deployment of renewable resources is significantly affected by policy and financial incentives. In 2011,

Europe had 51 GW of installed solar capacity, primarily because of policy incentives. In comparison, the U.S. only had 4.4 GW. In 2013, however, the U.S. had tripled its installed solar capacity to more than 13 GW, resulting from the combined effects of several policies to promote solar energy.[42]

3.3 Organic Materials for Photovoltaics and Electronics

Although PV-generated electricity would free the U.S. from reliance of foreign sources of oil, many of the current photovoltaic technologies require materials that are not produced in the U.S. Many of the necessary components of silicon-based and rare Earth metal-based technologies are not mined in the U.S. and, as a result, we are becoming more reliant on China for the importation of these materials. It does not make sense for the U.S. to pursue energy options for the purpose of decreasing our reliance on fuel imports from unstable nations if those energy options require materials that we must simply import from other unstable nations. In essence, it does not make sense to make a pivot from the Near-East to the Far-East. Most organic materials for photovoltaics and electronics applications are composed of relatively few elements (C, H, N, O, S, and halogens) all of which are very abundant on Earth and more or less equally distributed among the world's countries.

3.3.1 Benefits of Low-Cost Organic PV

Organic photovoltaics offer several advantages when compared to silicon-based technologies, but they are still much less efficient. Does this mean that one technology or the other should be favored? Photovoltaic technologies are expected to become a

sustainable source of terawatt energy. Producing this amount of energy will require vast amounts of raw materials. It doesn't make sense to favor just one technology; it is too risky to rely on just one set of materials since some materials are limited and future access to others is uncertain. For the benefit of sustainability, it makes sense to create a varied portfolio of solar energy technologies, so that if some materials become unavailable in the future, production of other technologies can be increased to mitigate the potential shortfalls in energy production. Surely, one technology in this portfolio will be organic photovoltaics since organic materials are incredibly cheap and abundant.

What is necessary to develop the photovoltaic industry into a source of terawatt energy? Dennler and Brabec outline several important factors: 1) cost, 2) availability of raw materials, 3) scalable, high-volume and low-cost production processes, 4) available land area, 5) energy storage systems, 6) distribution and grid efficiency for the energy mix, 7) centralized versus decentralized energy production.[43] Organic materials have the potential to make significant headway in several of these areas. Roll-to-roll manufacturing processes allow OPV modules to be produced at significantly lower unit costs than any other solar technology, with the added benefit that the printing and coating facilities already exist worldwide with huge capacities, relics of the photographic film, magnetic tape, and compact disc industries. As such, OPV technologies can outcompete most silicon-based technologies in terms of cost, availability of raw materials, and scalable, high-volume, low-cost production processes.

3.3.2 Organic Materials as Rare Earth Substitutes

Among other applications, rare Earth elements are used for batteries, magnets, and catalysts. Could organic materials ever replace rare Earth elements in these applications? The versatility of organic materials allows for a wide range of properties. For example, pure carbon can be an insulator (diamond) and a superconductor (carbon nanotubes).[44] Organic synthesis allows the tuning of material properties, such that we can tailor materials for certain applications. There are examples of organic batteries[45] and organic magnets.[46] This versatility will certainly create a new era of organic electronics, where many electronic materials will be organic.

3.4 Conclusions

The U.S. is dependent on foreign sources of oil for energy and rare Earth minerals for many electronics and weapons applications. Organic materials for photovoltaic and other electronic devices could relieve our dependence on foreign oil and rare Earth minerals. Energy independence is an attractive goal, both economically and in terms of national security, and organic materials offer a path to achieve this goal. The U.S. should invest in R&D for organic electronic materials and develop policies that promote their use and integration.

Chapter IV: Smectic E Mesogens for OFET: n,2-OBTTT Series

4.1 Introduction: The Smectic E Phase for OFETs

Small molecule, organic semiconductors have reached charge carrier mobilities equivalent to amorphous silicon, and even beyond in some cases.[47] In addition to equivalent or better device performance than amorphous silicon, organic materials are solution-processable, low-cost, and flexible, spawning the development of a new plastic electronics industry.[20] An essential component of many plastic electronic devices is the organic field effect transistor (OFET).[13] The most important property of OFETs is charge carrier mobility, the velocity of the electron and/or hole through the organic semiconductor material. There are many factors affecting charge carrier mobility, but from a device perspective, two of the most important are intermolecular π-stacking distance (a function of molecular structure) and the degree of molecular order within thin films (a function of processing conditions).[48] Liquid crystal mesophases offer a route to enable close intermolecular π-stacking distances, as well as create thin films with highly ordered morphologies.[20]

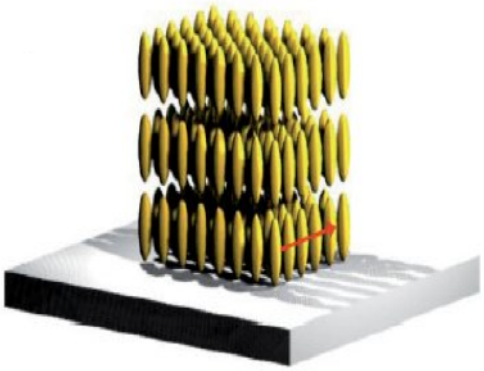

Figure 4-1. A homeotropically aligned smectic phase. The arrow indicates the direction of charge transport in an OFET. [Source: Macromol. Rapid Commun. 2009, 30, 1179–1202]

The direction of charge transport within an OFET is from source to drain, parallel to the surface of the device.[20,49] The nature of charge transport in liquid crystalline materials is still unclear, but many researchers believe that charge transport occurs via a hopping mechanism, from molecule to molecule.[14,17,49,50] In this model, the electron/hole pairs are localized onto single molecules and electron-phonon interactions create small polarons to drive charge transport.[51] Thus, a homeotropically aligned smectic mesophase would present an ideal morphology for charge transport (figure 4-1).[20] The charge could potentially move in two dimensions through a homeotropically aligned smectic layer, presenting an advantage over discotic liquid crystal phases. However, not all smectic mesophases display equivalent charge carrier mobility.[49] Table 4-1 shows some typical values of charge carrier mobility for calamitic organic materials in different smectic mesophases. As can be seen from the table, smectic mesophases have charge carrier mobilities spanning three orders of magnitude!

Table 4-1. Charge Carrier Mobility of Calamitic Mesogens in Smectic Phases

Compound	Number	Mobility		Phase
		μ_h	μ_e	
		$cm^2 \cdot V^{-1} \cdot s^{-1}$	$cm^2 \cdot V^{-1} \cdot s^{-1}$	
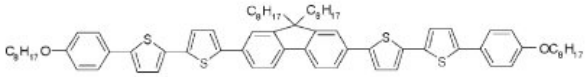	**14**	10^{-3}	–	nematic
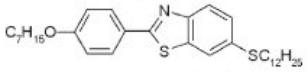	**15**	10^{-4}	10^{-4}	SmA
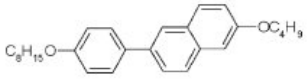	**16**	10^{-2} 4×10^{-4}	10^{-2} 4×10^{-4}	SmE SmA
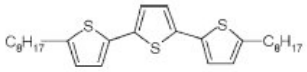	**17**	10^{-2} 2×10^{-3}	10^{-2} 2×10^{-3}	SmG SmF SmC
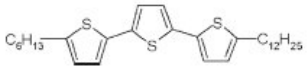	**18**	2×10^{-3}	–	SmF
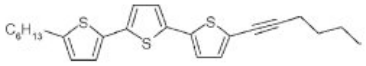	**19**	10^{-2}	10^{-2}	SmE
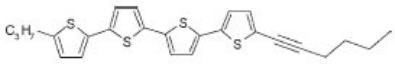	**20**	10^{-1}	–	SmB_{cryst}

[Source: Macromol. Rapid Commun. 2009, 30, 1179–1202]

It is not surprising that smectic A (SmA) has the lowest mobility of the smectic phases; in SmA and SmC (the *fluid-smectic* phases), the molecular packing in the layers is fluid-like and there is significant translational and rotational motion.[48,49] As the calamitic molecule rotates around its long axis, the π-orbital overlap is significantly diminished, potentially decreasing charge transport. On the other end of scale of thermodynamic stability lie the *crystal-smectic* phases. Compared to SmA and SmC, these phases are much more highly ordered and solid-like; included among the crystal-smectic phases are SmE, SmG, SmF, and SmB.[20,52]

These highly ordered crystal smectic phases have no fluidity and are the closest to ordered crystals.[53,54] The SmE phase, in particular, has generated much interest in the

field of small molecule semiconductors. In the SmE phase, the calamitic mesogens are packed so densely that free rotation around the long axis no longer occurs.[53] The rigid aromatic cores, then, are better approximated by boards than rods, since they are flat and no longer rotating. The resulting herringbone packing within the layers can potentially yield strong π-π interactions among the aromatic cores (figure 4-2). The very short π-stacking distance of 4 Å or less in the SmE phase can facilitate the hypothesized hopping mechanism of charge transport in liquid crystal systems.[49,51]

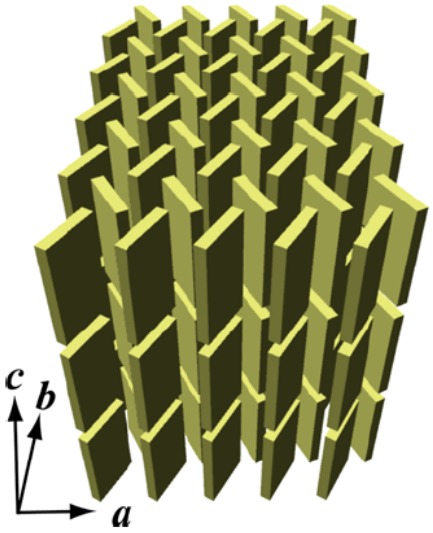

Figure 4-2. Herringbone array of rigid aromatic cores in SmE phase, [Source: J. Phys. Chem. B 2013, 117, 8293−8299]

Unlike most smectic mesophases, where separate layers are uncorrelated, XRD studies of the SmE phase have discovered three-dimensional periodicity.[53,54] The SmE phase displays a much more ordered structure than other smectic mesophases. Studies suggest that the structure of the SmE phase for an asymmetric, aromatic mesogen with a long alkyl chain contains nanosegregated domains with alkyl sublayers consisting of alkyl chains from both upper and lower sublayers (figure 4-3).[56] This alkyl chain

interdigitation is one potential source of interlayer correlation in the SmE phase. The anisotropy of the interaction among the cores in this up-down arrangement stabilizes the herringbone structure of the mesophase. This proposed structure for the SmE phase is further corroborated with evidence from various crystal structures presented in chapter 6 of this thesis.

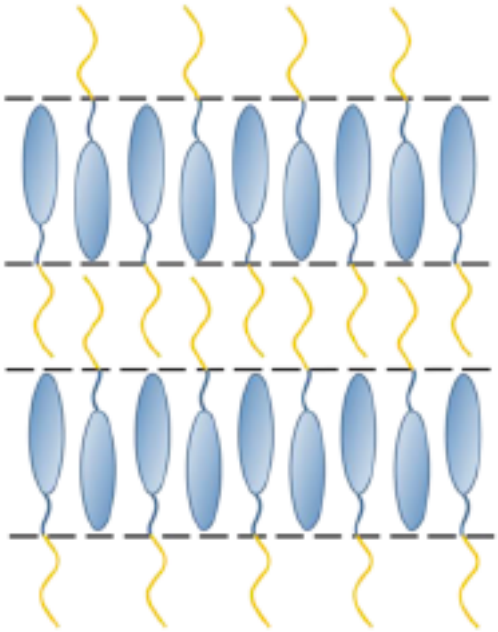

Figure 4-3. New model of SmE structure of asymmetric mesogen with long, interdigitated alkyl chains. [Source: J. Phys. Chem. B 2013, 117, 8293−8299]

What, then, is the difference between a *bona fide* crystal and a material in the SmE phase? The entropies of transitions calculated from the DSC results were plotted against the alkyl chain length for a series of SmE mesogens.[57] It was found that upon heating, during the crystal phase-SmE phase transition, the entropy of transition directly correlated to alkyl chain length, but for the SmE-Isotropic transition, no such correlation existed. The authors concluded that the alkyl chains in the SmE phase are fully *melted*, as it were.[57] This result is seen even in the mesophase closest in structure to an ordered

crystal, suggesting that the alkyl chains are fully melted in all mesophases.[56,57] However, disorder in the alkyl chains should not affect charge transport along the π-system, which is the preferred direction of charge transfer in conjugated organic materials, as already discussed. Further, judging from the high mobility values achieved in the SmE phase, the conformational disorder in the alkyl chains seems to have no effect. The SmE phase, then, seems to be a good platform for conferring a high degree of molecular order upon a thin film before cooling into a solid phase.

4.2 Design of SmE Mesogens with High Charge Carrier Mobility

Inducing short π-π distances can be achieved by designing molecules with specific structural features. General formation of smectic phases is a function of intermolecular nano-segregation of rigid, aromatic cores and flexible alkyl chains. But what subtle molecular features are responsible for the formation of specific mesophases is unclear. For example, although all of the members of the n-alkyl series of mesogens shown in figure 4-4 display some smectic phase or phases, certain members displayed the SmE phase, while others did not.[55,58-60] As such, one strategy employed when attempting to synthesize new mesogens with a specific mesophase is to synthesize a series that varies only by alkyl (or alkoxy) chain length. Different members of the series will display different mesophases and, with more homologs, the odds of obtaining the desired mesophase are increased.

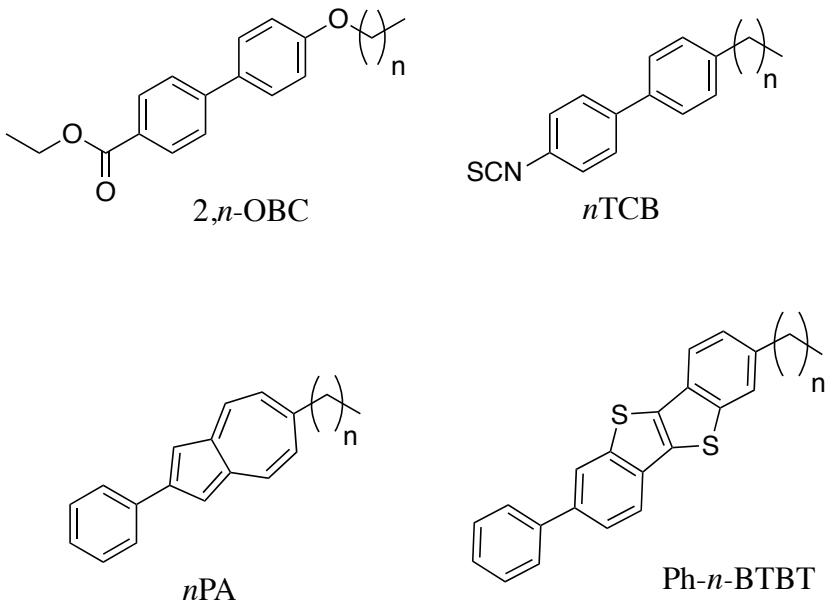

Figure 4-4. Calamitic mesogens displaying the SmE liquid crystal phase.

4.2.1 Molecular Features Affecting Short π-π Distances

Maximizing charge carrier mobility is the most important consideration for OFET semiconductors. Several factors affect charge mobility, including intermolecular distance and π-π overlap.[14,17,49,61] It makes intuitive sense that rigid systems of conjugated π-orbitals would maximize intermolecular π-π overlap. The degree of π-π overlap and the distance between molecules is a function of the crystal structure of a molecule, which is notoriously difficult to predict based on molecular structure alone. A material with particularly high charge carrier mobility is the polymer, poly[2,5-bis(3-tetradecylthiophen-2-yl)thieno[3,2-b]thiophene] (pBTTT, figure 4-5a), a thiophene-based material.[62] Figure 4-5b shows a potential morphology for the pBTTT mesophase; it can be seen that the alkyl chains interdigitate to create flat lamellar sheets. The π-π spacing in C14-pBTTT has been measured at d = 3.63 Å.[63] This π-π distance is relatively short. *The pBTTT aromatic core is nicely suited for short π-π distances.*

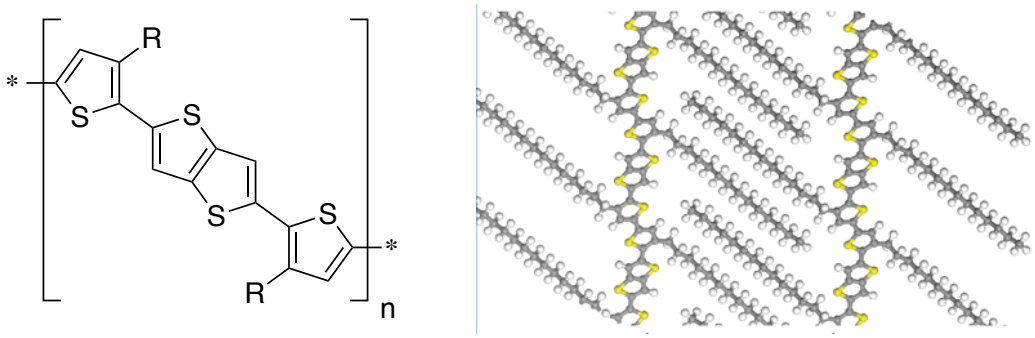

Figure 4-5. (a) Repeating structure of a semiconducting polythiophene (pBTTT) that was designed to self-assemble into large crystalline domains and to possess an extended, planar π-electron system. (b) Interdigitated alkyl chains in highly ordered mesophase of pBTTT. [Source: nature materials VOL 5 APRIL 2006, 328-333]

4.2.2 Molecular Features Affecting Formation of the SmE Phase

It is speculated that the *sanidic* mesophase, characterized by lamellar sheets of conjugated polymer backbones (figure 4-6), is responsible for the highly ordered morphologies of thin films of pBTTT and other thiophene-based polymer materials. The thin films are often annealed into a mesophase above room temperature, where it is believed that a favorable alkyl side-chain density allows for alkyl interdigitation, increasing charge carrier mobility.[50,62] Much like the interdigitation responsible for the interlayer correlation in the SmE phase (figure 4-3), the alkyl chains of pBTTT allow correlations between polymer chains (figure 4-5b). This alkyl chain interdigitation creates a very ordered structure. The mesophase exhibited by pBTTT is characterized as a highly-ordered *sanidic* phase of stacked polymer backbones. This morphology allows very close π-π interactions in the aromatic cores, similar to SmE (figure 4-6). When the material cools from this mesophase, the alkyl chains recrystallize, maintaining the highly ordered morphology achieved during annealing.[62] *Alkyl chains can potentially increase the order observed in thin films of polymer materials.*

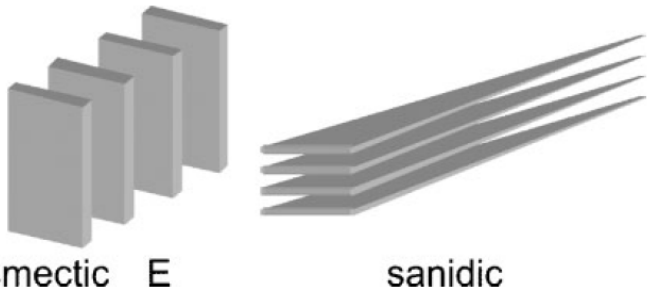

Figure 4-6. Comparison of the molecular packing in the SmE and sanidic phases. Both mesophases possess close π-stacking of aromatic cores. [Source: Macromol. Rapid Commun. 2009, 30, 1179–12]

The desired material for OFET devices is a small molecule mesogen that exhibits the SmE phase and close π-π interactions. The previously reported studies suggest that mesogens with a rigid, aromatic core and asymmetric alkyl chains of varying length will often induce the SmE phase.[56,57] Further, the aromatic core of pBTTT has been shown to exhibit very close π-π interactions, attributing to its high charge carrier mobility.[62] A series of mesogens was designed with these considerations in mind (figure 4-7).

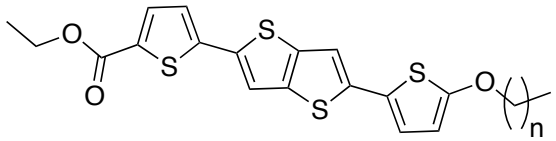

Figure 4-7. A calamitic mesogen designed to display the SmE phase for improvements in thin film processing and close π-stacking of aromatic cores to maximize charge carrier mobility: the n,2-OBTTT series.

The electron-rich thiophene rings of the desired compound contribute to a low ionization potential and also help to induce smectic phases through nanosegregation. The aromatic core is flat, similar to pBTTT, with very little inter-annular twisting because of the fused thieno[3,2-b]thiophene moiety. The aromatic core contains a high C/H ratio,

which facilitates close π-π stacking and helps to induce a cofacial arrangement. This morphology is believed to provide significant orbital overlap, which increases charge carrier mobility. The n,2-OBTTT series will exhibit varying alkoxy chain length to investigate how this affects the formation of highly ordered liquid crystal phases, as well as the crystal structure.

4.3 Synthesis of the n,2-OBTTT Series

The synthesis of the series of target mesogens (figure 4-7) required a thieno[3,2-b]thiophene unit. The synthesis was carried out according to previous literature methods (scheme 4-1).[64]

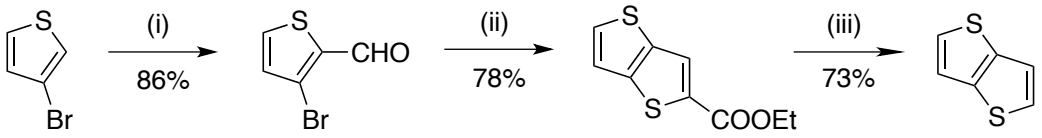

Scheme 4-1. (i) 1) LDA, THF, 0°C; 2) N-formylpiperidine; (ii) Ethyl thioglycolate, K_2CO_3, DMF; (iii) 1) LiOH, THF, reflux; 2) Quinoline, Cu, reflux

The synthetic pathway to the n,2-OBTTT series is illustrated in schemes 4-2 and 4-3. The final product (3) can be seen as a central thieno[3,2-b]thiophene core flanked by an electron-rich thiophene (2) and an electron-poor thiophene (the ester). Kirsch et al.[65] studied coupling reactions of thieno[3,2-b]thiophene and aryl halides and found that organozinc compounds coupled with aryl iodides (Negishi coupling) provided higher yields than the corresponding Suzuki or Stille reactions. Accordingly, Negishi coupling with aryl iodides was the coupling method employed in the current study.

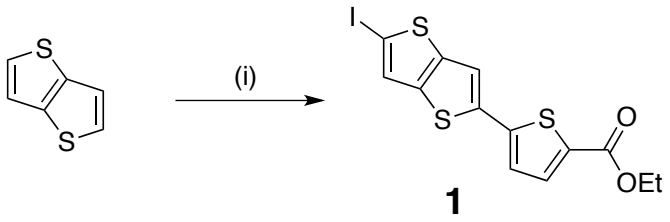

Scheme 4-2: (i) 1) n-BuLi, THF, −78°C, 2) $ZnCl_2$, THF, rt, 3) $Pd(dba)_2$, PPh_3, NMP, ethyl 5-iodo-2-thiophenecarboxylate, 70°C, 4) N-iodosuccinimide, $CHCl_3$:AcOH, rt

Coupling reactions of aryl halides and organometallic reagents are promoted by electron withdrawing groups on the aryl halide; as such, ethyl 5-iodothiophene-2-carboxylate was prepared and coupled to thieno[3,2-b]thiophene. Thieno[3,2-b]thiophene was prepared and treated with n-BuLi and anhydrous $ZnCl_2$ in dry and degassed THF to generate an organozinc compound *in situ* that was coupled to ethyl 5-iodothiophene-2-carboxylate via a Pd-mediated Negishi coupling. The resulting product was iodinated with NIS to yield compound (1).

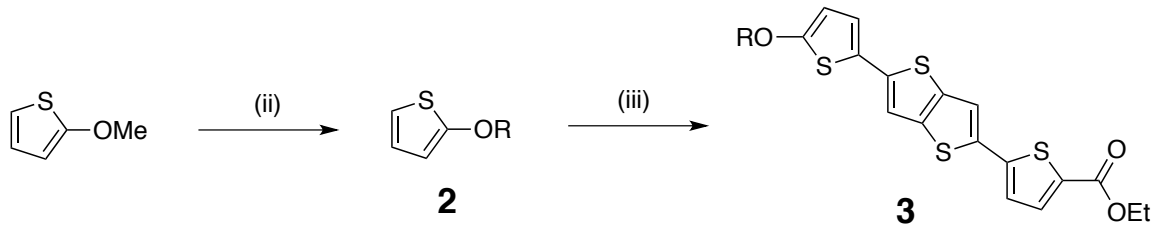

Scheme 4-3: (ii) HCl (5 mol%), ROH (excess), toluene, reflux; (iii) 1) n-BuLi, THF, −78°C, 2) $ZnCl_2$, THF, rt, 3) $Pd(dba)_2$, PPh_3, NMP, **1**, 70°C

Until recently, an efficient route to 2-alkoxythiophenes has not been reported. The method reported by Tietz et al.[66] utilizes a two-step procedure: an oxidation of a 2-thienyltrifluoroborate, followed by a Mitsunobu etherification, for an overall yield of

68% or less. Our group has recently developed an improved route to 2-alkoxythiophenes from 2-methoxythiophene utilizing a one-step procedure: an acid-catalyzed nucleophilic aromatic substitution. 2-methoxythiophene was prepared according to literature methods[67], dissolved in toluene, and treated with the appropriate alcohol and catalytic HCl. The reaction was heated and methanol was distilled to drive the reaction forward. The corresponding 2-alkoxythiophene **2** was produced in 50-70% yield. Compounds **1** and **2** were coupled via a Negishi reaction to afford compound **3** (scheme 4-3).

4.3.1 Synthesis of 2-Alkoxythiophenes

A necessary component of the desired target structure **1** is a 2-alkoxythiophene unit **2**. An exhaustive search of the literature revealed only one method to obtain 2-alkoxythiophenes and this method was only recently published, in 2012.[66] The only members of the 2-alkoxythiophene series that appeared in the literature prior to 2012 were 2-methoxythiophene and 2-ethoxythiophene. These two compounds were synthesized using a basic, nucleophilic aromatic substitution reaction with 2-bromothiophene, the appropriate alkoxide ion, and catalytic CuBr (scheme 4-4).

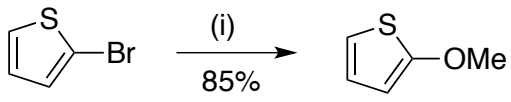

Scheme 4-4. (i) NaOMe, MeOH, CuBr, reflux.

However, this is not a viable route to 2-alkoxythiophenes with longer alkoxy chains because the longer chain alkoxides are not commercially available and are cumbersome to work with. It is difficult to prepare the alkoxide separately and add it to

the starting material later because the longer chain alkoxides are very insoluble in all aprotic solvents that were tried. It is difficult to make the alkoxide ions *in-situ* because sodium hydride will reduce the thiophenes. This synthesis proved to be an ineffective route to general 2-alkoxythiophenes due to the low yield, difficulty synthesizing long-chain alkoxide ions, and the large mixture of products. Further, the increasing insolubility of longer chain alkoxide ions precluded any product from being obtained for alcohols of 6 carbons and longer.

A procedure was located in an old German patent that describes an acid-catalyzed trans-etherification reaction utilizing 2-methoxythiophene, the appropriate alcohol, and catalytic *p*-toluenesulfonic acid in refluxing toluene (scheme 4-5). As the reaction progresses, methanol is distilled from the mixture to drive the equilibrium forward according to Le Chatlier's principle. The yield of the reaction is usually around 50%, but this value often varied quite dramatically and could be as low as 20%.

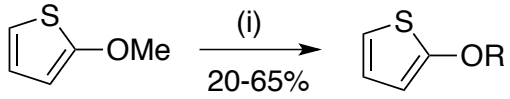

Scheme 4-5. (i) ROH (excess), TsOH (catalytic), toluene, reflux.

Due to the varying nature of the yield, an investigation was conducted as to the cause and to attempt to improve the yield. The final color of the reaction mixture usually varied from light yellow to dark red. After several iterations of the reaction, a correlation was noted between the final color of the reaction and the overall yield of desired product: the darker the color, the lower the yield. It was also noted that the order in which the reactants were added attributed to the generation of the color: if *p*-toluenesulfonic acid

was added directly to 2-methoxythiophene, an intensely dark red color was generated almost immediately, whereas if *p*-toluenesulfonic acid was first dissolved in toluene, followed by addition of 2-methoxythiophene, the generation of color was delayed and never became as intensely red, but rather stayed a lighter yellow-orange color. This suggested that perhaps 2-methoxythiophene was somehow reacting with *p*-toluenesulfonic acid, although a reasonable mechanism could not be elucidated. Since the identity of the acid was unimportant to affect the desired transformation and it was hypothesized that the electrophilicity of the TsOH was responsible for undesired side reactions, the TsOH was replaced with a non-electrophilic acid. It was discovered that the yield could be improved to 50-70% and the generation of red color could be avoided by replacing the TsOH with catalytic concentrated HCl (scheme 4-6). Using this new synthetic route to 2-alkoxythiophenes, 13 novel 2-alkoxythiophenes have been produced.

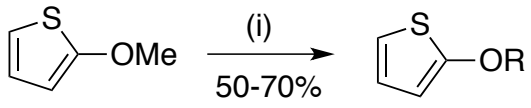

Scheme 4-6. (i) ROH (excess), HCl (catalytic), toluene, reflux.

4.3.2 Nomenclature of the n,2-OBTTT Series

The designation of the n,2-OBTTT series was arrived at in the following manner: 1) the core of the mesogen is based on the polymer pBTTT, but the mesogen is not a polymer, so the 'p' is dropped; 2) there is an alkoxy linkage from the alkyl chain to the aromatic core, so an 'O' is added; and 3) there are two potential alkyl chains, one on the ester side and one on the ether side, so the prefix n,n is denoting the lengths of the alkyl

tails, ether first, then ester. Since all of the homologs in this thesis have an ester tail length of two, the series is designated: n,2-OBTTT.

4.3.3 Experimental Procedures

All chemicals were purchased from Sigma-Aldrich and were used as received. Starting Materials thieno[3,2-b]thiophene[65] and 2-methoxythiophene[67] were prepared according to literature methods. ^{1}H and ^{13}C NMR spectra were recorded on a Bruker Avance-III 300 spectrometer and are reported in ppm relative to residual solvent. Mass Spectra were recorded on a Waters Synapt G2 spectrometer; compounds were analyzed in either positive or negative mode ESI by direct infusion of compounds in acetonitrile or methanol at approximately 10 pmol/ μL. In cases where ionization efficiency was low, LiCl was added to the compound solution in order to promote Li+ adducts. Accurate mass measurements were provided by lockmass correction using the +1 charge state of leucine enkephalin.

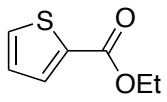

Ethyl thiophene-2-carboxylate

To a solution of 2-thiophene carboxylic acid (30 g, 0.234 mol) in ethanol (250 mL) in a 1000-mL round bottom flask was added concentrated sulfuric acid (1.3 mL, 10 mol%). The solution was refluxed for 24 hours and then cooled to room temperature. 150 mL of dichloromethane was added to the solution and the organic layer was washed with saturated sodium bicarbonate (3 x 50 mL), then saturated sodium chloride (3 x 50 mL). The organic layer was dried over anhydrous magnesium sulfate, filtered, and the solvent

removed *in vacuo* to yield the product as a pale yellow oil (35 g, 96%); the product did not require further purification and was used as obtained in the next step. δH(300 MHz; CDCl3) 1.40 (3 H, t, J 7.1 Hz), 4.37 (2 H, q, J 7.1 Hz), 7.12 (1 H, dd, J 5.0, 3.8 Hz), 7.56 (1 H, dd, J 5.0, 1.3 Hz), 7.82 (1 H, dd, J 3.7, 1.3 Hz); δC(75 MHz, CDCl3) XXX; m/z (TOF-ES+) 157.0315 [MH+] (calcd. 157.0323).

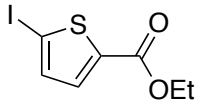

Ethyl 5-iodothiophene-2-carboxylate

N-iodosuccinimide (50.5 g, 0.224 mol) was added to a solution of ethyl thiophene-2-carboxylate (35 g, 0.224 mol) in a 1:1 mixture of chloroform (115 mL) and glacial acetic acid (115 mL) in a 1000-mL round bottom flask covered with aluminum foil. The solution was refluxed for 48 hours in the dark and then cooled to room temperature. The solution was washed with saturated sodium thiosulfate (3 x 100 mL), 1.0M sodium hydroxide (3 x 100 mL), and saturated sodium chloride (3 x 100 mL). The organic layer was dried over anhydrous magnesium sulfate, filtered, and the solvent was removed in vacuo. The resulting mixture, containing product (~85%) and starting material (~15%), was placed into a freezer at −20°C overnight. The product solidifies at this temperature and the starting material remains a liquid and can be removed by pipette to yield pure product (pale yellow solid, 51.8 g, 82%). δH(300 MHz; CDCl3) 1.40 (3 H, t, J 7.1 Hz), 4.37 (2 H, q, J 7.1 Hz), 7.12 (1 H, dd, J 5.0, 3.8 Hz), 7.56 (1 H, dd, J 5.0, 1.3 Hz), 7.82 (1 H, dd, J 3.7, 1.3 Hz); δC(75 MHz, CDCl3) XXX; m/z (TOF-ES+) 282.9286 [MH+] (calcd. 282.9290).

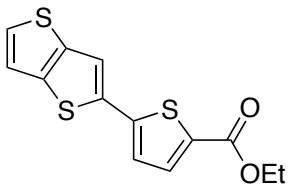

Ethyl 5-(thieno[3,2-b]thiophen-2-yl)thiophene-2-carboxylate

A three-neck, 1000-mL round bottom flask was flame dried and placed under high vacuum. The flask was vacuum purged for 10 minutes under high vacuum, then back-filled with argon; this process was repeated three times. The flask was charged with thieno[3,2-b]thiophene (20 g, 0.143 mol) and anhydrous tetrahydrofuran (150 mL) that was degassed using the freeze-pump-thaw method. The solution was cooled to −78°C using an acetone/dry ice bath and n-butyllithium (1.6M, 90 mL, 0.143 mol) was slowly added, dropwise. The solution was stirred at −78°C for 30 minutes, then stirred at room temperature for 30 minutes, at which time anhydrous zinc (II) chloride (19.45 g, 0.143 mol) was added in small portions and stirred at room temperature for 30 minutes. Degassed N-methyl-2-pyrrolidone was added (100 mL) and the solution was stirred at room temperature for an additional 30 minutes. Ethyl 5-iodothiophene-2-carboxylate (40.33 g, 0.143 mol), bis(dibenzylideneacetone)palladium(0) (1.67 g, 2 mol%), and triphenylphosphine (1.52 g, 4 mol %) in degassed N-methyl-2-pyrrolidone (50 mL) was added and the solution was stirred at 70°C for 2 hours. The solution was then poured into cold, distilled water (1000 mL), and filtered. The filtered solids were purified by silica gel column chromatography (dichloromethane) to yield the product (yellow solid, 32.4 g, 77%). δH(300 MHz; CDCl3) 1.41 (3 H, t, J 7.1 Hz), 4.39 (2 H, q, J 7.1 Hz), 7.18 (1 H, d, J 3.9 Hz), 7.25 (1 H, dd, J 5.3, 0.7 Hz), 7.43 (1 H, d, J 5.3 Hz), 7.47 (1 H, d, J 0.6 Hz),

7.72 (1 H, d, J 3.9 Hz); δC(75 MHz, CDCl3) 14.37, 61.28, 117.21, 119.46, 123.94, 128.28, 132.09, 134.06, 137.95, 139.12, 139.82, 144.27, 162.01; m/z (TOF-ES+) 594.9851 [2MLi+] (calcd. 594.9846).

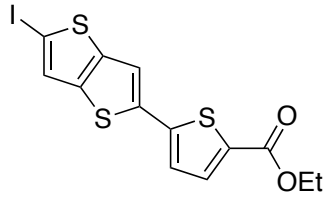

Ethyl 5-(5-iodothieno[3,2-b]thiophen-2-yl)thiophene-2-carboxylate (1)

N-iodosuccinimide (17.6 g, 0.078 mol) was added to a solution of ethyl 5-(thieno[3,2-b]thiophen-2-yl)thiophene-2-carboxylate (23 g, 0.078 mol) in a 1:1 mixture of chloroform (100 mL) and glacial acetic acid (100 mL) in a 1000-mL round bottom flask covered with aluminum foil. The solution was stirred at room temperature, in the dark, for 24 hours. The solution was washed with saturated sodium thiosulfate (3 x 100 mL), then 1.0M sodium hydroxide (3 x 100 mL), then saturated sodium chloride (3 x 100 mL). The organic layer was dried over anhydrous magnesium sulfate, filtered, and the solvent was removed *in vacuo*. The residue was purified by silica gel column chromatography (dichloromethane) to yield the product (pale yellow solid, 27.5 g, 84%). δH(300 MHz; CDCl3) 1.41 (3 H, t, J 7.1 Hz), 4.38 (2 H, q, J 7.1 Hz), 7.16 (1 H, d, J 3.9 Hz), 7.36 (1 H, d, J 0.6 Hz), 7.38 (1 H, d, J 0.6 Hz), 7.71 (1 H, d, J 3.9 Hz); δC (75 MHz, CDCl3) 14.38, 61.35, 76.04, 116.29, 124.15, 128.39, 132.41, 134.07, 137.84, 139.11, 143.63, 144.45, 161.93; m/z (TOF-ES+) 846.7768 [2MLi+] (calcd. 846.7780).

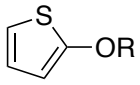

2-Alkoxythiophene (2)

The general procedure reported here for the synthesis of 2-butoxythiophene was used for the synthesis of all of the 2-alkoxythiophenes.

A 250-mL round bottom flask was equipped with a fractional distillation head. The flask was charged with a solution of 2-methoxythiophene (10 g, 0.088 mol) in toluene (100 mL). To the solution was added 1-butanol (25 mL) and concentrated HCl (0.36 mL, 5 mol%). The solution was stirred at room temperature for 30 minutes and then slowly heated to 70°C. The temperature of the distillate was carefully monitored and when it exceeded the boiling point of methanol, the reaction was stopped and cooled to room temperature. The solution was washed with saturated sodium bicarbonate (3 x 50 mL) and saturated sodium chloride (3 x 50 mL). The solution was dried over anhydrous magnesium sulfate, filtered, and the solvent was removed *in vacuo*. The residue was purified by silica gel column chromatography (hexanes) to yield the product (10.02 g, 73%). δH(300 MHz; CDCl3) 1.00 (3 H, t, J 7.3 Hz), 1.51 (2 H, m), 1.80 (2 H, m), 4.06 (2 H, t, J 6.5 Hz), 6.23 (1 H, ddd, J 3.7, 1.4, 0.6 Hz), 6.56 (1 H, ddd, J 5.7, 1.4, 0.6 Hz), 6.74 (1 H, ddd, J 5.7, 3.7, 0.6 Hz); δC (75 MHz, CDCl3) 13.78, 19.11, 31.23, 73.66, 104.50, 111.65, 124.67, 165.87; m/z (TOF-ES+) 157.0692 [MH+] (calcd. 157.0682).

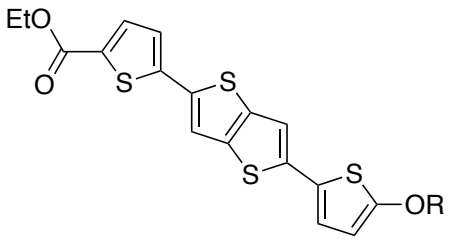

Ethyl 5-(5-(5-alkoxythiophen-2-yl)thieno[3,2-b]thiophen-2-yl)thiophene-2-carboxylate (3)

The general procedure reported here for the synthesis of 4,2-OBTTT was used for the synthesis of all of the members of the n,2-OBTTT series.

A three-neck, 100-mL round bottom flask was flame dried and placed under high vacuum. The flask was vacuum purged for 10 minutes under high vacuum, then back-filled with argon; this process was repeated three times. The flask was charged with 2-butoxythiophene (0.78 g, 5 mmol) and anhydrous tetrahydrofuran (15 mL) that was degassed using the freeze-pump-thaw method. The solution was cooled to −78°C using an acetone/dry ice bath and n-butyllithium (1.6M, 3.13 mL, 5 mmol) was slowly added, dropwise. The solution was stirred at −78°C for 30 minutes, then stirred at room temperature for 30 minutes, at which time anhydrous zinc (II) chloride (680mg, 5 mmol) was added in small portions and stirred at room temperature for 30 minutes. Degassed N-methyl-2-pyrrolidone was added (10 mL) and the solution was stirred at room temperature for an additional 30 minutes. Compound 1 (2.10 g, 5 mmol), bis(dibenzylideneacetone)palladium(0) (58 mg, 2 mol%), and triphenylphosphine (52 mg, 4 mol %) in degassed N-methyl-2-pyrrolidone (5 mL) was added and the solution was stirred at 70°C for 2 hours. The solution was then poured into cold, distilled water (150 mL), and filtered. The filtered solids were purified by silica gel column chromatography (dichloromethane) to yield the product (bright yellow solid, 32.4 g,

77%). δH(300 MHz; CDCl3) 1.00 (3 H, t, J 7.4 Hz), 1.41 (3 H, t, J 7.1 Hz), 1.51 (2 H, m), 1.81 (2 H, m), 4.09 (2 H, t, J 6.5 Hz), 4.38 (2 H, q, J 7.1 Hz), 6.16 (1 H, d, J 4.0 Hz), 6.88 (1 H, d, J 4.0 Hz), 7.12 (1 H, d, J 0.4 Hz), 7.16 (1 H, d, J 3.9 Hz), 7.38 (1 H, d, J 0.6 Hz), 7.71 (1 H, d, J 3.9 Hz); δC(75 MHz, CDCl3) 13.75, 14.37, 19.07, 31.12, 61.26, 73.76, 105.43, 113.90, 117.22, 122.16, 123.41, 123.64, 131.73, 134.10, 136.82, 137.45, 139.65, 141.12, 144.31, 162.03, 165.53; m/z (TOF-ES+) 903.0731 [2MLi+] (calcd. 903.0751).

4.4 Conclusions

A series of small molecule semiconductors was designed to exhibit the SmE liquid crystal phase in order to achieve highly ordered materials for organic electronics. Several other mesogens with a rigid, aromatic core attached to at least one alkyl chain exhibit the SmE phase, so the design of the target molecule included at least one alkyl chain of varying length. The liquid crystalline, semiconducting polymer, pBTTT, has among the highest charge carrier mobility of any organic material and it is hypothesized that this is due to the short distance of the intermolecular π-π overlap in the aromatic core. The thiophene-based aromatic core of pBTTT was also included in the design of the target molecule to maximize intermolecular π-π overlap and charge carrier mobility.

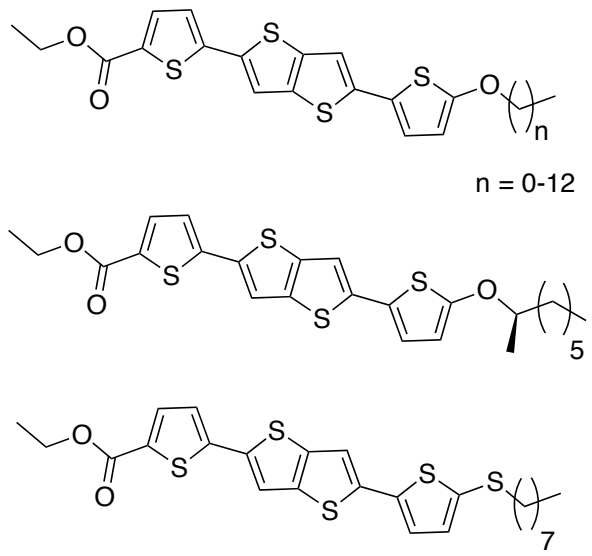

Figure 4-8. The n,2-OBTTT series (and 8,2-SBTTT); 15 mesogens synthesized as a series of small molecule semiconductors designed to exhibit the SmE phase and close intermolecular π-π overlap.

The synthetic route required synthesis of a new class of molecules not previously (before 2012) reported in the literature, 2-alkoxythiophenes. A recent paper describes a 2-step route to general 2-alkoxythiophenes utilizing a Mitsunobu etherification reaction.[66] The overall yield of the two-step Mitsunobu reaction is about 65%. The synthetic route to 2-alkoxythiophenes described here employs only one step with an overall yield of 50-70%. The synthesis of the target series of molecules was successful. Figure 4-8 displays the 15 mesogens that were synthesized as part of this series.

Chapter V: Liquid Crystal Behavior of the n,2-OBTTT Series

5.1 Introduction: Paramorphosis as a Route to Monodomain Films

Often, one factor that limits charge carrier mobility in OFETs is poor molecular alignment throughout the bulk of the organic semiconducting thin film, the presence of grain boundaries.[13,18,19,20] Although crystalline, organic semiconductors typically have higher charge carrier mobilities than materials in liquid crystal mesophases, it is difficult to prepare highly ordered thin films with good molecular alignment from crystalline organic materials. This is because of the formation of crystal grain boundaries in polycrystalline materials (figure 2-3) and the difficulty of aligning solid materials. Although the molecules within a single grain are aligned, the grains are not necessarily aligned with each other. In polycrystalline samples, this creates several crystal grain boundaries that act as trap sites for charges moving through a material.

Liquid crystal phases offer a route to achieve large-area, highly ordered, semiconducting films.[5,20,49,68,69] Liquid crystal phases respond to shear, electric fields, temperature gradients, alignment layers, etc., so they are easier to align than solid and isotropic phases.[20] Assuming that the bulk morphology of the film changes very little upon crystallization from a highly ordered, aligned smectic phase (a process called *paramorphosis* (figure 5-1)), then the formation of crystal grain boundaries can be avoided.[68,69,72]

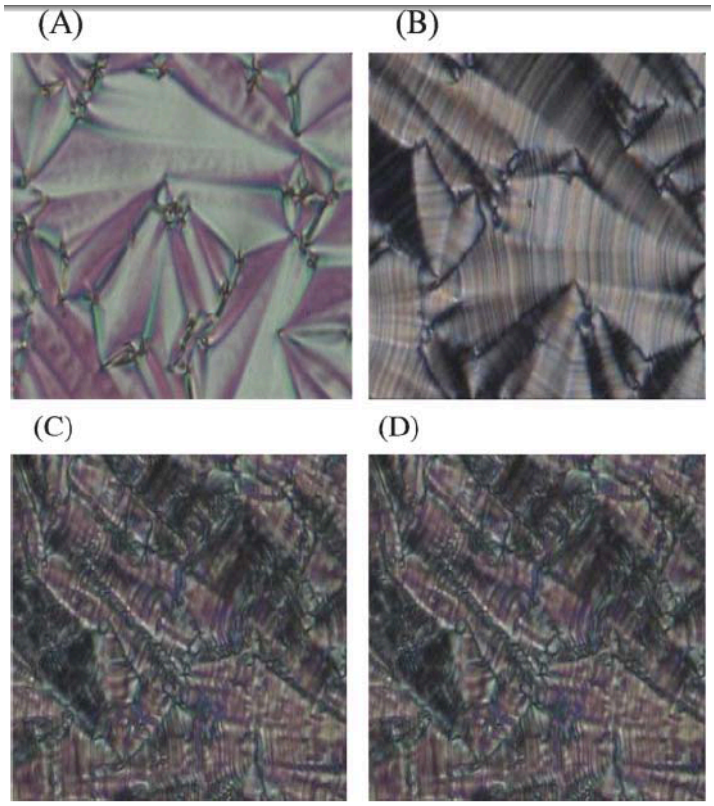

Figure 5-1. Textures exhibiting paramorphosis upon cooling. (A) SmA phase, (B) SmE phase, (C) Sm3 phase, (D) crystal. [source: Chem. Commun., 2005, 2921–2923]

Paramorphosis is the term applied when a material cooled from one smectic phase (SmA) into a more highly ordered smectic phase (SmE) exhibits the optical texture of the smectic phase above it rather than its own, more thermodynamically stable, texture.[53,68,73] This indicates that the defects in the lower temperature phase were inherited from the higher temperature phase. Thus, if there are few or no defects in the higher temperature phase, then this order will be maintained in the lower temperature phases, including the crystal, upon cooling. This strategy has been used to control the morphology of thin films of organic semiconductors.[68,69,72]

New research into the SmE phase has elucidated structural features of the phase that make it a good platform for charge transport, like close intermolecular π-π overlap.[70,71] The SmE phase is the mesophase closest in structure to an ordered crystal,

exhibiting three-dimensional interlayer correlation.[53] Conversely, the SmA phase is the most fluid-like smectic phase and can be aligned into a monodomain from an isotropic melt.[72] The ideal phase sequence would be I - SmA - SmE - crystal. Utilizing this phase sequence, a material could be deposited onto a substrate, heated and annealed into the SmA mesophase, aligned into a monodomain[72], and cooled into first the SmE mesophase, then the crystal phase. The gradual increase in order as the material passes through the smectic phases is expected to suppress the formation of a multidomain structure. Materials that exhibit paramorphosis could potentially retain the monodomain alignment conferred in the SmA phase all the way throughout cooling, into the crystal phase, without the formation of crystal grain boundaries. A similar strategy has been used to create a 150mm in diameter monodomain of thin film, liquid crystalline semiconductor.[69]

5.1.1 Liquid Crystal Characterization of n,2-OBTTT

The experimental methods used to characterize the liquid crystal behavior of the n,2-OBTTT series are: 1) differential scanning calorimetry (DSC); 2) polarized light microscopy (PLM); and 3) x-ray diffraction (XRD). Phase diagrams for all the compounds in the series are presented at the end of this chapter (Table 5-1).

5.2 Differential Scanning Calorimetry

Differential scanning calorimetry is a thermoanalytical technique that measures the heat capacity of a substance as a function of temperature, allowing phase transitions to be located. Phase transitions were determined with a Mettler Toledo DSC823e and a heating and cooling rate of 10° C/min. The compounds were weighed into aluminum

crucibles (1-5 mg of material). The DSC data for the n,2-OBTTT series indicate that all of the members of the series are liquid crystalline and have at least one mesophase, even the compound with only a methoxy tail: 1,2-OBTTT. In fact, 1,2-OBTTT has at least two distinct mesophases (figure 5-2). This is surprising considering that formation of liquid crystalline phases is said to be driven by nanosegregation of alkyl and aromatic sub-regions and a chain length of one does not provide much substance for nanosegregation. This is a subject for future investigation. The DSC data divide the mesogens into two distinct groups: compounds with at least two mesophases (figure 5-2) and compounds with only one mesophase (figure 5-3). Of course, it is possible that there are subtle second order phase transitions that do not appear on the DSC data. The compounds with short alkoxy chains (# of carbons = 1-3) and long alkoxy chains (# of carbons = 10-13) seem to exhibit at least two mesophases, whereas the compounds with medium alkoxy chains (# of carbons = 4-9) seem to exhibit only one mesophase, as shown by the DSC spectrum of 4,2-OBTTT (figure 5-3).

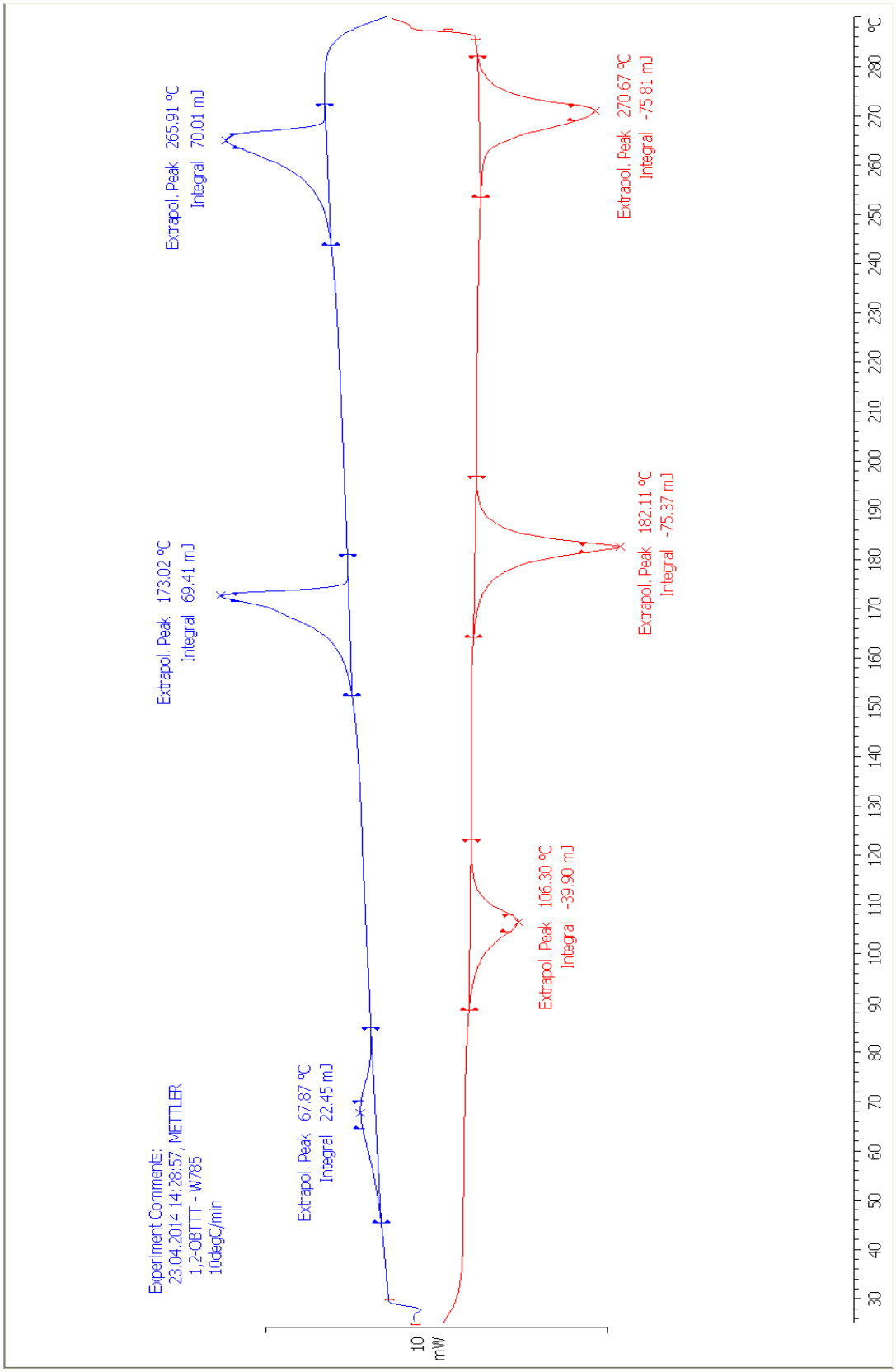

Figure 5-2. Differential scanning calorimetry data for 1,2-OBTTT obtained at 10°C/min.

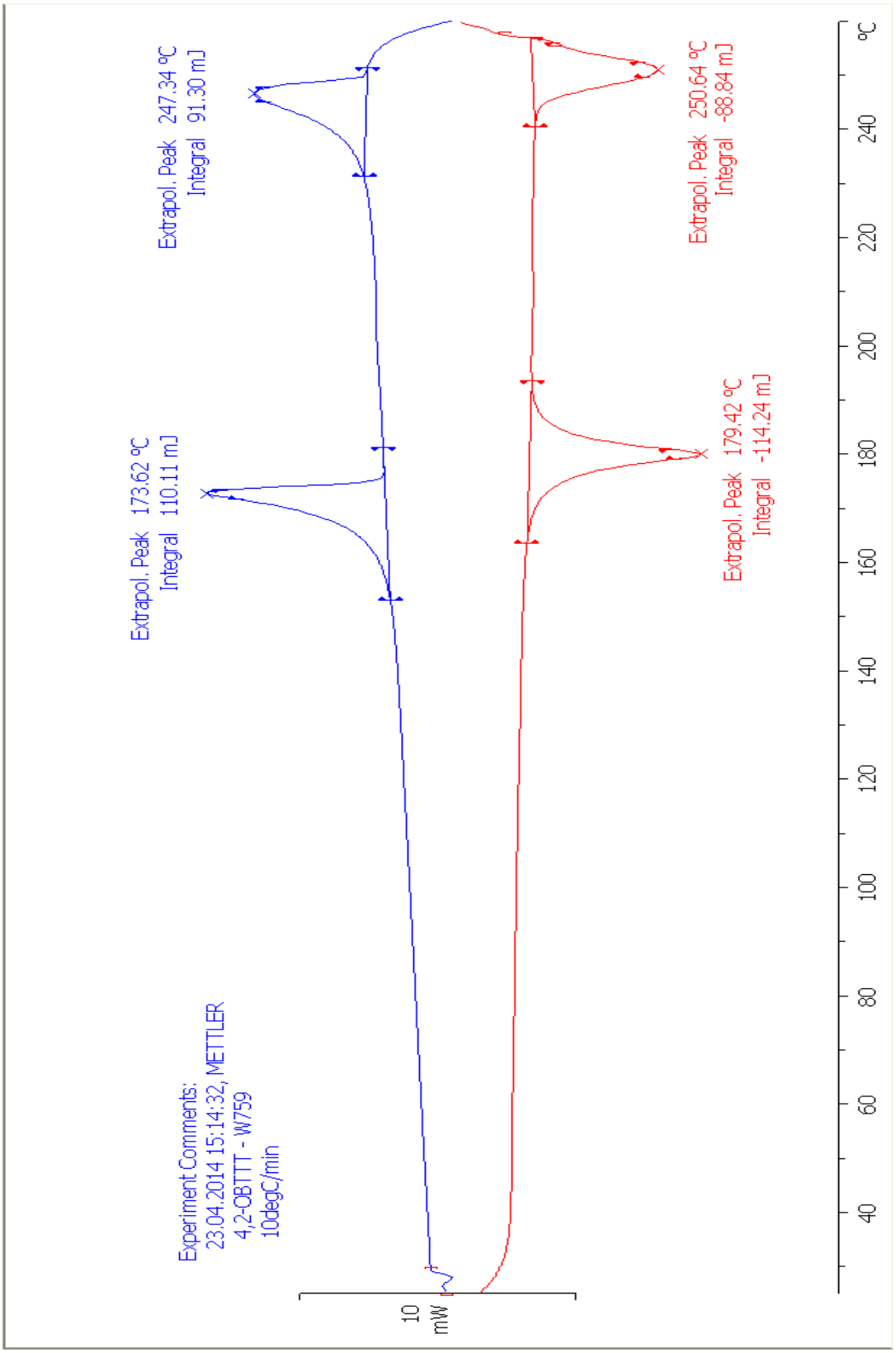

Figure 5-3. Differential scanning calorimetry data for 4,2-OBTTT obtained at 10°C/min.

5.2.1 Trends in Transition Temperatures

The clearing points of all the compounds in the series but one are quite high: between 210-270°C. This is not surprising; the structure of the aromatic core was chosen to allow close, and therefore strong, π-π overlap. These strong π-π interactions hold the molecules together and increase the clearing point. The clearing points decrease slightly with increasing alkoxy tail length. Again, this is to be expected; alkyl chains are non-polar and so the intermolecular forces between them are much weaker than the π-π interactions of the cores. The longer the chain gets, the weaker are the intermolecular forces holding the molecules together. For device applications, these temperatures are likely too high to be cost effective or amenable to certain industrial deposition techniques.

Three isomers with 8 carbons in their alkyl chains were synthesized as part of this series: 8,2-OBTTT, (R)8,2-OBTTT (enantiomerically pure), and 8,2-SBTTT (a thioether linkage replacing the alkoxy linkage) (figure 4-7). The compound (R)8,2-OBTTT that possesses a branched alkoxy tail with and a stereocenter has a much lower clearing point than the n-alkoxy homolog, though this is not surprising. Mesogens with branched tails often have lower clearing points resulting from an inability to pack closely, causing disorder in the crystal structure. The compound 8,2-SBTTT also has lower transition temperatures than the corresponding 8,2-OBTTT by about 20°C. Figure 5-4 displays the minimum energy conformations, as determined by a Merck molecular force field energy minimization (MMFF), of the isomers in the n,2-XBTTT series with eight carbons in their tails. The n-alkoxy linkage of 8,2-OBTTT allows a very straight, unkinked conformation with a dihedral angle between the plane of the thiophene ring and the plane

of the alkoxy tail of virtually zero, an all anti conformation (figure 5-4a). Conversely, when the octyl tail is connected to the oxygen at the 2-position (an *iso* connection), the preferred dihedral angle between the plane of the thiophene ring and the plane of the alkoxy tail is gauche, with a dihedral angle of about 30° (figure 5-4b). Lastly, replacing the alkoxy linkage with a thioether linkage creates a serious kink in the alkyl chain, as seen in the minimum energy conformation of 8,2-SBTTT (figure 5-4c). The C-S-C bond lengths of the thioether are much longer than the C-O-C bond lengths of the alkoxy linkage. Similarly, the C-S-C bond angle is more compressed than the corresponding alkoxy, causing the tail to kink to avoid steric repulsion between hydrogen atoms. The measured dihedral angle between the plane of the thiophene ring and the plane of the alkyl chain in 8,2-SBTTT is 60°, a fully gauche conformation.

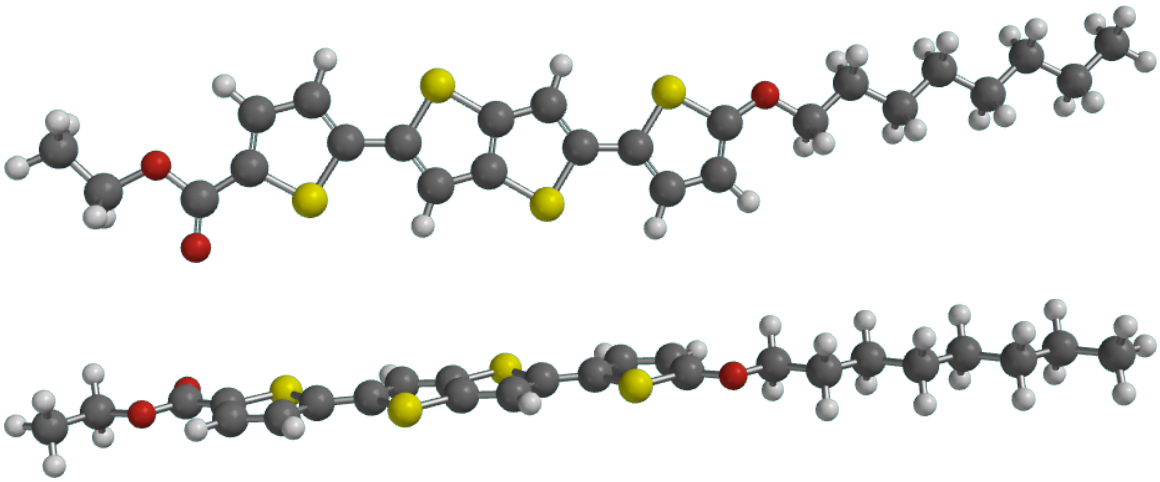

Figure 5-4. (a) MMFF energy minimization of 8,2-OBTTT. The dihedral angle between the plane of the core and that of the alkoxy tails is nearly zero, an all anti conformation.

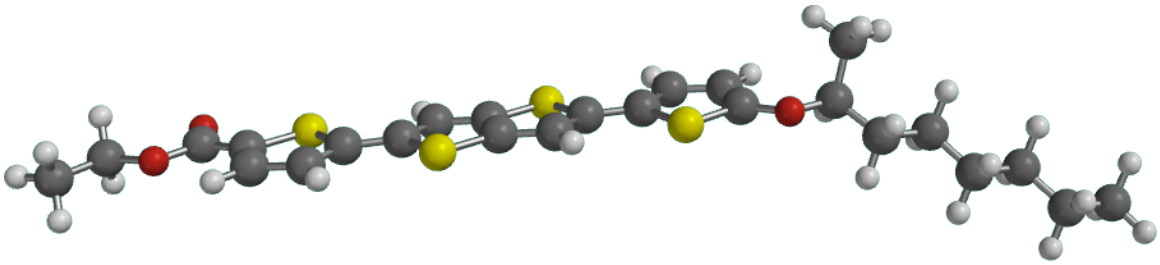

(b) MMFF energy minimization of (R)8,2-OBTTT. The branched tail shifts the dihedral angle between the plane of the core and that of the alkoxy tails to about 30°, a partial-gauche conformation.

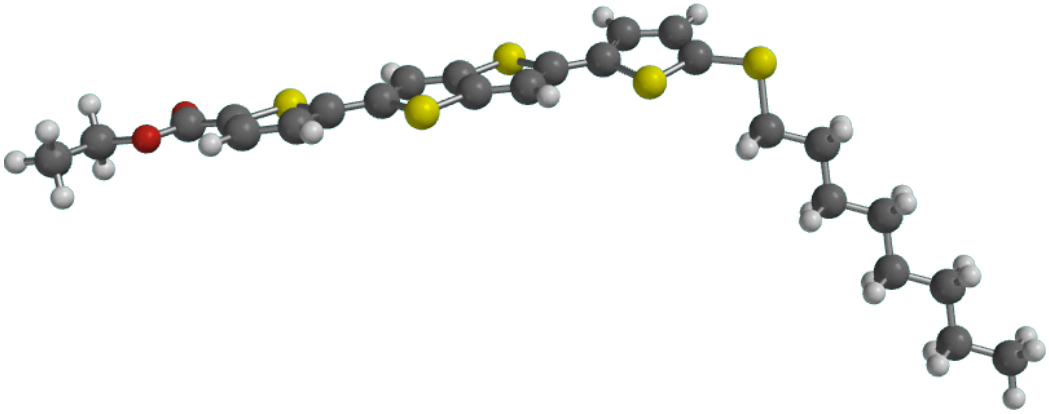

(c) MMFF energy minimization of 8,2-SBTTT. The sulfur atom in the thioether shifts the dihedral angle between the plane of the core and that of the thioether tails to about 60°, a fully-gauche conformation.

The transition temperatures as a function of alkoxy tail length are plotted in figure 5-5. The temperatures of the transitions (Iso - SmA; blue) and (SmA - SmX/crystal; red) seem to be inversely correlated to alkyl chain length, as previously discussed. There are a couple of interesting anomalies, however. First, the presence of a smectic phase below the SmA phase in short-chain mesogens and again in long-chain mesogens and puzzling absence from the medium-chain mesogens. Second, the long-chain mesogens 10,2-OBTTT and 12,2-OBTTT do not fall on the trendline (figure 5-5). 10,2-OBTTT has

transition temperatures slightly lower and 12,2-OBTTT, slightly higher, than would be expected from the effects of the alkyl chain length alone. This behavior is unexpected and, presently, unexplainable, except to say that there is possibly some odd-even effect of alkyl chain length at longer lengths. This behavior warrants future investigation.

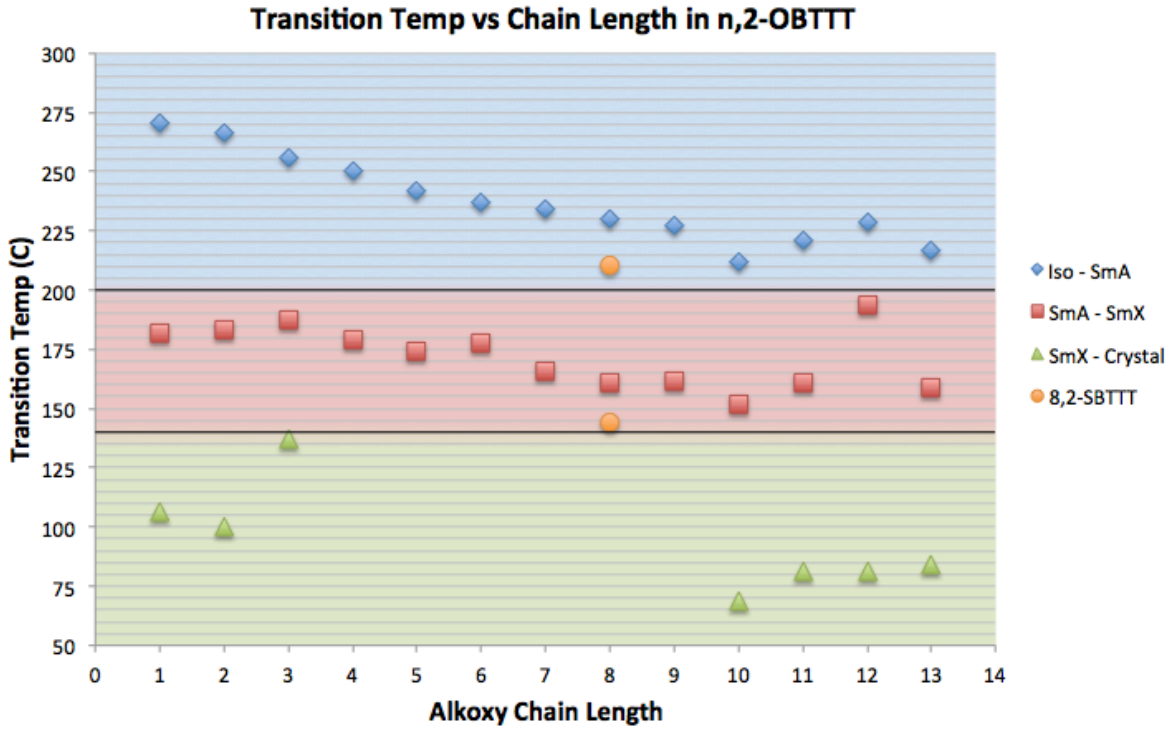

Figure 5-5. Transition temperatures as a function of alkoxy (or thioether) chain length.

5.2.2 Formation of Crystal Smectic Phases as a Function of Chain Length

The possession of an alkyl chain length attached to a rigid, aromatic core has previously been discussed as potential driving forces of the SmE phase. However, it does not seem to be as simple as the mere possession of an alkyl chain of any length. One possible explanation for this behavior has to do with the asymmetry of the alkyl chains as well as the possession of a molecular dipole. The ester chain length is constant, at about

4 atoms long (C-O-C-C), whereas the length of the alkoxy chain varies. In the short-chain compounds (# of carbons = 1-2), the ether chain is shorter than the ester chain. In medium-chain compounds (# of carbons = 3-9), the ether chain is between 1-2 times the length of the ester chain. In long-chain compounds (# of carbons = 10-13), the ether chain is more than 2 times the length of the ester chain. In the medium-chain compounds, the tails are nearly of equal length. This alone should not affect the formation of the SmE phase, since many mesogens with symmetric chains display the SmE phase (C8-BTBT, for example; figure 4-4). However, C8-BTBT is a completely symmetric mesogen, so there is no difference between head and tail, whereas n,2-OBTTT is asymmetric. Even though the chains may be of similar length in some members of the n,2-OBTTT series, there is a definite difference between the head and tail of the mesogens. When there is a large mismatch between the lengths of the ester and ether chains, the chains between smectic layers must interdigitate; this is the case for both short-chain compounds and long-chain compounds (figure 5-6a), but not for medium-chain, nearly symmetric compounds (figure 5-6b).

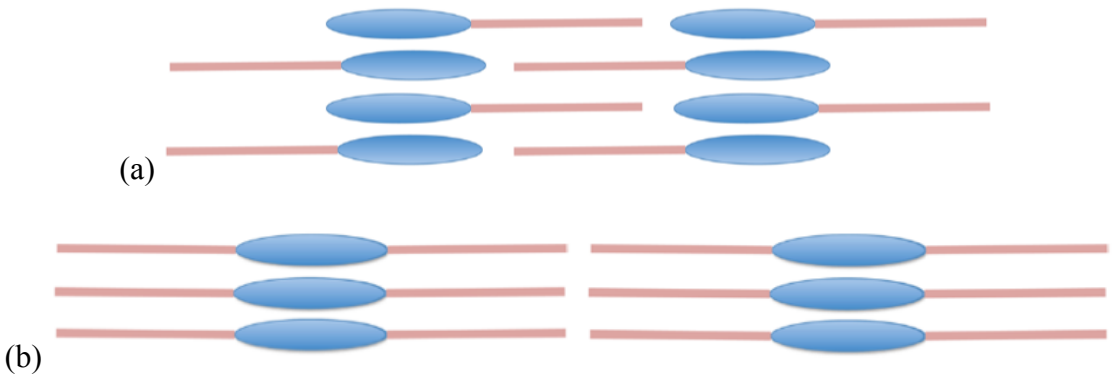

Figure 5-6. (a) Asymmetric calamitic mesogens must interdigitate their alkyl chains between layers to maintain a nanosegregated structure with sublayers of cores and

sublayers of alkyl chains; (b) symmetric calamitic mesogens do not interdigitate their alkyl chains.

Thus, maybe the mesogens with two, nearly symmetric chains must be completely symmetric, like C8-BTBT (figure 4-4), in order to form low temperature, crystal smectic phases. This could be a function of the point group symmetry of the mesogens relative to the direction (and magnitude) of the molecular dipole. This hypothesis could be tested further to examine the effect of molecular dipole moments on smectic phase formation.

5.3 Polarized Light Microscopy

Liquid crystal mesophases can be identified by examining the optical textures they produce through a polarized light microscope. Each phase has a characteristic texture and defect structures when viewed through crossed polarizers that change during a phase transition, allowing identification of the type of phase. Liquid crystal cells were produced and the optical textures analyzed using PLM to identify the mesophases. Liquid crystal cells were prepared by heating on a hotplate a small amount of material at the junction of a cover slip and microscope slide so that as the material melted, it was drawn into the cavity between the cover slip and slide by capillary force to form a thin film without air bubbles. Liquid crystal cells were heated to an isotropic melt and cooled at a rate of 10°C/min to examine the optical textures produced. Cells were examined using a Nicon-HCS400 microscope with an Instec-STC200 temperature-controlled stage.

5.3.1 Assignment of Mesophases by Texture Analysis

DSC data confirmed that all of the compounds in the n,2-OBTTT series exhibit at least one mesophase. Careful examination of the textures produced upon cooling from an isotropic melt at a cooling rate of 10°C/min allowed the following phase determinations to be made for the n,2-OBTTT series:

Smectic A

The high temperature mesophase that appears directly below the isotropic melt is remarkably similar for all members of the n,2-OBTTT series. Although there are subtle differences in the textures of this high temperature phase, these differences have been attributed to differences in alignment (planar vs. homeotropic) and/or second order phase transitions that are not apparent from the DSC data but have subtle effects on texture. As such, the high temperature mesophase that appears directly beneath the isotropic liquid has been identified as the smectic A phase for all members of the series.

Figure 5-7A displays a texture exhibited by 8,2-OBTTT at 230°C upon cooling from the isotropic at a rate of 10°C/min and figure 5-7B displays an image of the anisotropic growth of *batonnets*, a feature associated with the formation of the SmA phase from an isotropic melt. The images are incredibly similar and, as such, the structures from 8,2-OBTTT have been identified as SmA *batonnets*. Although only 8,2-OBTTT is shown here, all members of the n-2-OBTTT series exhibited similar *batonnets* upon cooling from an isotropic melt.

(A) (B)

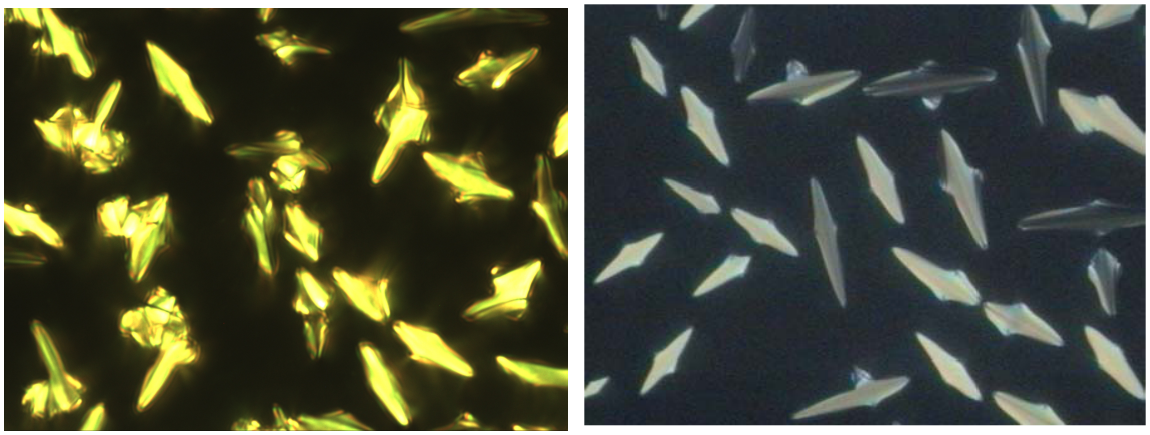

Figure 5-7. (A) Texture exhibited by 8,2-OBTTT at 230°C upon cooling from an isotropic melt at the rate of 10°C/min.; (B) growth of *batonnets* associated with the SmA phase. [Source: Textures of Liquid Crystals, Ingo Dierking, 2003, Wiley-Verlag]

Figure 5-8A displays a texture of 8,2-OBTTT at 215°C upon cooling at a rate of 10°C/min. This texture is representative of the textures exhibited by the other mesogens in the series, as well. Figure 5-8B displays a texture of the focal conic defect associated with the SmA phase. The dark lines that form a '+' in the image result from the alignment of molecules along the direction of the crossed polarizer and analyzer. When the optic axis (slow axis) of the birefringent sample is parallel or perpendicular to the polarizers, dark lines known as *extinction brushes* result. The presence of extinction brushes in the textures exhibited by the n,2-OBTTT series (figure 5-8A) is further support for an assignment of SmA.

(A) (B)

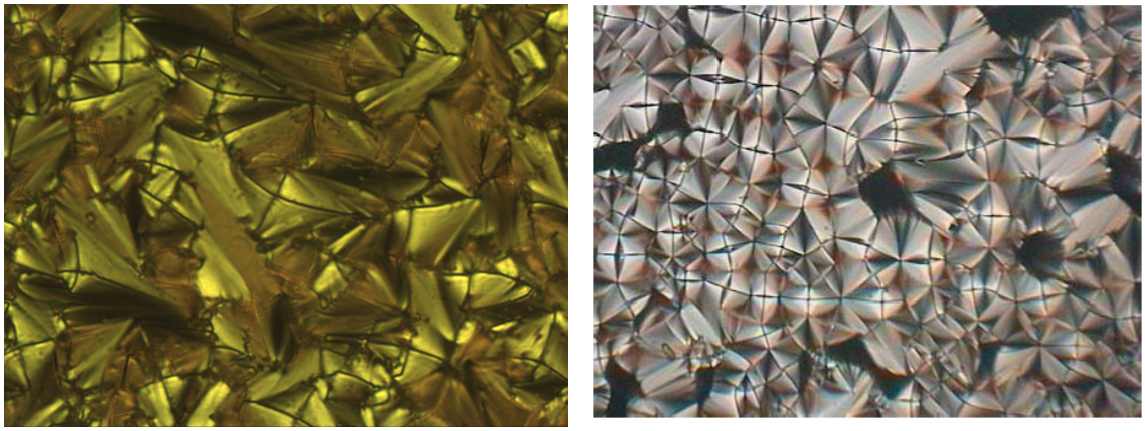

Figure 5-8. (A) Texture exhibited by 8,2-OBTTT at 212°C upon cooling from an isotropic melt at the rate of 10°C/min.; (B) typical focal conic texture associated with the SmA phase. [Source: Textures of Liquid Crystals, Ingo Dierking, 2003, Wiley-Verlag]

Finally, figure 5-9B displays another typical texture resulting from the SmA phase, the fan texture. Figure 5-9A displays a texture exhibited by 9,2-OBTTT (and typical of the other members of the n,2-OBTTT series) at 212°C upon cooling at a rate of 10°C/min. Again, the image in figure 5-9A is taken to be the same texture as that in figure 5-9B, providing more evidence that the high temperature mesophase of the n,2-OBTTT series is, indeed, the SmA phase.

(A) (B)

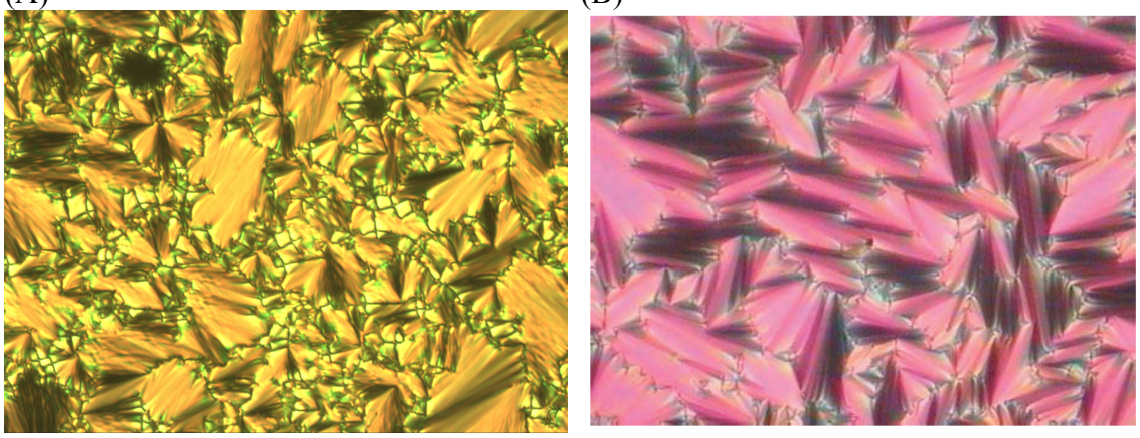

Figure 5-9. (A) Texture exhibited by 9,2-OBTTT at 215°C upon cooling from an isotropic melt at the rate of 10°C/min.; (B) typical fan texture associated with the SmA phase. [Source: Textures of Liquid Crystals, Ingo Dierking, 2003, Wiley-Verlag]

Smectic C

Although not apparent from the DSC data, the textures exhibited by some of the members of the n,2-OBTTT series indicated that a smectic C (SmC) phase may be formed upon cooling from the SmA. Figure 5-9A shows the texture of 1,2-OBTTT at 202°C upon cooling from an isotropic melt at a rate of 10°C/min. The texture has been assigned as belonging to the SmA phase. Figure 5-9A contains regions of planar-aligned SmA (the golden focal conic and fan textures), as well as regions of homeotropically-aligned SmA (the dark regions interrupting the focal conic texture). During the paramorphic phase transition from SmA to a lower temperature smectic phase shown in figure 5-9B, the regions of homeotropically aligned aligned mesogens that appeared dark in the SmA phase have become bright and exhibit what looks like a mosaic texture. Thus, 1,2-OBTTT seems to transition from SmA to a more highly ordered, low temperature smectic phase without passing through a SmC phase. The phase transition is first-order and is apparent from the DSC data (figure 5-2).

(A)

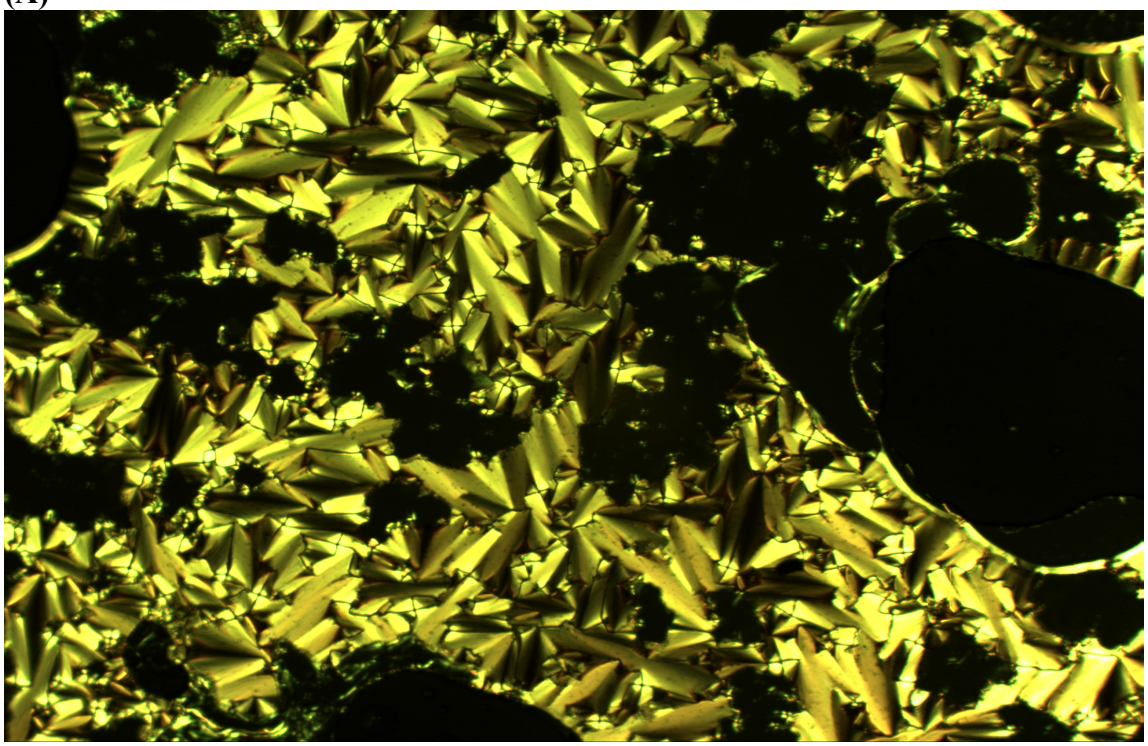

(B)

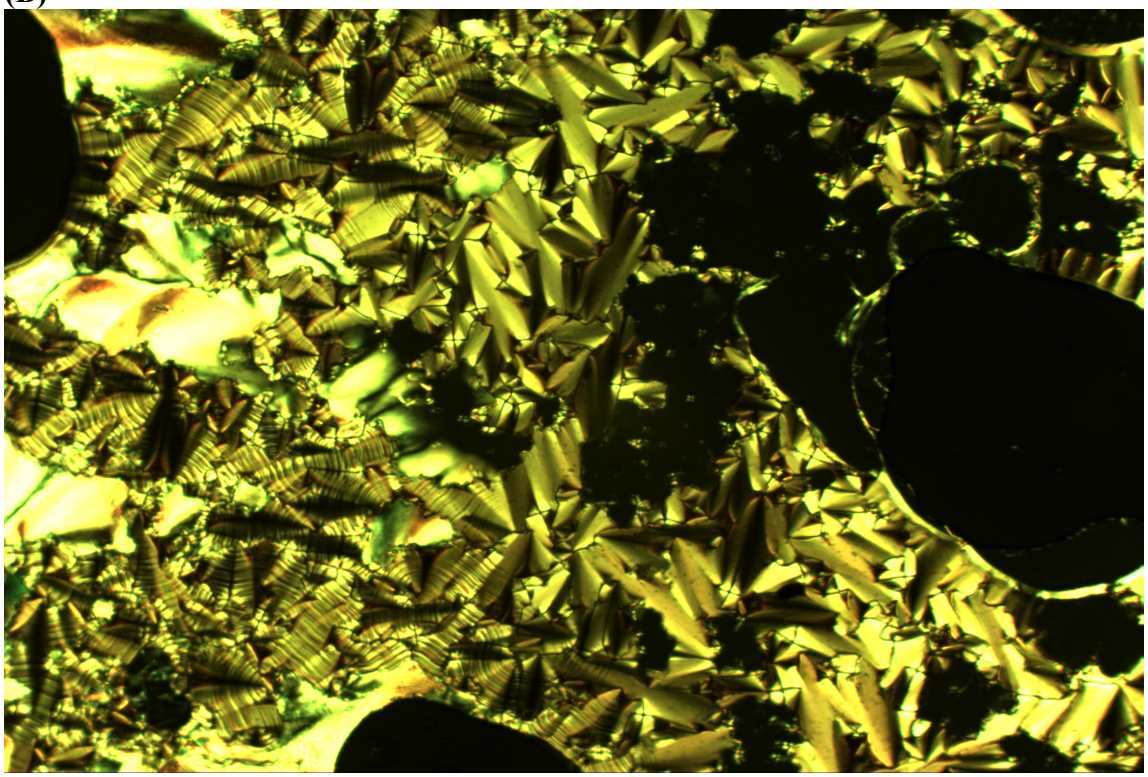

Figure 5-10. PLM textures of 1,2-OBTTT produced on cooling from an isotropic melt at 10°C/min; (A) SmA texture at 202°C, dark homeotropically aligned regions interrupting fan texture; (B) SmA - SmE transition at 174°C, dark homeotropic regions forming a mosaic texture and planar regions forming a striated fan texture with concentric arcs.

Figure 5-10 displays several textures exhibited by 10,2-OBTTT upon cooling from an isotropic melt at a rate of 10°C/min. Similar to what was seen in figure 5-9A, the image in figure 5-10A displays a texture containing regions of planar-aligned SmA (the golden focal conic and fan textures) and regions of homeotropically-aligned SmA (the dark regions spotted throughout the focal conic texture). However, markedly different from the behavior of 1,2-OBTTT, as the cell is further cooled through the SmA phase, 10,2-OBTTT develops a subtle texture in the homeotropically-aligned regions (figure 5-10B, C, and D). The texture becomes brighter as the cell cools until it is just as bright (or more) than the planar-regions.

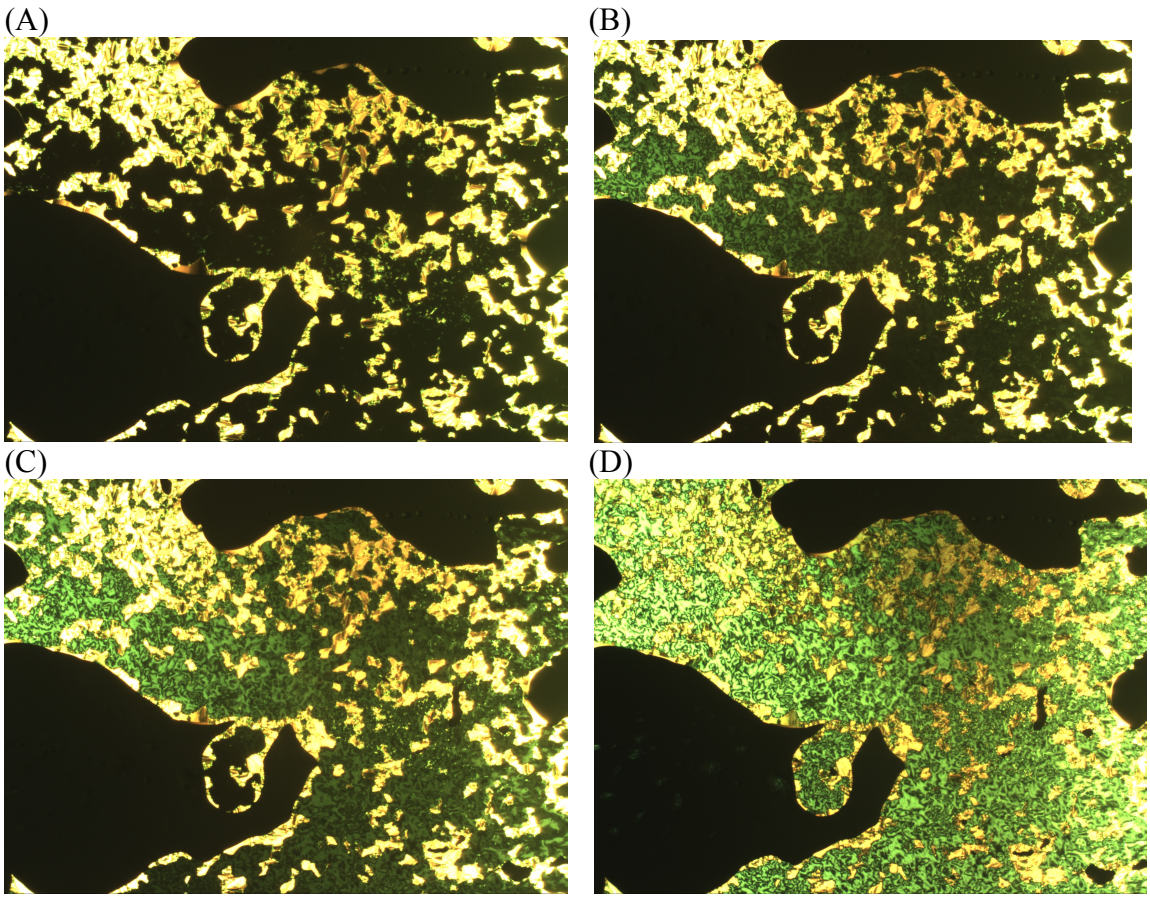

Figure 5-11. PLM textures of 10,2-OBTTT produced on cooling from an isotropic melt at 10°C/min; (A) SmA texture at 205°C; (B) beginning of second-order SmA-SmC transition at 195°C; (C) SmA-SmC transition at 185°C; (D) SmC texture at 175°C.

Though this behavior is indicative of a phase transition, there is no evidence of any such transition in the DSC data across the series, suggesting that the transition is second-order.

Closer examination of the homeotropically-aligned regions of the texture produced by 10,2-OBTTT revealed a Schlieren texture (figure 5-11). Although homeotropically aligned SmA would appear dark between crossed polarizers, homeotropically aligned SmC would appear as a Schlieren texture and this is precisely what is seen.

(A) (B)

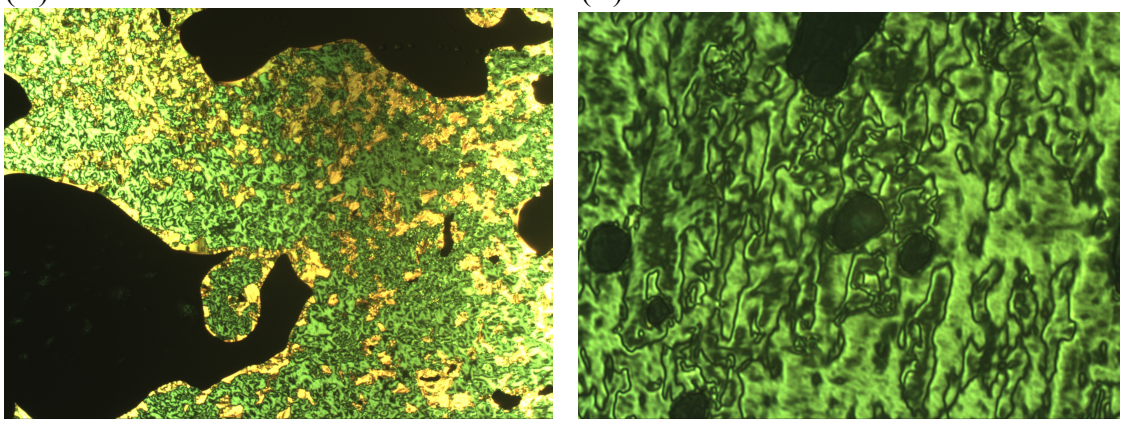

Figure 5-12. PLM textures of 10,2-OBTTT produced on cooling from an isotropic melt at 10°C/min; (A) SmC texture with planar regions (golden) and homeotropic regions (green); (B) increased magnification of homeotropic regions reveals a Schlieren texture.

Further evidence of a SmC phase was obtained by examining the textures produced by 9,2-OBTTT (figure 5-12). Figure 5-12A is presumed to be the SmA phase at 220°C obtained upon cooling from an isotropic melt at a rate of 10°C/min. The literature states that the fan texture of SmA exhibits well-formed extinction brushes (figure 5-13A), but the *broken fan* texture of SmC has softened edges and lightened extinction brushes due to the different tilt directions of the director with respect to the layer normal (figure 5-13B).

The textures exhibited by 9,2-OBTTT in figure 5-12 greatly resemble the textures indicative of a SmA-SmC transition, as reported in the literature (figure 5-13).

(A) (B)

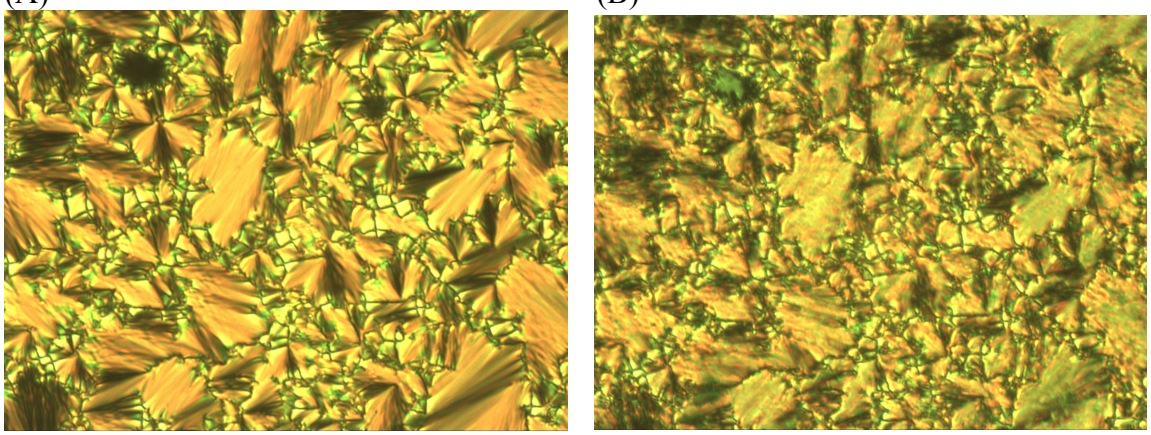

Figure 5-13. PLM textures of 9,2-OBTTT produced on cooling from an isotropic melt; (A) SmA texture at 205°C; (B) beginning of second-order SmA-SmC transition at 195°C, broken fan texture.

(A) (B)

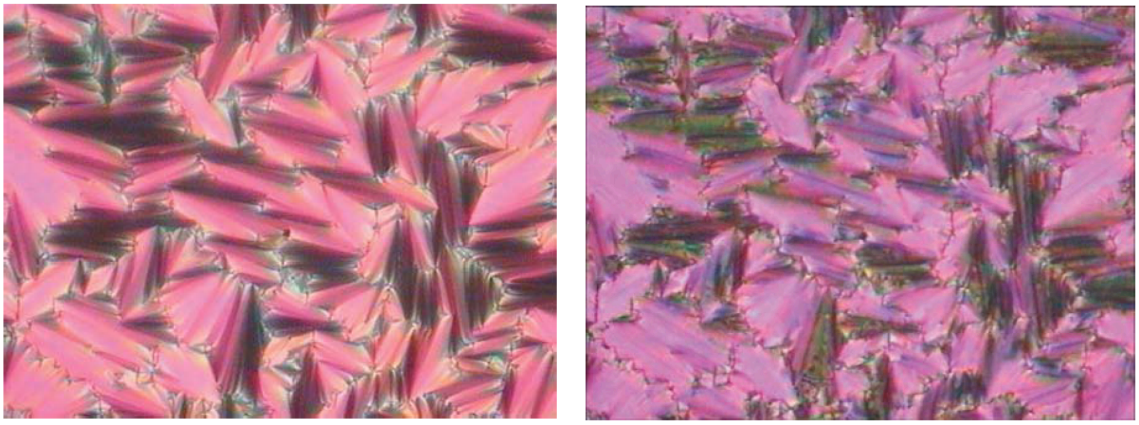

Figure 5-14. (A) literature report of SmA fan texture; (B) literature report of SmC broken fan texture. [Source: Textures of Liquid Crystals, Ingo Dierking, 2003, Wiley-Verlag]

Most of the mesogens in the n,2-OBTTT series displayed the second-order SmA-SmC transition proposed above. An examination of the optical textures of the series revealed that only 1,2-OBTTT and 2,2-OBTTT do not indicate the appearance of some

degree of tilt upon cooling from the SmA phase. The tilt of the director is potentially driven by alkyl chain length since it is absent only in the short-chain mesogens.

Smectic E

In the short-chain mesogens (# of carbons = 1-3) and the long-chain mesogens (# of carbons = 10-13), there is DSC evidence (figure 5-5) of a lower-temperature liquid crystal phase below the SmA (for short-chains) or the SmC (for long-chains). DSC evidence for this lower-temperature phase is absent for the medium-chain compounds (# of carbons = 4-9). The texture of the lower-temperature phase is different for long-chain compounds than for short-chain compounds, presumably because the long-chain compounds are tilted relative to the layer normal and the short-chain compounds are not. As such, the two phases will be assigned separately.

The texture of the phase that appears directly beneath the SmA phase of 2,2-OBTTT upon cooling retains the structural features of the SmA phase above it (figure 5-13). The new texture contains striated focal conics and fans, with equally spaced, concentric arcs across the fans (figure 5-13B). The arcs are not transition bars, as they remain long after the transition.

(A) (B)

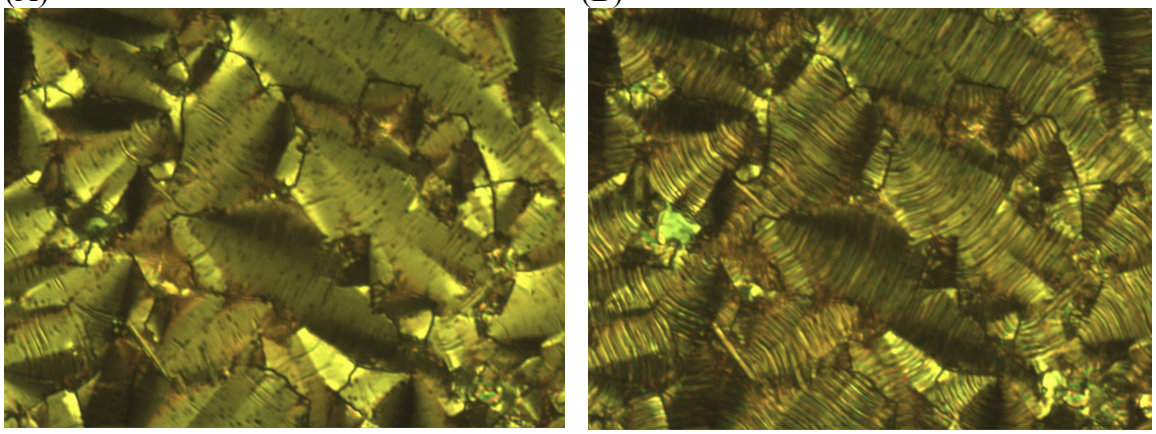

Figure 5-15. PLM textures of 2,2-OBTTT produced on cooling from an isotropic melt; (A) SmA texture at 205°C; (B) beginning of second-order SmA-SmC transition at 195°C, broken fan texture.

The textures in figure 5-15 are literature reports depicting a SmA-SmE transition. The fan texture of the SmA phase is apparent in figure 5-15A and the striated fan with equally spaced concentric arcs seen in figure 5-15B is typical of the SmE phase. The textures in figure 5-14 are consistent with the literature reports of the SmA-SmE transition seen in figure 5-15. The evidence is consistent with a phase assignment of SmE for the short-chain mesogens: 1,2-OBTTT and 2,2-OBTTT.

(A) (B)

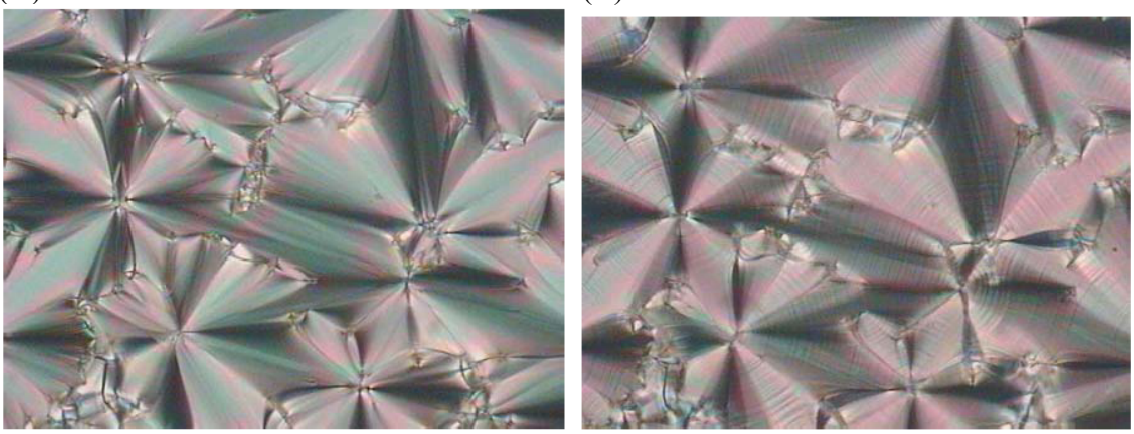

Figure 5-16. (A) literature report of SmA fan texture; (B) literature report of SmC broken fan texture. [Source: Textures of Liquid Crystals, Ingo Dierking, 2003, Wiley-Verlag]

Smectic G

There is DSC evidence of a lower-temperature liquid crystal phase in both the short-chain mesogens and the long-chain mesogens and the textures indicate that these are two distinct phases. The textures in figure 5-16, although similar to the textures exhibited by the short-chain mesogens, were distinctly different. First, the edges of the homeotropic domains were spherical when the sample was in the SmA phase; however, when the sample cooled into the lower-temperature phase, the edges of the homeotropic domains changed into "snowflake" shapes (figure 5-16A). The formation of snowflake domains is indicative of the SmG phase (figure 5-17A). Second, although the broken fan texture of the SmC texture yielded to the lower-temperature phase while retaining structural features of the phase above it, similar to the transition seen in the short-chain mesogens (figure 5-14), the striated bands seem to make interconnected paths between what were once distinct focal conic structures, blurring the boundaries (figure 5-16B). This behavior was not seen in the short-chain mesogens and is similar to what is seen in the SmG tilted hexatic crystal phase (figure 5-17B).

(A) (B)

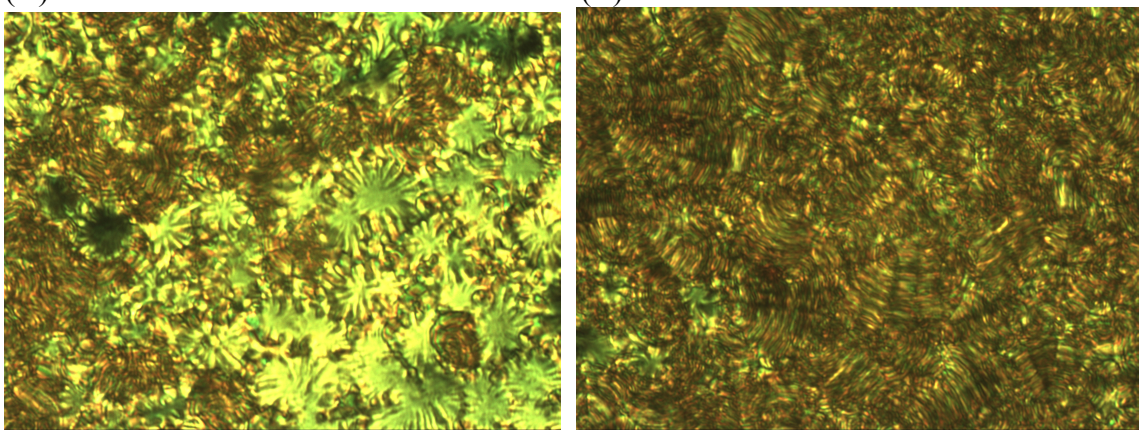

Figure 5-17. PLM textures of 12,2-OBTTT produced on cooling from an isotropic melt at a rate of 10°C/min; (A) SmG "snowflake" texture at 185°C; (B) striated band structure of SmG texture at 185°C.

(A) (B)

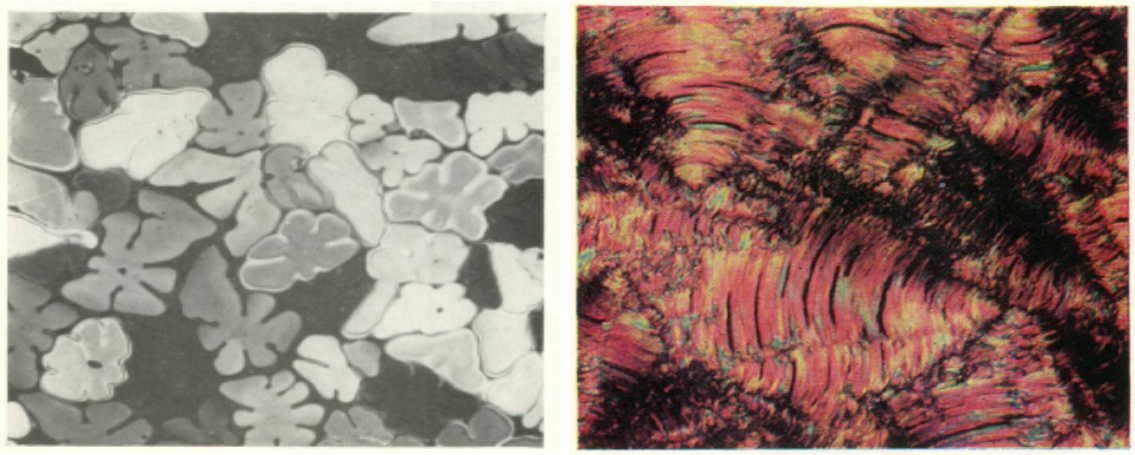

Figure 5-18. (A) Literature report of SmG "snowflake" texture; (B) literature report of SmG striated band texture. [Source: Textures of Liquid Crystals, Ingo Dierking, 2003, Wiley-Verlag]

The assignment of SmG to the long-chain mesogens is consistent with the observation that the long-chain mesogens seem to exhibit a second-order SmA-SmC transition. It has been noted that tilted smectic phases typically yield to lower-temperature tilted phases and that non-tilted smectic phases typically yield to non-tilted smectics. Definitive phase assignment of the crystal smectic phases is not possible by DSC and PLM alone. X-ray data need to be collected to gather more information about the three dimensional structure of these lower-temperature phases.

5.3.2 Materials that Exhibit Paramorphic Smectic Transitions

Paramorphic phase transitions are those that occur while retaining the structural features and defects of the preceding phase. Paramorphic phase transitions can occur in either direction, while heating or cooling. Figure 5-18 displays two paramorphic phase transitions occurring in 2,2-OBTTT: 1) from SmA-SmE (figure 5-18B and C) and 2)

from SmE-crystal (figure 5-18C and D). This designation is consistent with the literature example of paramorphic phase transitions described at the beginning of this chapter (figure 5-1).

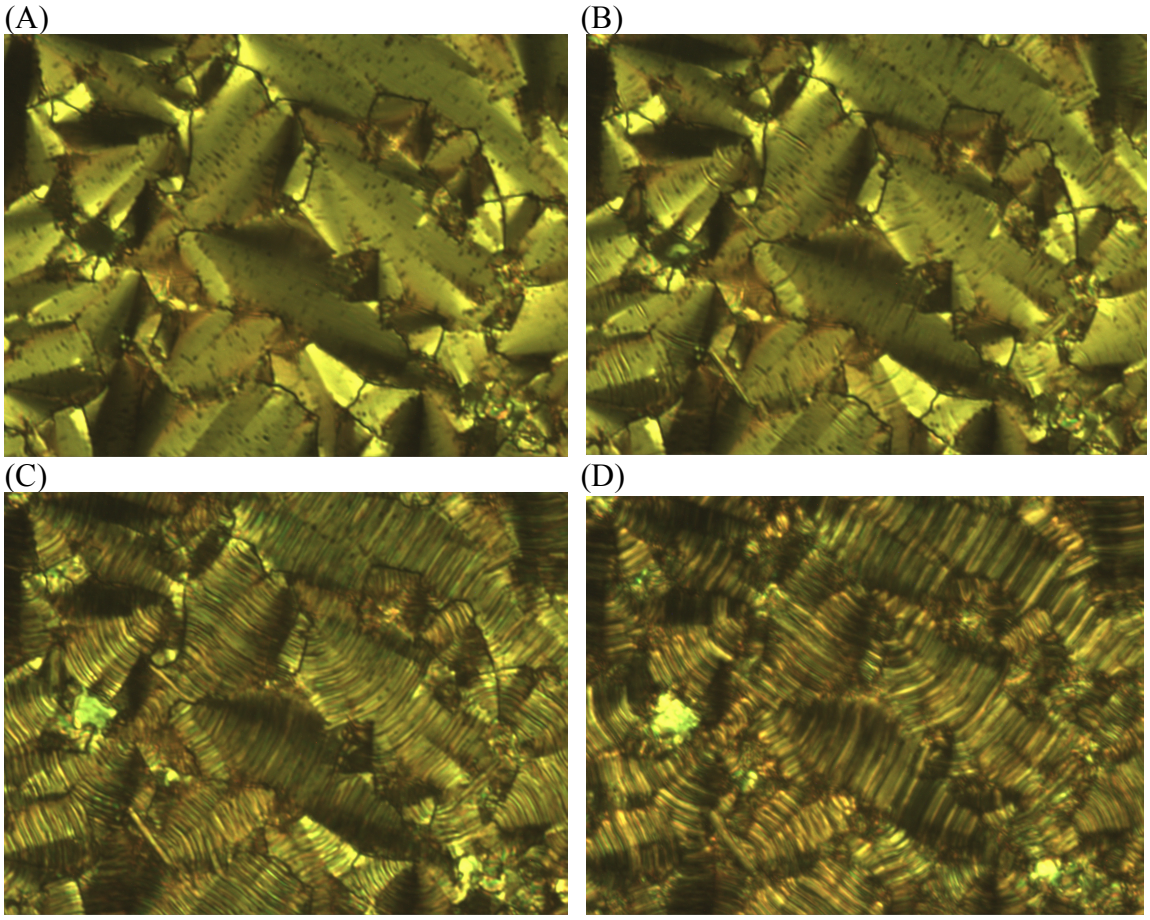

Figure 5-19. PLM textures of 2,2-OBTTT produced on cooling from an isotropic melt at 10°C/min; (A) SmA texture at 200°C; (B) SmA - SmE transition at 185°C; (C) SmE texture at 145°C, paramorphic with SmA; (D) crystal texture at 70°C, paramorphic with SmE.

Figure 5-19 displays paramorphic phase transitions in both short-chain (1,2-OBTTT) and long-chain (10,2-OBTTT) mesogens from a more fluid smectic phase (SmA or SmC) to a highly ordered smectic phase (SmE or SmG). The paramorphic transition from SmA-SmE is ideal for a strategy involving the alignment of a material while in the

SmA phase and the retention of that structure throughout crystallization. In both images, the transition occurs while retaining the boundaries of the homeotropic and planar domains, as well as the general structural features of the smectic focal conic and fan textures. Although the medium-chain mesogens don't seem to display a low-temperature, highly ordered smectic phase (like SmE or SmG), they do exhibit what are taken to be paramorphic SmC-crystal transitions. The assignment of paramorphic crystal transitions in the medium-chain mesogens is made based on the transition pictured in figure 5-20. This type of transition is representative of all of the medium-chain mesogens.

(A) (B)

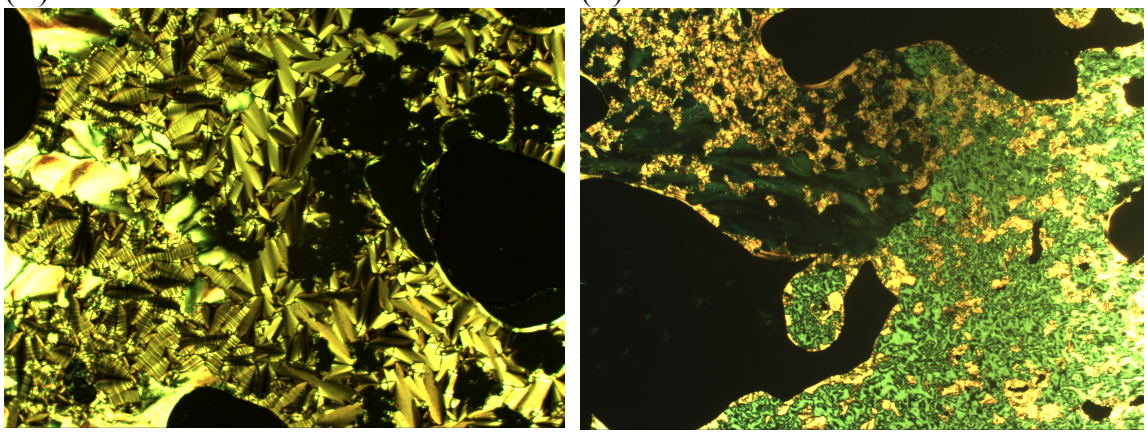

Figure 5-20. Paramorphic transitions produced on cooling from an isotropic melt at 10°C/min; (A) SmA-SmE transition of 1,2-OBTTT at 174°C; (B) SmC-SmG transition of 10,2-OBTTT at 153°C.

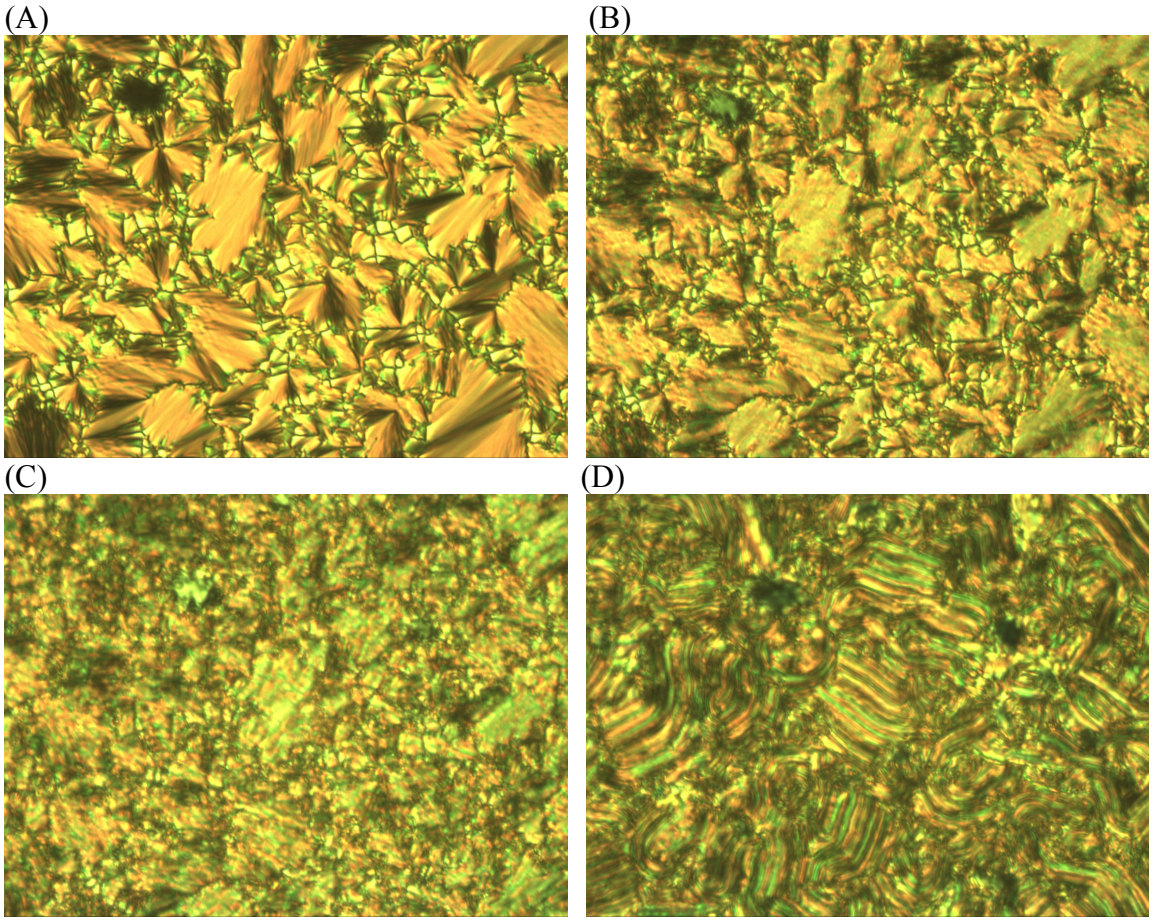

Figure 5-21. PLM textures of 5,2-OBTTT produced on cooling from an isotropic melt at 10°C/min; (A) SmA texture at 215°C, fan texture; (B) SmA-SmC transition at 195°C, broken fan texture; (C) SmC texture at 185°C, paramorphic with SmA; (D) SmC-crystal transition at 183°C, paramorphic with SmC.

In fact, the only member of the series that does not seem to exhibit paramorphic phase transitions is 4,2-OBTTT. Figure 5-21 displays the textures exhibited during the SmC-crystal phase transition in 4,2-OBTTT. Clearly, the incoming crystal texture does not retain any of the structural features of the smectic phase preceding it. The formation of crystal lancets disrupts the focal conic texture. Paramorphosis does not occur if the crystal structure is significantly different than the structure of the mesophases.(LC semiconductors book) As such, 4,2-OBTTT does not seem particularly well suited to form highly ordered thin films using the presently employed strategy.

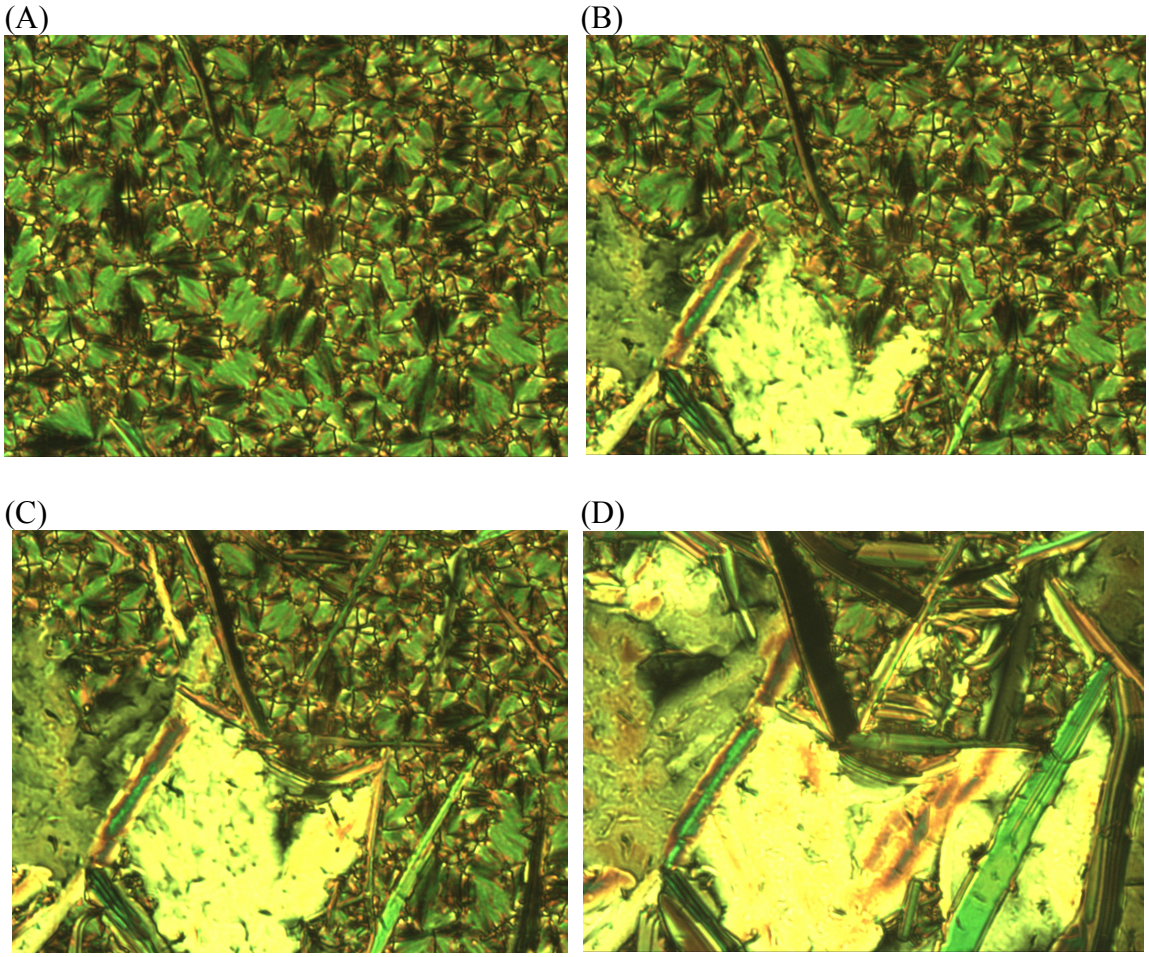

Figure 5-22. Non-paramorphic transitions exhibited by 4,2-OBTTT produced on cooling from an isotropic melt at 10°C/min; (A) SmA texture at 180°C; (B) SmA - crystal transition at 179°C; (C) SmA - crystal transition at 178°C; (D) crystal texture at 80°C.

5.4.3 X-Ray Diffraction

X-ray experiments were temperature-controlled with an Instec STC200 hotstage, and data were collected using a point detector mounted on a Huber four-circle goniometer and utilizing synchrotron radiation at beamline X10A of the National Synchrotron Light Source (NSLS), Brookhaven National Laboratory. The data were collected by Dr. Yongqiang Shen of the Liquid Crystal Materials Research Center at the University of Colorado at Boulder. Due to time constraints, it was not possible to obtain

x-ray data for all members of the series across the entire temperature range of mesogenicity.

4,2-OBTTT

Figure 5-22 is a plot of layer thickness (measured by XRD) as a function of temperature for 4,2-OBTTT. This is the only member of the series that does not exhibit paramorphic phase transitions. The plot shows that the thickness of the smectic layers (d = 24.92 Å) is slightly less than the molecular length of the mesogen in the lowest energy conformation (d = 25.03 Å), as determined using a MMFF calculation. This suggests that the mesogens in the smectic layers are un-tilted and fully stretched out, indicating a SmA phase. However, the texture of 4,2-OBTTT clearly shows the presence of a Schlieren texture in co-existence with a planar region of focal conic texture. A Schlieren texture in homeotropically aligned SmA is not possible, presenting the possibility that this is some orthogonal phase besides SmA and SmE. The only other possibilities are SmB_{hex} and $SmB_{crys.}$ The mesogen crystallizes around 180°C, as seen in the PLM data of figure 5-21 and the DSC data of figure 5-3. At 180°C, the x-ray signal for 4,2-OBTTT exhibits three dimensional order, indicating crystallization (figure 5-23). It is unclear why 4,2-OBTTT would deviate from the series. The ether tail (d = 7.005 Å) of 4,2-OBTTT is slightly longer than the ester tail (d = 5.650 Å). This behavior is a topic for future investigation.

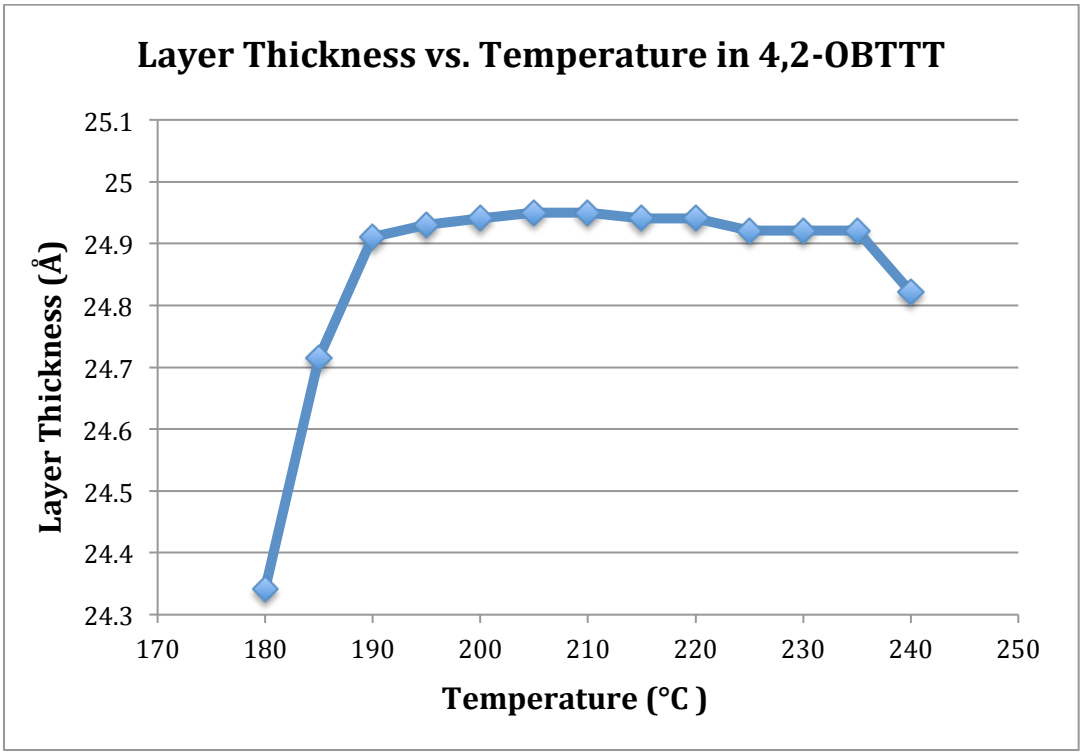

Figure 5-23. XRD generated plot of smectic layer thickness (Å) of 4,2-OBTTT as a function of temperature (°C). Molecular length = 25.03 Å (MMFF calculation).

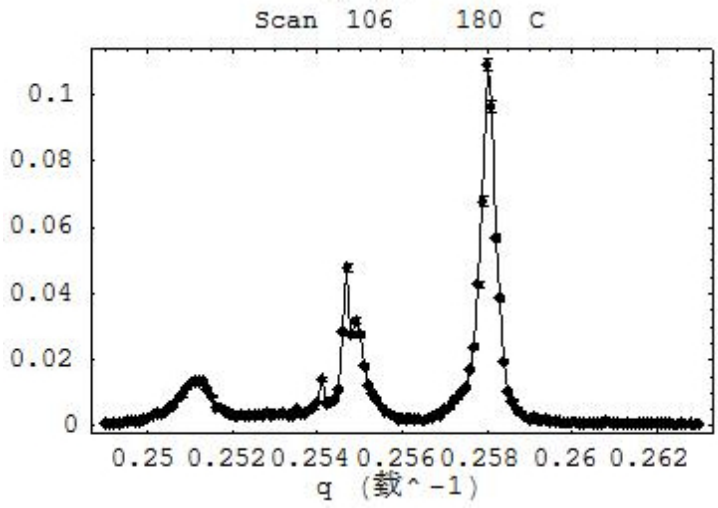

Figure 5-24. Diffractogram of 4,2-OBTTT showing scattering from the three-dimensionally ordered crystal structure.

Medium Chain Mesogens

The medium chain mesogens in the n,2-OBTTT series exhibited similar behavior. The layer spacing of the phase observed immediately upon cooling from an isotropic melt is nearly the same as the molecular length for each of the compounds reported (figure 5-24). This is consistent with an orthogonal phase and since the PLM data already indicated a SmA phase, this seems to be a reasonable phase assignment. It is also apparent that the layer spacing decreases with decreasing temperature. Again, the PLM data indicated a second-order SmA-SmC transition for the medium chain mesogens and the XRD data support this hypothesis.

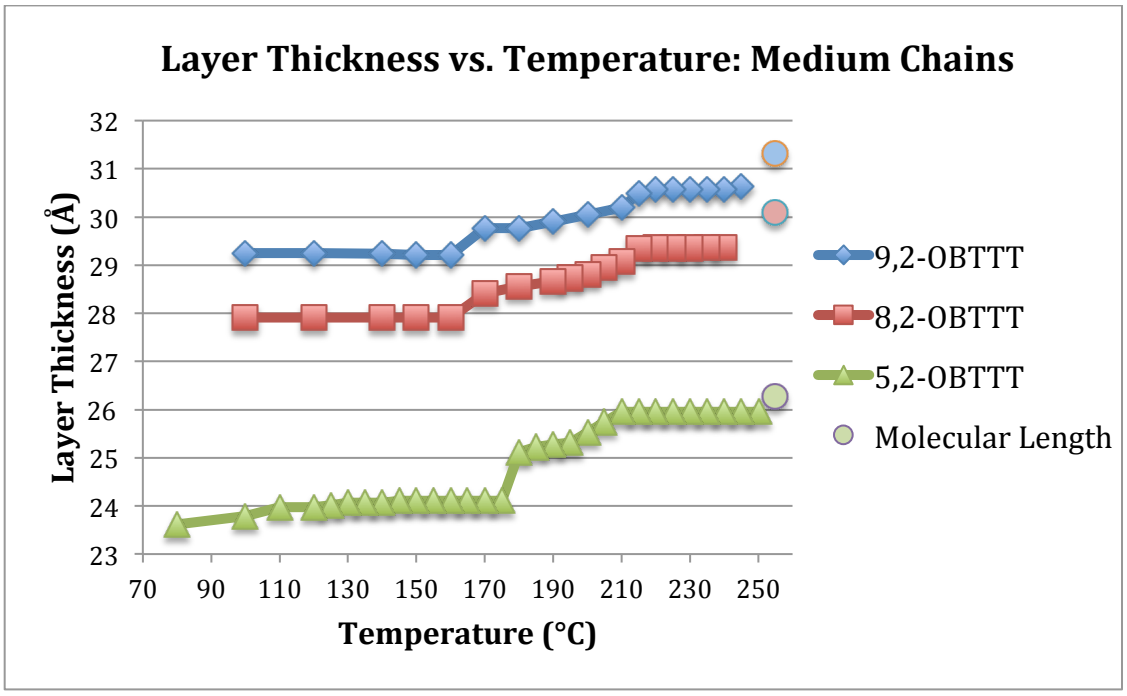

Figure 5-25. Layer thickness of medium chain members of the n,2-OBTTT series as a function of temperature. Molecular length (MMFF) is also reported.

Long Chain Mesogens

The layer spacing of the phase directly beneath the isotropic of both 12,2-OBTTT and 13,2-OBTTT is significantly shorter than the molecular length, as determined by MMFF calculation (figure 5-25). There are at least two possible explanations for this behavior: 1) the molecules are tilted relative to the layer normal or 2) the alkoxy chains are somewhat interdigitated. If the molecules are tilted relative to the layer normal, then this should be evident in the PLM texture of the material: tilted phases should not have dark homeotropically aligned domains. Upon re-visiting the PLM data, it was discovered that, indeed, the phase directly beneath the isotropic does not contain dark homeotropic domains (figure 5-26). In light of this new discovery, the mesophase observed upon cooling from an isotropic melt in the long chain mesogens was re-designated as one of the tilted, fluid-smectic phases, either SmI or SmF. Another interesting feature of this data is the increase in layer spacing as the temperature decreases below 150°C. Typically, a tilted mesophase will stay tilted as the temperature is decreased, though it is not unheard of for a tilted phase to stand back up upon cooling.

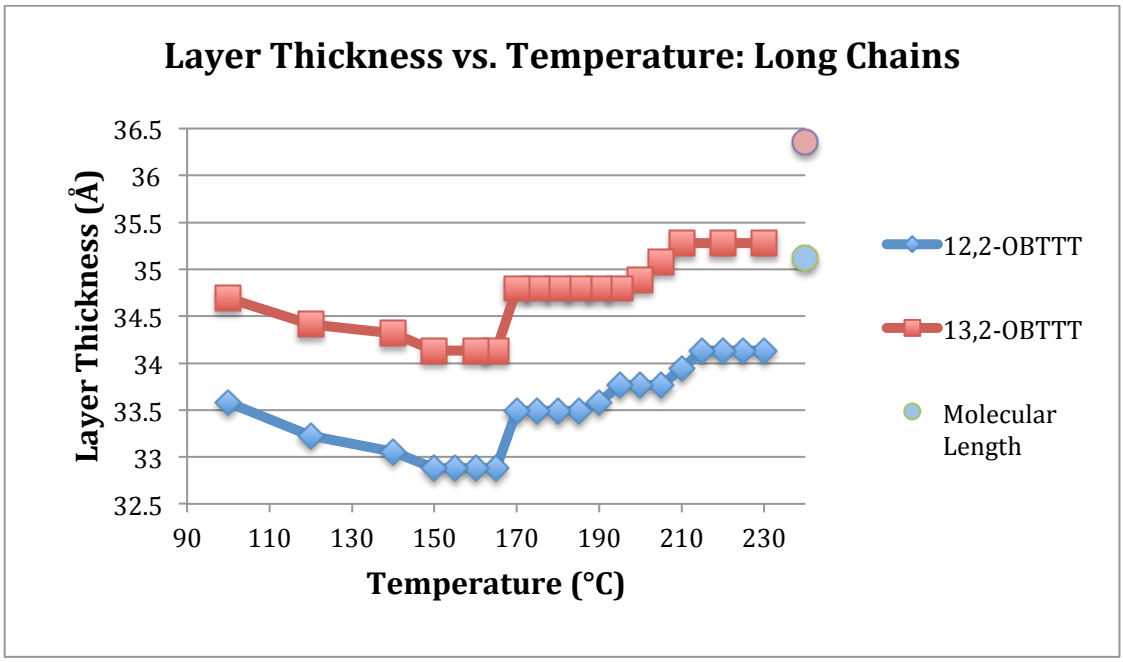

Figure 5-26. Layer thickness of long chain members of the n,2-OBTTT series as a function of temperature. Molecular length (MMFF) is also reported.

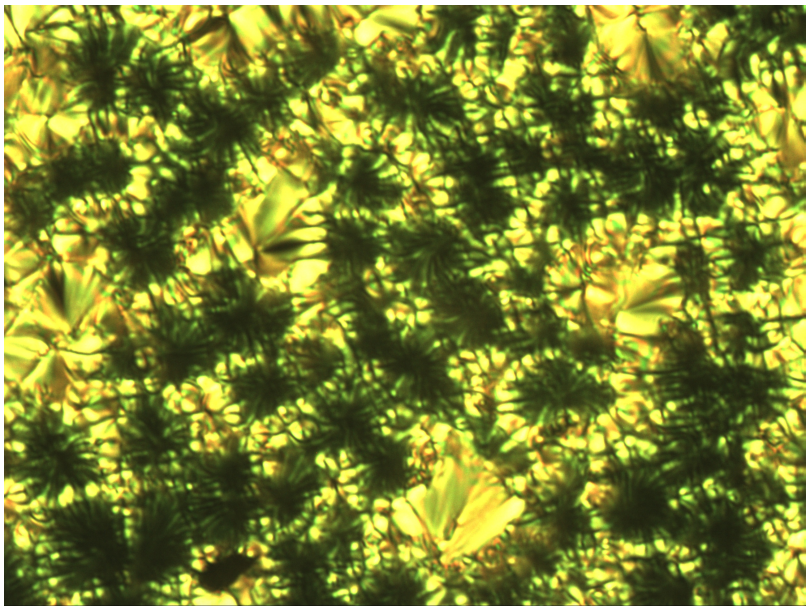

Figure 5-27. PLM texture of 12,2-OBTTT produced at 225°C upon cooling from an isotropic melt at a rate of 10°C/min. The lack of dark homeotropic domains indicates a tilted, fluid mesophase, SmI perhaps.

5.5 Conclusions

The DSC, PLM, and XRD data presented in this chapter have allowed the tentative phase assignment of the n,2-OBTTT series (table 5-1). Without more extensive x-ray studies, definitive phase assignments cannot be made. There is certainly a significant effect of mesogen tail length on transition temperature and formation of mesophases. The short chain compounds are untilted; this is consistent with the Boulder Model for mesogen tilt. This model proposes that the cores tilt to maximize enthalpic interactions among the aromatic rings while giving more space to the melted alkyl tails. This might explain why these short chain mesogens didn't tilt. The medium chain compounds did not seem to exhibit any of the highly ordered, crystal smectic phases. This could have something to do with chain asymmetry: the medium chain compounds have two chains of similar length. This hypothesis is supported by the formation of crystal smectic phases in the long chain compounds; as one chain increases in length as the other stays constant, they become more asymmetric. Perhaps some threshold is reached starting with compound 10,2-OBTTT, since it exhibits an ordered, crystal smectic phase and 9,2-OBTTT does not. This is a topic for future investigation.

Ultimately, at least some of the mesogens of the n,2-OBTTT series exhibited low-temperature, crystal-smectic phases. As such, the approach of designing a molecule to exhibit a certain phase based on the structure of other mesogens that also exhibit that phase seems to be successful. Further, most of the mesogens exhibited paramorphic phase transitions. Perhaps more importantly, one mesogen did not; this suggests that the crystal structure of 4,2-OBTTT is significantly different than not only the structures of its own mesophases, but also the structures of the crystals for other members of the series. It

would be useful to know what structural features affect paramorphic phase transitions. A potential strategy for lowering transition temperatures was discovered: substituting the alkoxy linkage for a thioether linkage. This strategy potentially retains the liquid crystalline behavior of the series while lowering transition temperatures by about 20°C

Table 5-1. Phase Assignments and Paramorphic Behavior of the n,2-OBTTT Series.

Compound	W#	Phase Transitions Upon Cooling	Paramorphic
1,2-OBTTT	W785	Iso → SmA → SmE → crystal	Yes
2,2-OBTTT	W786	Iso → SmA → SmE → crystal	Yes
3,2-OBTTT	W787	Iso → SmA → SmC → SmG → crystal	Yes
4,2-OBTTT	W759	Iso → SmA → SmB? → crystal	No
5,2-OBTTT	W760	Iso → SmA → SmC → crystal	Yes
6,2-OBTTT	W761	Iso → SmA → SmC → crystal	Yes
7,2-OBTTT	W762	Iso → SmA → SmC → crystal	Yes
8,2-OBTTT	W763	Iso → SmA → SmC → crystal	Yes
8,2-SBTTT	W768	Iso → SmA → SmC → crystal	Yes
(R)8,2-OBTTT	W769	Iso → SmA* → SmC* → crystal	Yes
9,2-OBTTT	W756	Iso → SmA → SmC → crystal	Yes
10,2-OBTTT	W764	Iso → SmA → SmC → SmG → crystal	Yes
11,2-OBTTT	W765	Iso → SmA → SmC → SmG → crystal	Yes
12,2-OBTTT	W766	Iso → SmA → SmC → SmG → crystal	Yes
13,2-OBTTT	W767	Iso → SmA → SmC → SmG → crystal	Yes

Chapter VI: Solid-State Characterization of n,2-OBTTT Series

6.1 Introduction: Short Contacts and Monodomain Thin Films

As charges hop across molecules in a material, charge mobility is significantly affected by even small molecular displacements.[74] The nature of molecular packing within the crystal phase of organic semiconductors with very similar aromatic cores can affect charge mobility values by more than 5 orders of magnitude.[16] Typically, molecules with rigid aromatic cores crystallize in a herringbone structure (figure 6-1a); the herringbone structure offers little or no intermolecular π overlap. A better arrangement would be a cofacial π-stack (figure 6-1b).[74,75] Even in cofacial π-stacks, the charge mobility is greatly affected by intermolecular distance. Figure 6-2 is a plot of charge mobility as a function of the distance between π systems.[6,75] The typical intermolecular distance between π-stacks in organic molecules that exhibit this cofacial arrangement is between 3.5 - 4.0 Å. As can be seen from the plot, charge mobility is affected significantly even at these relatively short distances.

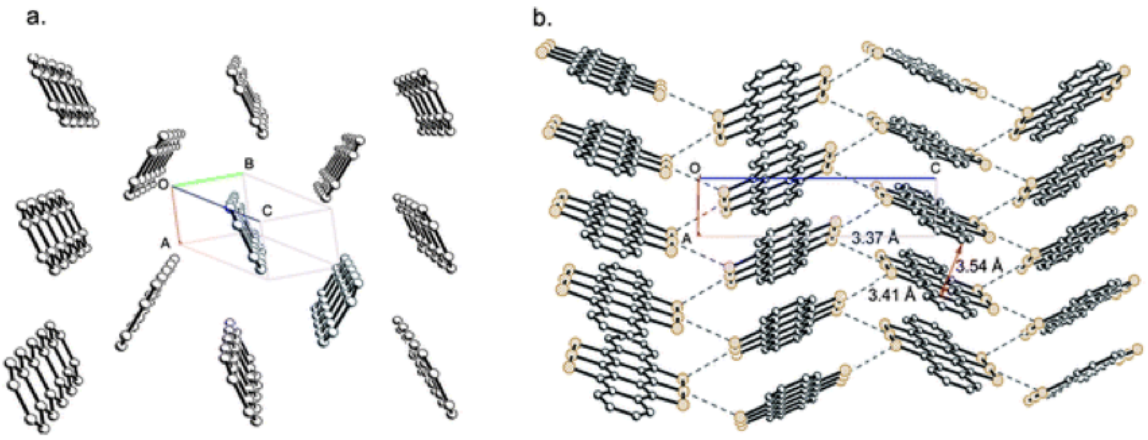

Figure 6-1. (a) Herring bone structure of pentacene; (b) cofacial π-stack structure of hexathiapentacene, π-stack distance = 3.54 Å. [Source: J. Mater. Chem.,2011, **21**, 1329-1337]

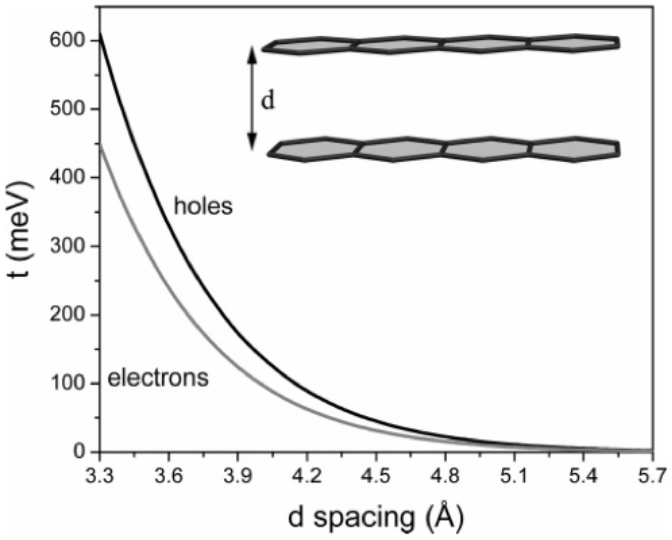

Figure 6-2. Charge carrier mobility as a function of the intermolecular distance in cofacial π-stacks. [Source: Chemical Reviews, 2007, Vol. 107, No. 4, 951]

It is incredibly difficult to predict a crystal structure based on a molecular structure. Subtle effects of conformation can have significant effects on crystal structure. As such, it is difficult to predict the effect of varying alkoxy chain length on otherwise identical molecules. Unsubstituted oligothiophenes crystallize in a herringbone structure with very little π-overlap, similar to unsubstituted oligoacenes.[76] However, the introduction of alkyl side chains causes a lamellar structure, where the main chains are forced into a more cofacial arrangement.[6] Further, a series of compounds with the same aromatic backbone, but different length alkyl chains showed an increase in charge mobility as a function of increasing alkyl chain length.[78,80] It is reasonable, then, to expect that the introduction of alkyl side chains onto a rigid aromatic core might cause a cofacial crystal arrangement. In the present work, the crystal structures of the n,2-OBTTT series are examined to determine the effect of alkoxy chain length on the crystal structure and intermolecular π-distance.

In addition to a favorable intermolecular distance and cofacial arrangement in the

crystal structure, charge mobility values are improved upon limiting the number of grain boundaries in a thin film.[18,19] Controlling the growth a crystal is very difficult and nucleation is a kinetic process that often occurs simultaneously in several regions of a thin film. Grain boundaries and other structural defects trap charge carriers and limit device efficiency.[77,79] It is possible to grow a perfect, defect-free molecular crystal[20], but this is not a trivial process. Crystal grain boundaries can also be avoided by preparing a monodomain crystalline sample by utilizing liquid crystal mesophases.[68,69] Monodomain thin films have achieved charge carrier mobilities one order of magnitude higher than multidomain thin films of the same material.[78] Solution deposition of a mesogen onto a substrate containing an alignment layer, like polyimide, and subsequent annealing in the fluid-smectic phases, like SmA or SmC, can yield highly aligned monodomain thin films.[68-69,80-81] Figure 6-3a displays a spin-cast, multidomain thin film, as spun, and figure 6-3b displays a spin-cast, monodomain thin film of the same material obtained by coating the substrate with an alignment layer and annealing the as spun thin film into the SmA phase for realignment.[81]

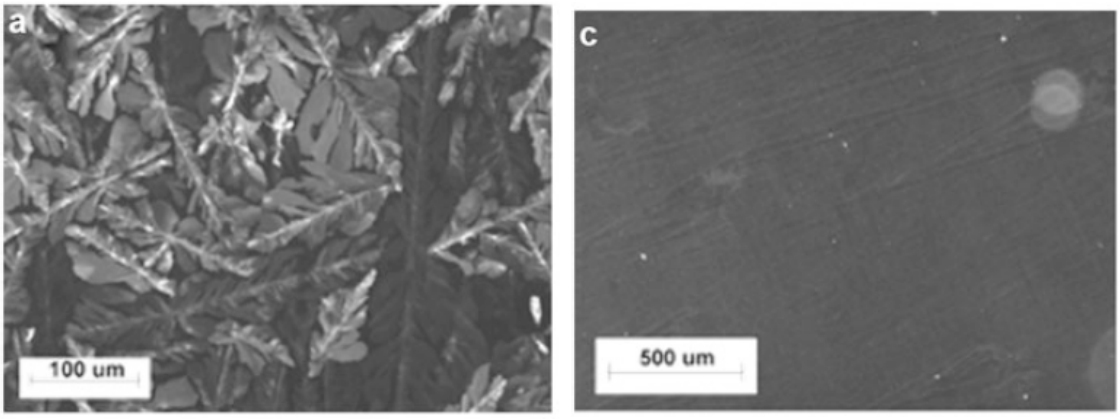

Figure 6-3. (a) Leaf-like, multidomain thin film obtained from spin-casting without annealing; (b) monodomain thin film obtained from spin-casting onto an alignment layer and annealing into the SmA phase. [Source: J. Am. Chem. Soc. 128(7), 2336–2345 (2006)]

6.2 Single Crystal X-Ray Crystallography

All reflection intensities were measured at 110(2) K using a SuperNova diffractometer (equipped with Atlas detector) with Mo *K*α radiation (λ = 0.71073 Å) under the program CrysAlisPro (Version 1.171.36.32 Agilent Technologies, 2013). The program CrysAlisPro (Version 1.171.36.32 Agilent Technologies, 2013) was used to refine the cell dimensions. Data reduction was done using the program CrysAlisPro (Version 1.171.36.32 Agilent Technologies, 2013). The structure was solved with the program SHELXS-2013 (Sheldrick, 2013) and was refined on F^2 with SHELXL-2013 (Sheldrick, 2013). Analytical numeric absorption corrections based on a multifaceted crystal model were applied using CrysAlisPro (Version 1.171.36.32 Agilent Technologies, 2013). The temperature of the data collection was controlled using the system Cryojet (manufactured by Oxford Instruments). The H atoms were placed at calculated positions using the instructions AFIX 23, AFIX 43 or AFIX 137 with isotropic displacement parameters having values 1.2 or 1.5 times *U*eq of the attached C atoms.

The n,2-OBTTT series exhibits *crystallochromy*, changes in the color of the crystals. Even though all members of the series exhibit a fluorescent yellow color and nearly identical absorption spectra when in solution, the color of the solid crystals varies as a function of the molecular packing within the crystal. Figure 6-4 displays the change in color from yellow to orange and back to yellow in the n,2-OBTTT series. These color changes have been attributed to changes in the degree of π-overlap within the aromatic cores.[82] Figure 6-5 displays a series of different intermolecular arrangements of perylene bisimide dyes that yield drastically different colors depending on the degree of π-overlap.

(a)

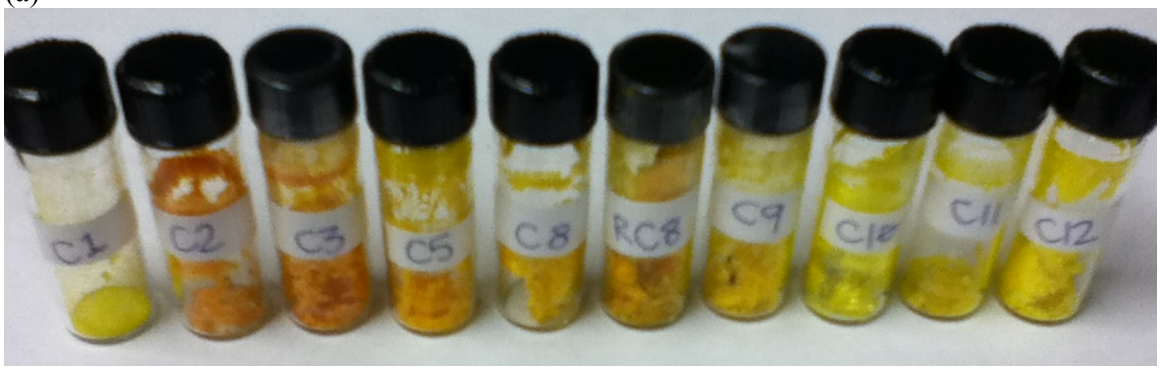

(b) (c)

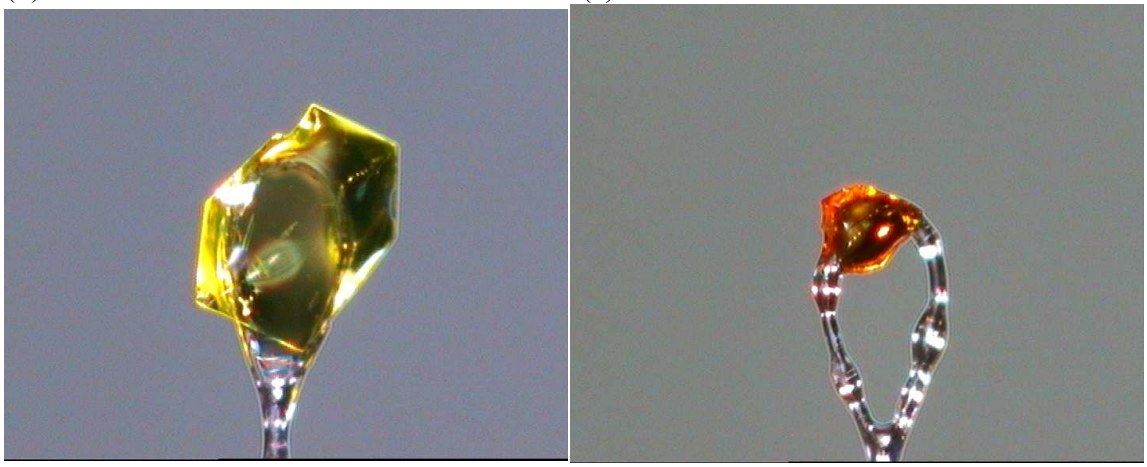

Figure 6-4. (a) Crystallochromy, changes in the color of the crystals, exhibited by the n-2-OBTTT series, indicating a range of intermolecular π-π arrangements; (b) a single crystal of 13,2-OBTTT, yellow plate; (c) a single crystal of 3,2-OBTTT, orange plate.

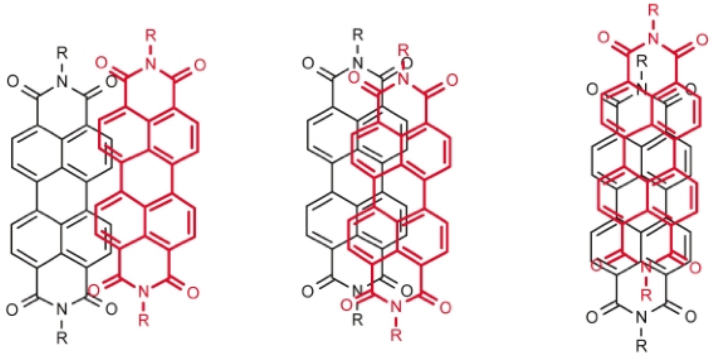

Figure 6-5. A series representing the π-π arrangements of perylene bisimide dyes; the structure on the left (red) displays the largest offset and, thus, the smallest π-π interactions; the structure in the middle (maroon) displays more band broadening as a result of increased π-π coupling; the structure on the right (black) experiences extensive band broadening and π-π coupling.

1,2-OBTTT: Small yellow plates, Monoclinic, P21/c

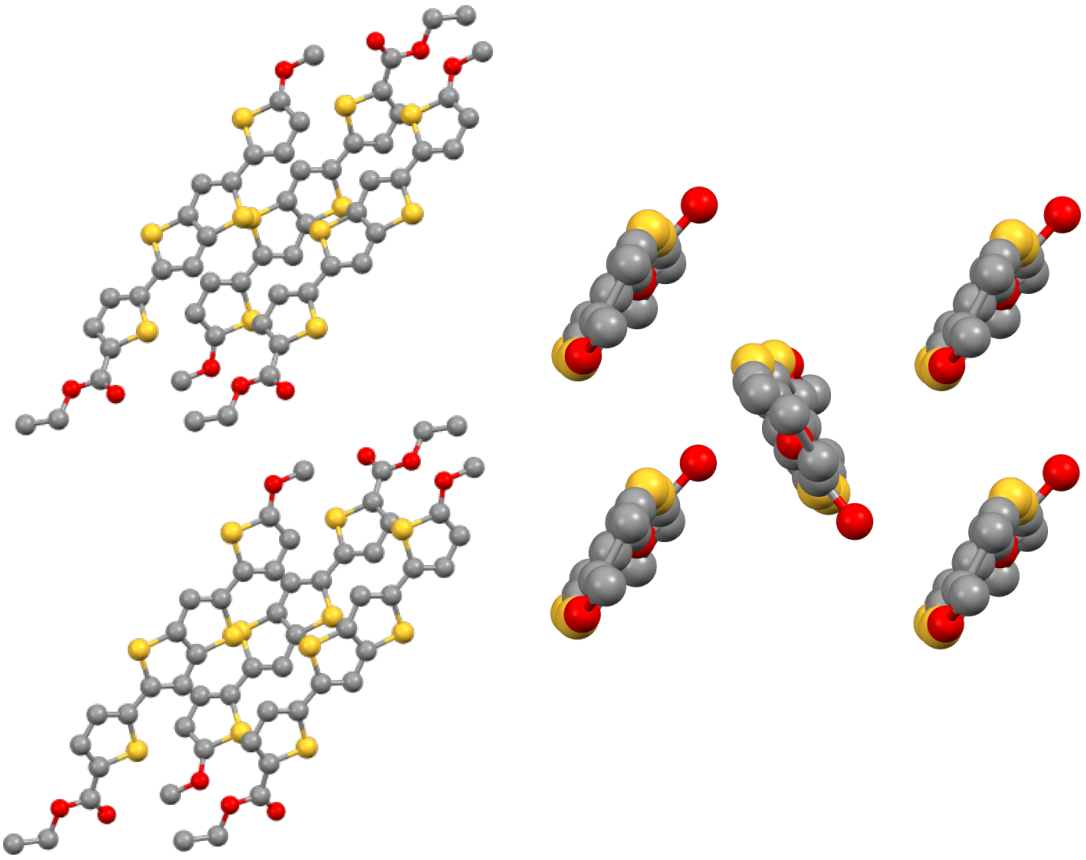

Figure 6-6. Crystal structure of 1,2-OBTTT displaying smectic-like layers of tilted molecules and a herringbone array. The π-π overlap is very minimal; π-π distance = 3.518 Å.

1,2-OBTTT crystallizes in the monoclinic space group with 4 molecules in the unit cell. The molecules display a herringbone arrangement, with edge-to-face interactions. This significantly limits π-overlap, as can been seen in figure 6-6. The distance between the cofacial aromatic rings is 3.518 Å, which is relatively close, but the minimal π-overlap will severely limit charge transport in this material. The crystal structure displays smectic-like layers of tilted molecules; this structure could help explain the paramorphic phase transitions observed in chapter 5. The structure is partly

disordered. The central thieno[3,2-b]thiophene ring and alkoxy-bearing thiophene ring are disordered over two orientations (figure 6-7).

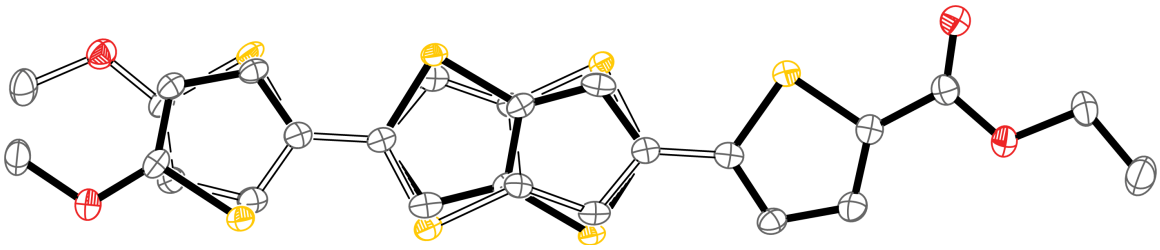

Figure 6-7. The molecular disorder inherent in the crystal structure of 1,2-OBTTT; the central thieno[3,2-b]thiophene and alkoxy-bearing thiophene ring are disordered over two orientations.

3,2-OBTTT: Orange plates, Monoclinic, C2/c

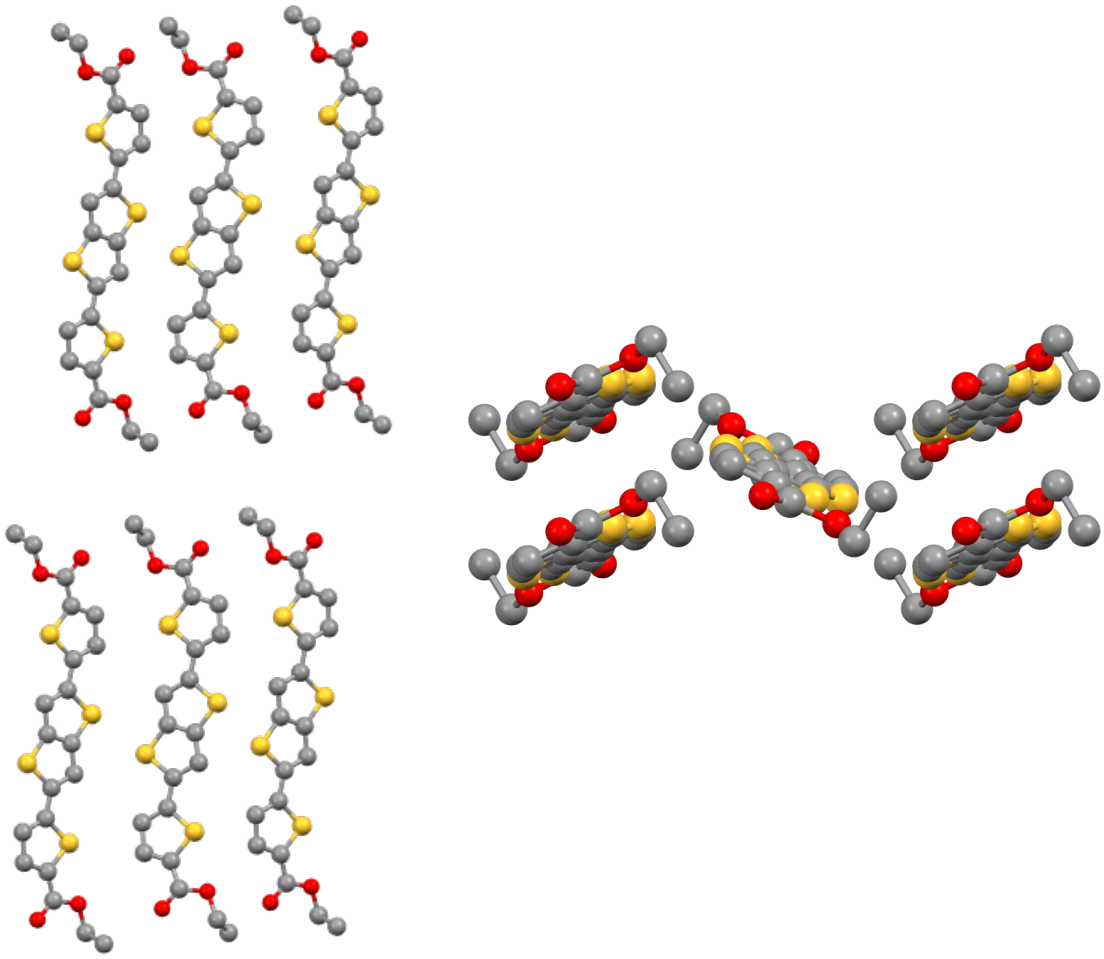

Figure 6-8. Crystal structure of 3,2-OBTTT displaying smectic-like layers of tilted molecules and a cofacial arrangement. The π-π overlap is significant in this orientation; π-π distance = 3.498 Å.

3,2-OBTTT crystallizes in the monoclinic space group. Unlike 1,2-OBTTT, the molecules display a cofacial arrangement, with face-to-face interactions. This significantly increases π-overlap, as can been seen in figure 6-8. The distance between the cofacial aromatic rings is 3.498 Å, which is relatively close and the significant π-overlap will facilitate charge transport in this material. The crystal structure displays smectic-like layers of tilted molecules; this structure could help explain the paramorphic phase transitions observed in chapter 5.

The molecules of 3,2-OBTTT are found at sites of inversion symmetry. The molecules are partially disordered as they do not have inversion symmetry (the fragment including the non-fused and fused thiophene rings are ordered though). To prevent impossible intermolecular short contacts along the **a** direction, both ether and ester groups must be disordered over two orientations (figure 6-9). The occupancy factors of the major components of the disorder were refined freely, and their values refine to 0.314(6) and 0.298(5) (note: the sum of the major/minor occupancy factors for both ether and ester groups must be equal to 0.5 in the asymmetric unit). In the figure below, the molecules are found at sites of inversion, and only one half of the molecule is crystallographically independent. Thus, both ether and ester groups must be disordered, and the occupancy factors of the major components of the disorder must be < 0.5.

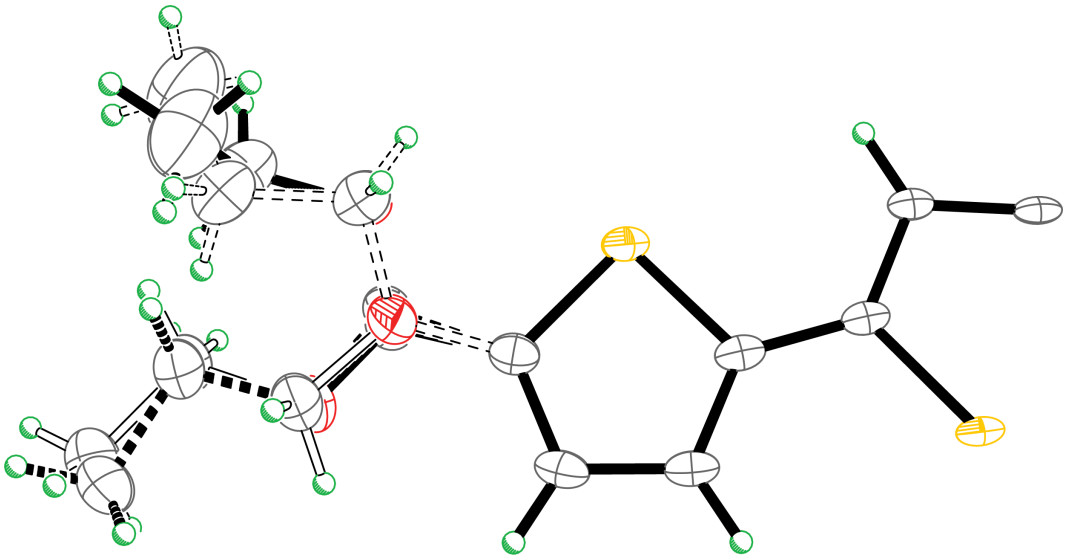

Figure 6-9. The molecular disorder inherent in the crystal structure of 3,2-OBTTT because the molecules are found are sites of inversion symmetry but the molecules don't possess inversion symmetry; both ether and ester groups must be disordered over two orientations.

5,2-OBTTT: Yellow plates, Triclinic, P-1

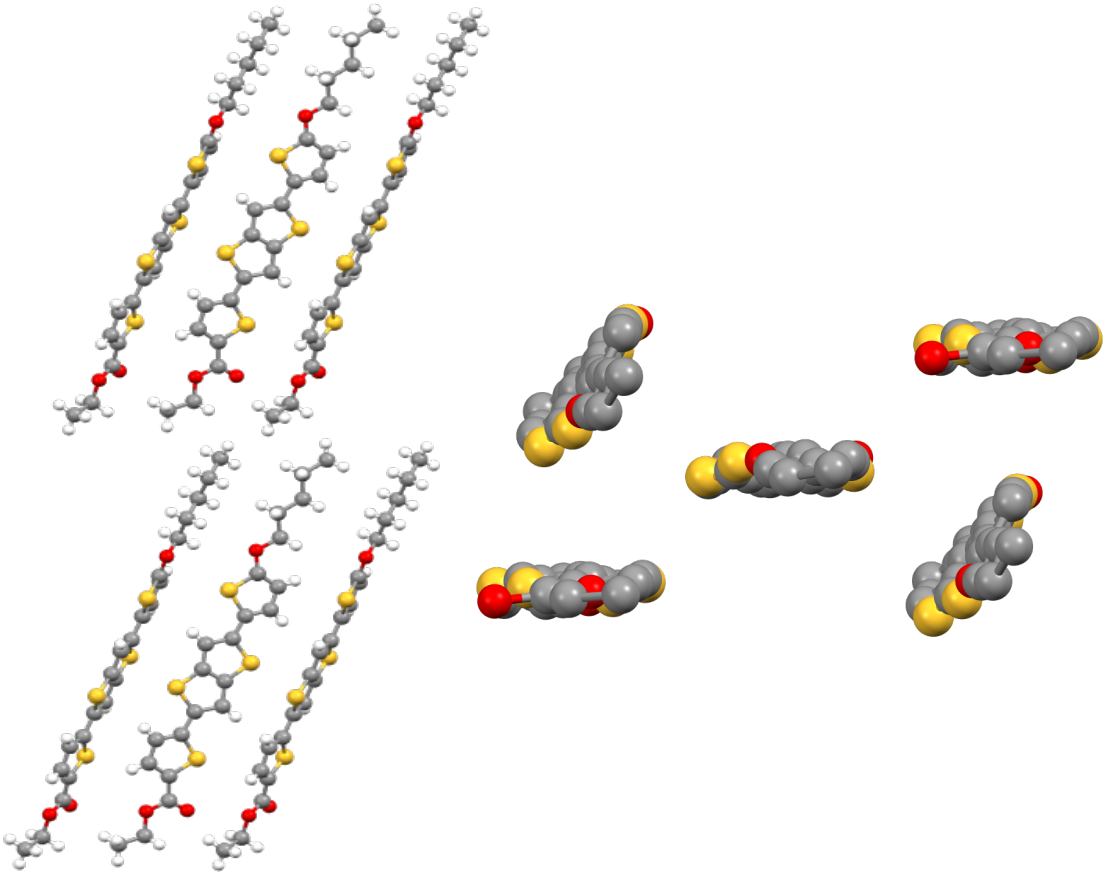

Figure 6-10. Crystal structure of 5,2-OBTTT displaying smectic-like layers of tilted molecules and a herringbone arrangement. The π-π overlap is negligible in this orientation; π-π distance = 3.650 Å.

5,2-OBTTT crystallizes in the triclinic space group with 2 independent molecules in the unit cell. Similar to 1,2-OBTTT, the molecules display a herringbone arrangement, with edge-to-face interactions. This significantly hinders π-overlap, as can been seen in figure 6-10. The distance between the cofacial aromatic rings is 3.650 Å. The crystal structure displays smectic-like layers of tilted molecules; this structure could help explain the paramorphic phase transitions observed in chapter 5. The structure is disordered. Both molecules are found to be wholly disordered (figure 6-11).

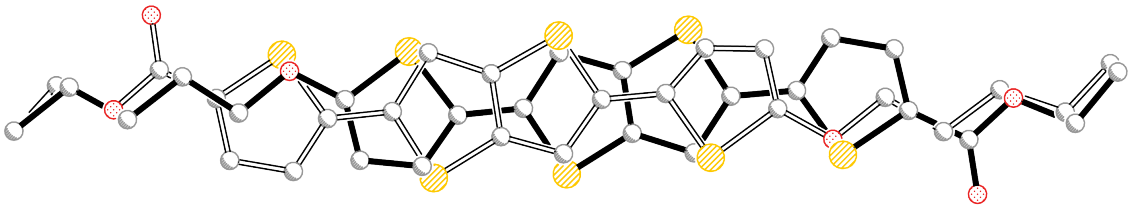

Figure 6-11. The molecular disorder inherent in the crystal structure of 5,2-OBTTT; Both molecules found in the unit cell are completely disordered.

6,2-OBTTT: Yellow plates, Triclinic, P-1

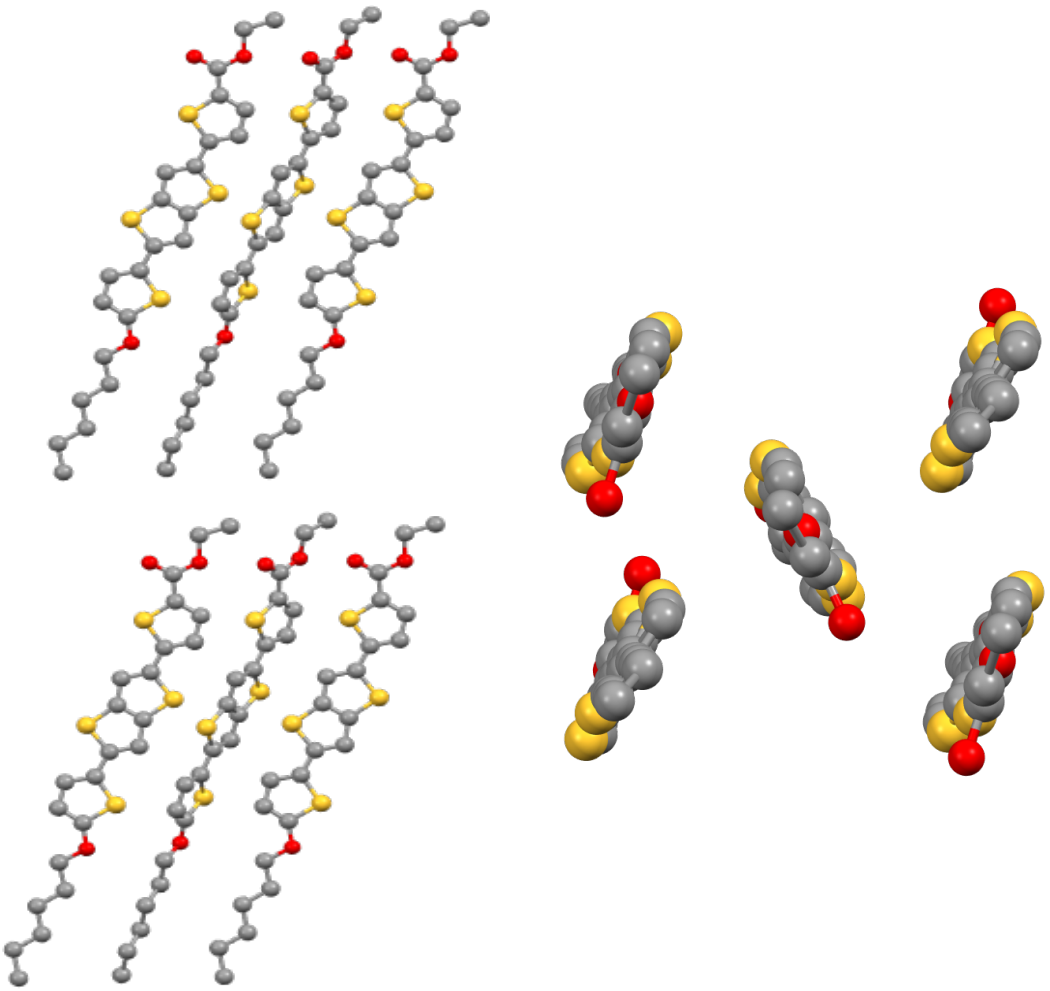

Figure 6-12. Crystal structure of 6,2-OBTTT displaying smectic-like layers of tilted molecules and a herringbone arrangement. The π-π overlap is negligible in this orientation; π-π distance = 3.571 Å.

6,2-OBTTT crystallizes in the triclinic space group with 2 independent molecules in the asymmetric unit cell. Similar to 1,2-OBTTT, the molecules display a herringbone arrangement, with edge-to-face interactions. This significantly hinders π-overlap, as can been seen in figure 6-12. The distance between the cofacial aromatic rings is 3.571 Å. The crystal structure displays smectic-like layers of tilted molecules; this structure could help explain the paramorphic phase transitions observed in chapter 5. In contrast to 5,2-OBTTT, which is almost completely disordered, the structure of 6,2-OBTTT is mostly ordered. The only disorder in the structure is found in the central thieno[3,2-b]thiophene ring, which is disordered over two orientations.

8,2-OBTTT: Small yellow plates, Orthorhombic, Pbca

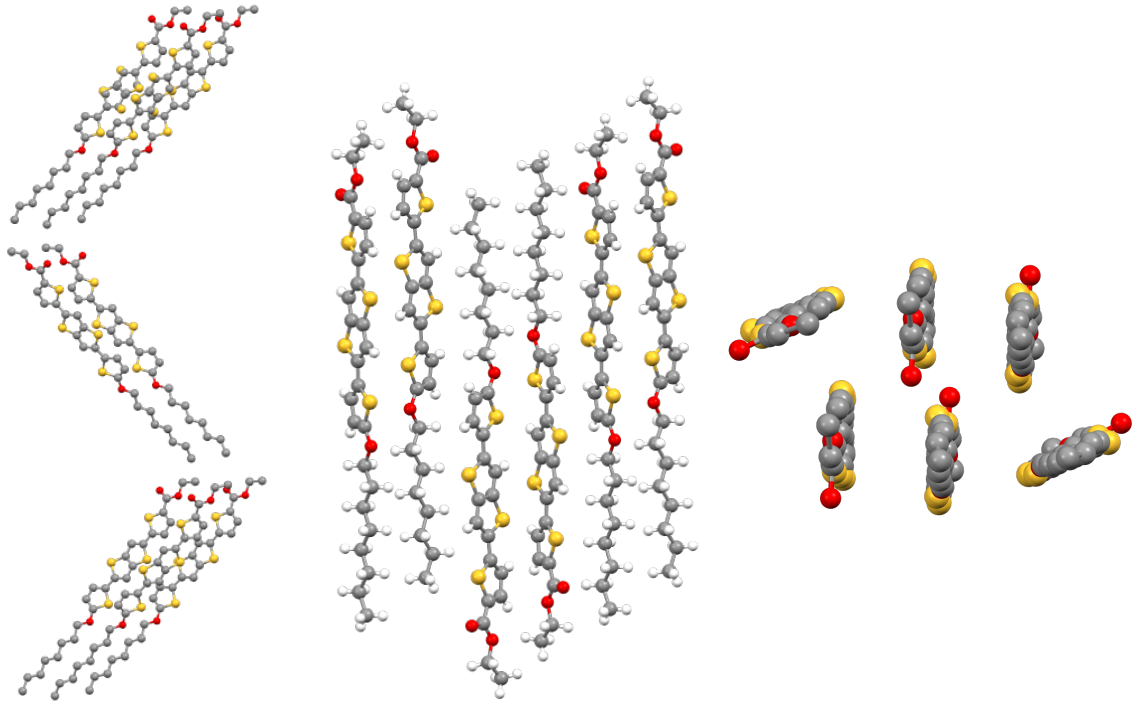

Figure 6-13. Crystal structure of 8,2-OBTTT displaying smectic-like layers of tilted molecules and a herringbone arrangement. The π-π overlap is negligible in this orientation; π-π distance = 3.617 Å.

8,2-OBTTT crystallizes in the orthorhombic space group with 2 independent molecules in the asymmetric unit cell. This compound exhibits significantly different crystal morphology than those members of the series already discussed. The layers are still smectic-like, though the layer interface displays anti-clinic orientation. This should not affect charge carrier mobility since charge transport within these materials in 2D, within the layers, not between. However, molecules within the layer do not form a continuous π-system as they do in the short chain members of the series. This is a function of the increasing asymmetry along the long axis of the molecules caused by the increasing alkoxy chain length. A head-to-tail orientation effectively disrupts the intermolecular π-overlap. The molecules in the short chain mesogens crystallize with a head-to-tail orientation, as well, but because the ester and alkoxy chains are similar in length, there is still significant π-overlap. This molecular arrangement is predicted to severely hinder charge transport. There is essentially zero π-overlap; though the overhead view in figure 6-13 gives the impression that there is a favorable cofacial arrangement, though the perspective in the middle shows the head-to-tail orientation that effectively limits π-overlap. Because the phase transition from SmC - crystal appears to be paramorphic, it raises the question whether the layer interfaces in the liquid crystal phase are syn-clinic or anti-clinic. The crystal structure of 8,2-OBTTT is mostly ordered. The only disorder in the structure is found in the central thieno[3,2-b]thiophene ring, which is disordered over two orientations.

9,2-OBTTT: Yellow Needles, Monoclinic, P21/c

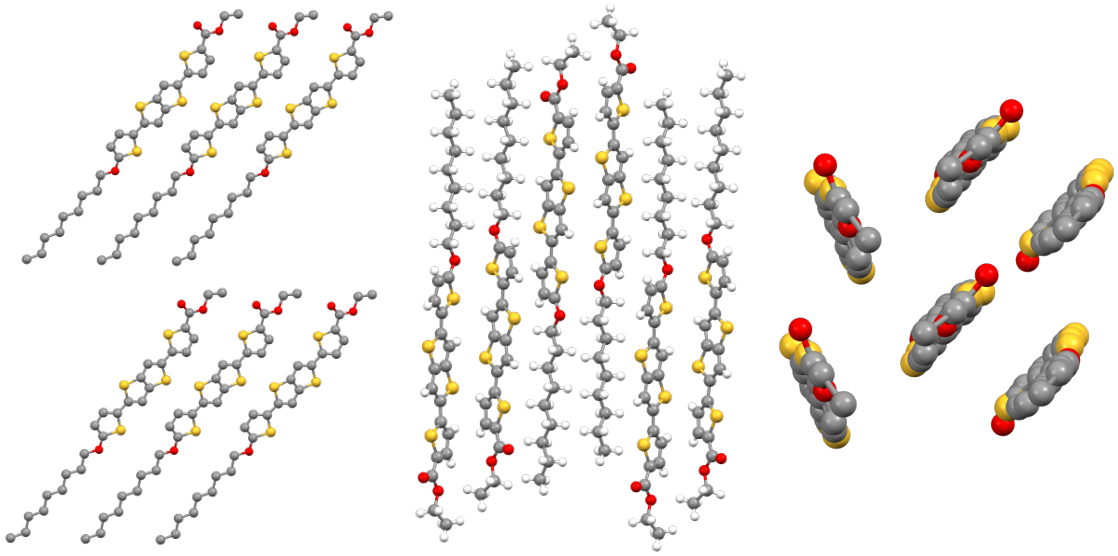

Figure 6-14. Crystal structure of 9,2-OBTTT displaying smectic-like layers of tilted molecules and a herringbone arrangement. The π-π overlap is negligible in this orientation because of the head-to-tail orientation; π-π distance = 3.644 Å.

9,2-OBTTT crystallizes in the monoclinic space group. Similar to 1,2-OBTTT, the molecules display a herringbone arrangement, with edge-to-face interactions. The asymmetry of the molecule resulting from the long alkoxy chain disrupts the continuous π-system, similar to 8,2-OBTTT. This significantly hinders π-overlap, as can been seen in figure 6-14. The distance between the cofacial aromatic rings is 3.644 Å. The crystal structure displays smectic-like layers of tilted molecules; this structure could help explain the paramorphic phase transitions observed in chapter 5. Similar to 8,2-OBTTT, the molecules are oriented in a head-to-tail fashion, which disrupts the π-overlap. However, 9,2-OBTTT has syn-clinic layer interfaces, like the shorter chain members of the series. The only disorder in the structure is found in the central thieno[3,2-b]thiophene ring, which is disordered over two orientations.

10,2-OBTTT: Small Yellow Plates, Orthorhombic, Pbca

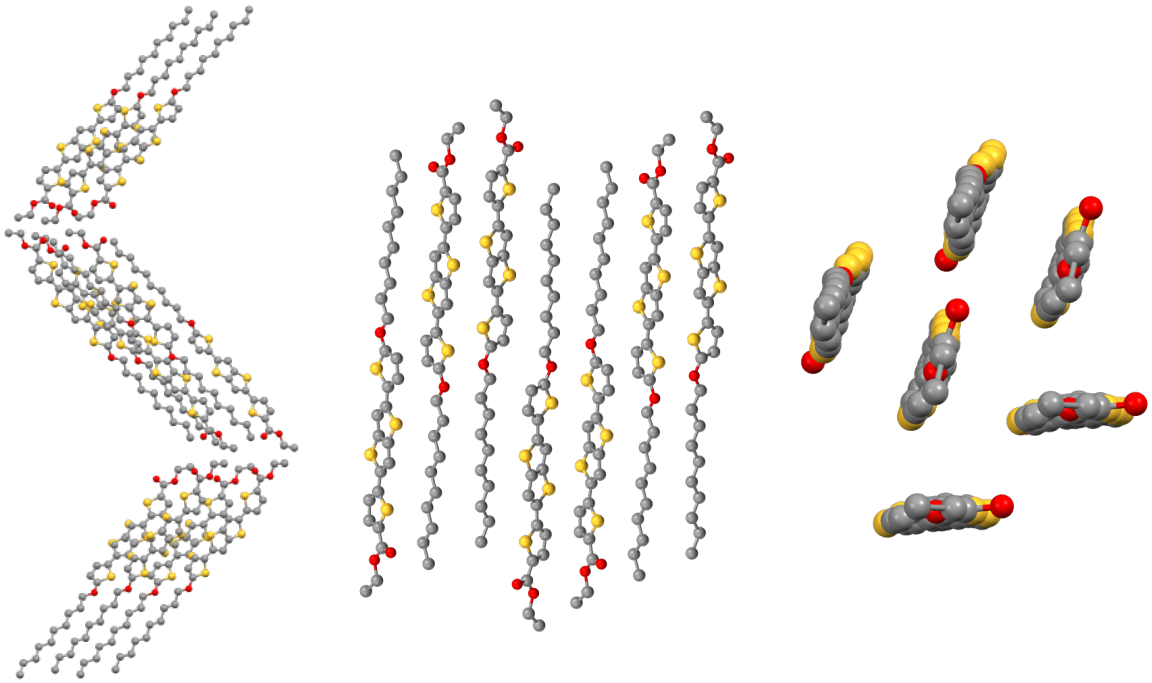

Figure 6-15. Crystal structure of 10,2-OBTTT displaying smectic-like layers of tilted molecules with anti-clinic layer interfaces and a herringbone arrangement. The π-π overlap is negligible in this orientation because of the head-to-tail orientation; π-π distance = 3.652 Å.

10,2-OBTTT crystallizes in the orthorhombic space group, like 8,2-OBTTT. Also similar to 8,2-OBTTT, the smectic-like layers in the crystal structure exhibit anti-clinic layer interfaces. The π-π distance is slightly larger than in 8,2-OBTTT at 3.652 Å. The fact that 9,2-OBTTT doesn't display the orthorhombic space group, but the members with 8 and 10 carbons is their alkoxy chains do. This suggests some type of even-odd switching behavior. Crystal structures of 11,2-OBTTT and 12,2-OBTT are not available, but it would be interesting to solve these structures and see if they follow this same trend. Again, it would be interesting to examine whether the tilted smectic phase exhibited by 10,2-OBTTT has syn-clinic or anti-clinic layer interfaces, since the SmC - crystal

transition appears paramorphic, suggesting structural similarity between the liquid crystal phase and the crystal phase. This crystal structure is not predicted to yield high charge carrier mobilities due to the low π-overlap. The structure is mostly ordered, but the thieno[3,2-b]thiophene ring is disordered over two orientations.

13,2-OBTTT: Yellow Plates, Monoclinic, P21/c

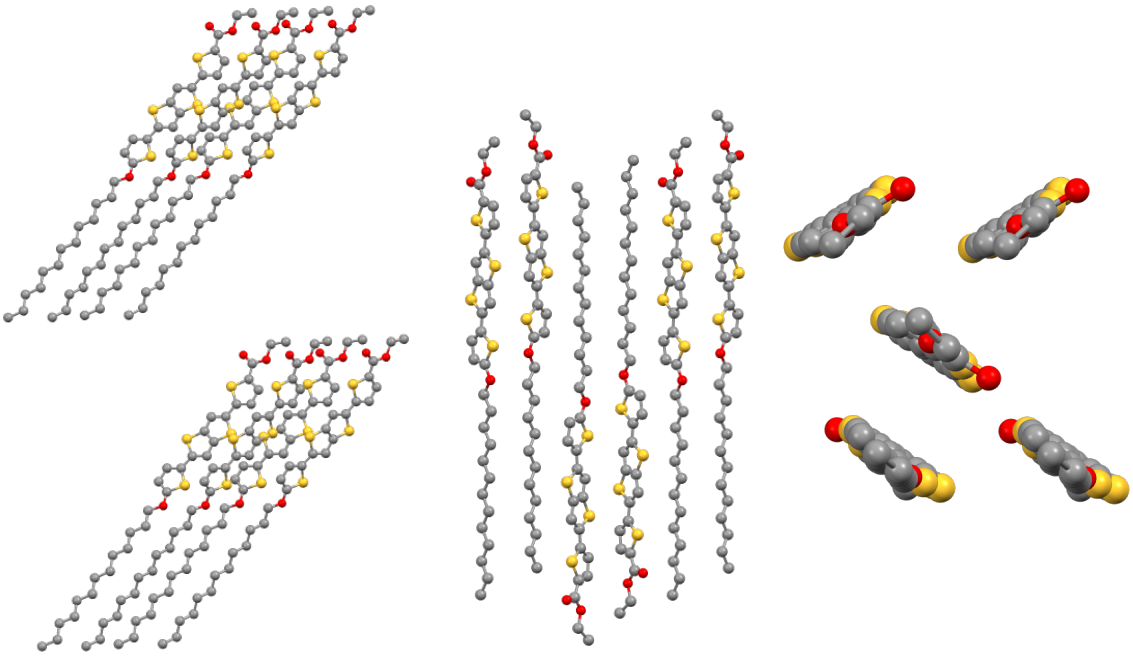

Figure 6-16. Crystal structure of 13,2-OBTTT displaying smectic-like layers of tilted molecules and a herringbone arrangement. The π-π overlap is negligible in this orientation because of the head-to-tail orientation; π-π distance = 3.581 Å.

13,2-OBTTT crystallizes in the monoclinic space group with 2 independent molecules in the unit cell. Similar to 1,2-OBTTT, the molecules display a herringbone arrangement, with edge-to-face interactions. This significantly hinders π-overlap, as can been seen in figure 6-10. The distance between the cofacial aromatic rings is 3.581 Å. The asymmetry of the molecule resulting from the long alkoxy chain disrupts the continuous π-system, similar to 8,2-OBTTT. This significantly hinders π-overlap, as can

been seen in figure 6-16. The distance between the cofacial aromatic rings is 3.581 Å. This distance is shorter than the distance in the 8, 9, and 10 carbon alkoxy isomers, which underlines the fact that there is no linear effect of alkoxy chain length on π-π distance. Again, the only disorder in the structure is found in the central thieno[3,2-b]thiophene ring, which is disordered over two orientations.

Table 6-1 summarizes the results obtained from crystal structures of the n,2-OBTTT series. A general conclusion that emerges from these results is that there is not a linear correlation between alkoxy chain length and crystal structure, although the crystal structure is profoundly affected by such small molecular changes.

Table 6-1. Crystal Properties of the n,2-OBTTT Series

Chain Length	Crystal Color	π-π Distance	Layer Interface	Regularity	Space Group
1	yellow	3.518 Å	synclinic	disordered	P21/c
2	orange				
3	orange	3.498 Å	synclinic	disordered	C2/c
4	yellow/orange				
5	yellow/orange	3.650 Å	synclinic	disordered	P-1
6	yellow	3.571 Å	synclinic	ordered	P-1
7	yellow				
8	yellow	3.617 Å	anticlinic	ordered	Pbca
9	yellow	3.644 Å	synclinic	ordered	P21/c
10	yellow	3.652 Å	antclinic	ordered	Pbca
11	yellow				
12	yellow				
13	yellow	3.581 Å	synclinic	ordered	P21/c

It is unclear what is responsible for the significant shortening of the π-π distance and the cofacial orientation in 3,2-OBTTT. This compound displays significant band broadening in the solid state resulting from the π-interactions, as evidenced by its different crystal

color caused by a red-shifted absorption. Though the crystal structure of 2,2-OBTTT was not solved, this material also formed orange crystals and it would be worthwhile to measure the π-π distance. The shorter chain members of the series also exhibited much more disorder in their crystal structures than the longer chain members. It is unclear what role crystal disorder plays in charge transport; it is possible that this disorder limits charge mobility, but it is also possible that this disorder could contribute to a productive phonon system, facilitating charge transport. This effect needs to be further studied. In addition to larger π-π distances, long chain members become more and more asymmetric, which further disrupts the π-overlap. Taking this into consideration, future mesogens should be designed with some maximum limit to the chain length asymmetry to prevent head-to-tail disruptions of the π-system.

The odd-even behavior of the layer interfaces in the crystal structures of 8,2-OBTTT, 9,2-OBTTT, and 10,2-OBTTT is certainly a topic for future investigation, as well. Odd-even trends are common in liquid crystal research, but it is strange that extending the length of an n-alkoxy chain could drive a shift from syn-clinic to anti-clinic layer interfaces. Further, that the effect is not extended to 13,2-OBTTT, which displays syn-clinic layer interfaces once again, is also unexpected. Another possible explanation of this behavior is that these materials exhibit more than one stable crystal phase. Perhaps all of the longer chain mesogens exhibit more than one stable crystal phase and it is only coincidental that even chain members happened to crystallize in that structure.

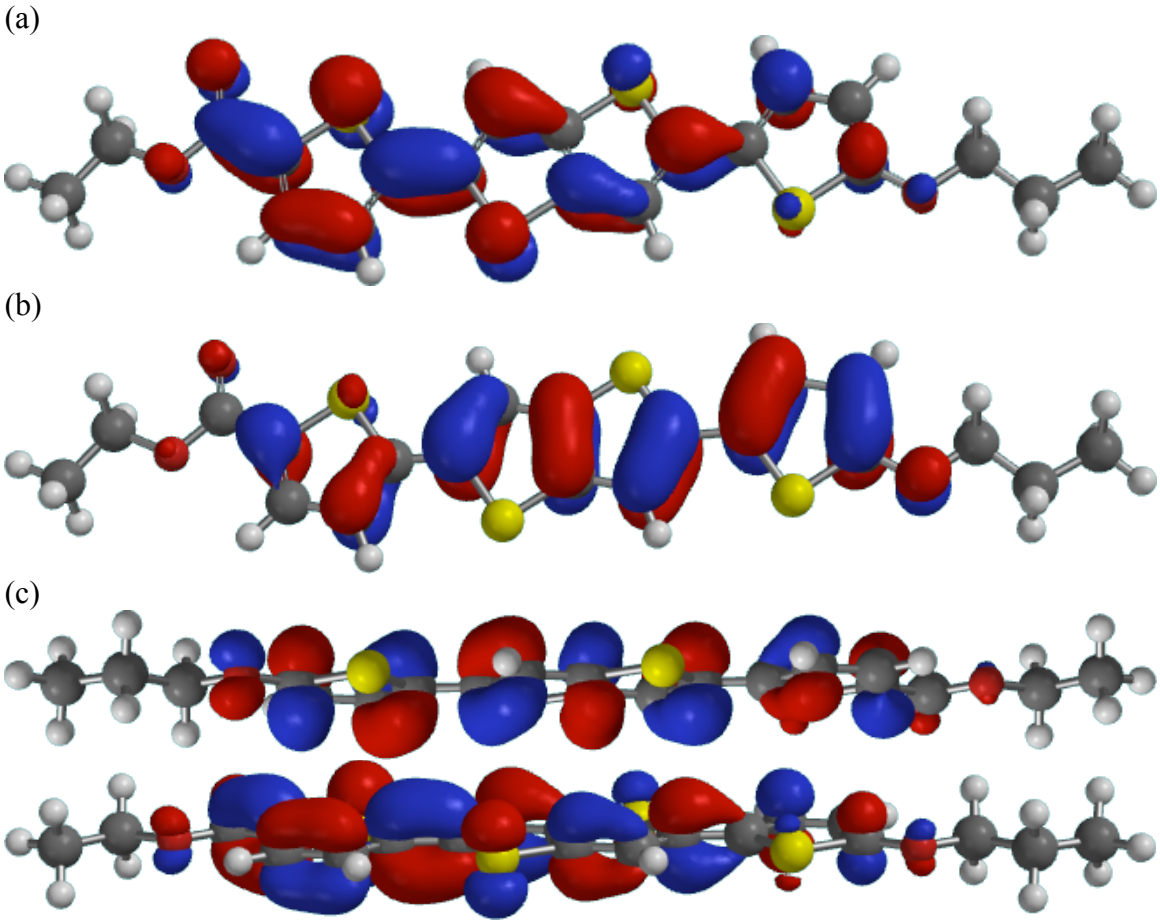

Figure 6-17. Molecular orbitals of 3,2-OBTTT; (a) HOMO; (b) LUMO; (c) overlap of HOMO-LUMO. Calculated by DFT using B3LYP/6-31G* starting from MMFF energy minimized geometry.

One final consideration is that short π-π distances do not necessarily ensure higher charge carrier mobilities. It is not spatial overlap that is important for charge transport; it is wavefunction overlap of the HOMO and LUMO of adjacent molecules. Figure 6-17 shows the molecular orbitals of 3,2-OBTTT. Because the molecule contains a molecular dipole moment, the frontier orbitals are not symmetric. This means that perfect cofacial arrangement might not lead to the highest charge carrier mobilities. To truly determine whether a specific molecular π-π arrangement is favorable, the charge carrier mobility of the material must be measured.

6.3 Thin-Films

The n,2-OBTTT series was designed to exhibit paramorphic liquid crystal phases to create highly ordered thin films. Though none of the mesophases have been confirmed by x-ray studies, it is believed that 1,2-OBTTT and 2,2-OBTTT exhibit the SmE phase. The SmE phase has been characterized as exhibiting charge carrier mobilities as high as solid crystalline materials. As such, these members of the series are excellent candidates for creating monodomain thin films. Even though 3,2-OBTTT exhibited shorter π-π distances than 1,2-OBTTT, the nature of the low-temperature smectic phase in 3,2-OBTTT is less clear. Since there is no crystal structure for 2,2-OBTTT and this information will be useful for the analysis of the thin film characteristics, 1,2-OBTTT was chosen as a pilot compound to make monodomain thin films and optimize the processing conditions.

Two different deposition techniques were examined: spin-casting and blade-casting. Figure 6-18 shows the morphology of an unannealed thin film of 1,2-OBTTT obtained from spin-casting a chloroform solution of 10 mg/mL at a rate of 1000 RPM. The film is a multidomain structure with needle-like regions meeting at grain boundaries. The film was visible to the naked eye on top of the substrate, so it is likely not particularly thin, though no measurements of film thickness were taken. Although this technique has been used to successfully deposit thin films with very high charge carrier mobilities, there is substantial variation in the specific execution of the technique, leading to difficulty obtaining reproducible results. Further, the radial force applied to the substrate as it spins will likely lead to a radially aligned thin film, which does not provide a channel for the anisotropic transport of charge through organic materials.

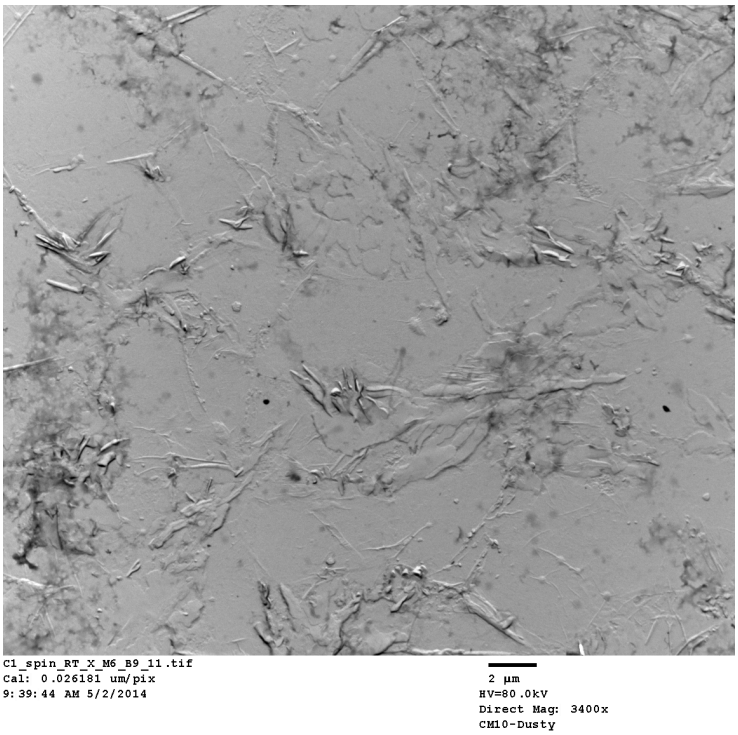

Figure 6-18. TEM image of an unannealed, spin-cast thin film of 1,2-OBTTT. Solution concentration = 10 mg/mL; spin speed = 1000 RMP. Multidomain morphology with several grain boundaries.

In contrast, figure 6-19 shows a TEM image of an unannealed, blade-cast thin film of 1,2-OBTTT from a chloroform solution of 10 mg/mL. Blade-casting offers the advantage of being able to control the deposition temperature, which for liquid crystalline materials, can be extremely useful. In a material is deposited at a temperature so that it is in a liquid crystal phase, it will be much easier to align. Further, blade-casting produces a uni-directional force on the thin film during deposition, potentially leading to uni-directional alignment, an ideal orientation for organic semiconductors. The film in figure 6-19 was deposited at 150° and was not annealed. As can been seen from the images, the structure produced from blade-casting is more homogenous, though more than one domain are still certainly present. The domains in figure 6-18 look crystalline, like

needles, suggesting that the solvent evaporated too quickly during spin-casting. Conversely, the domains in the film in figure 6-19 have far less severe grain boundaries and the edges of the domains are softer. This suggests that the film benefitted from the liquid crystallinity of the material during blade-casting.

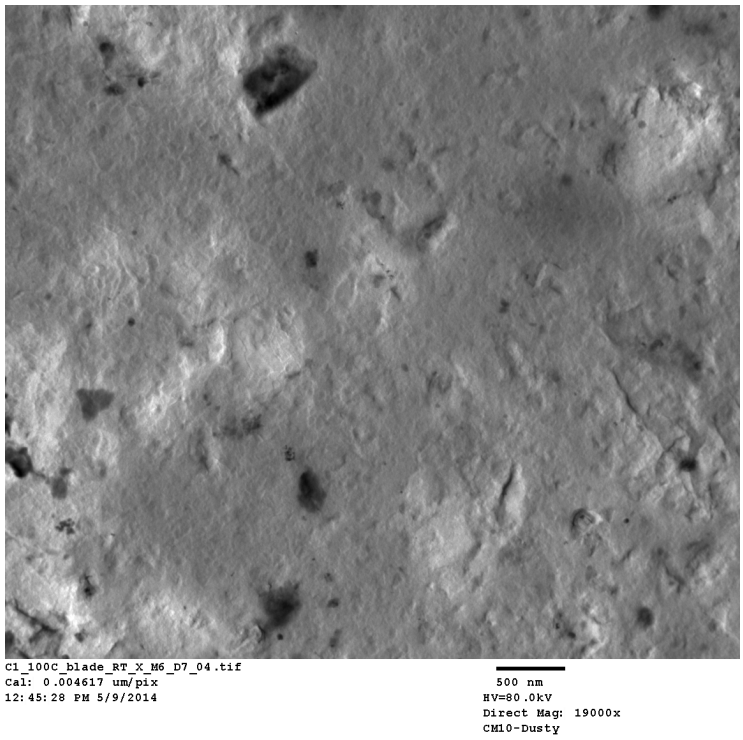

Figure 6-19. TEM image of an unannealed, thin film of 1,2-OBTTT blade-cast at 150°C. Solution concentration = 10 mg/mL. Multidomain morphology with several grain boundaries, though an improvement over spin-casting.

Although liquid crystallinity certainly affects the morphology of the thin films when deposited at different temperatures, this is also a function of the solvent boiling point: a low boiling point solvent will evaporate quickly, especially at high temperatures, and may not yield enough time for mesophase induced molecular alignment. As such, it was discovered that bromoform, with dissolving properties similar to chloroform but with a much higher boiling point, was a better solvent for deposition at elevated temperatures.

Thin films were also blade-cast at 100°C (figure 6-20) and 90°C (figure 6-21). Subtle variations in deposition conditions can have profound effects on the morphology of thin films, so several deposition temperatures, casting speeds, solution concentrations, and blade heights were tried. Of the several deposition temperatures that were explored, it was discovered that depositing at 90°C yielded films with the most homogenous morphologies. Figure 6-21 shows an image of a thin film of 1,2-OBTTT deposited at 90°C without further annealing. There is clearly an improvement in the morphology between the films deposited at 100°C and 150°C. There is a striking improvement in thin film morphology caused by a simple 10°C reduction in the deposition temperature (figure 6-20 vs 6-21).

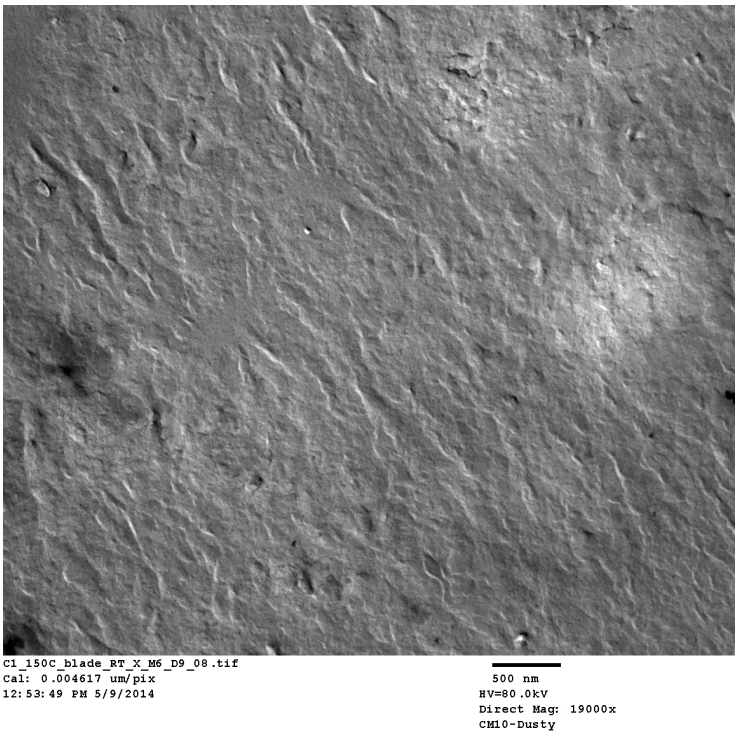

Figure 6-20. TEM image of an unannealed, thin film of 1,2-OBTTT blade-cast at 100°C. Solution concentration = 10 mg/mL. Multidomain morphology with several grain boundaries, though an improvement over both spin-casting and blade-casting at 150°C.

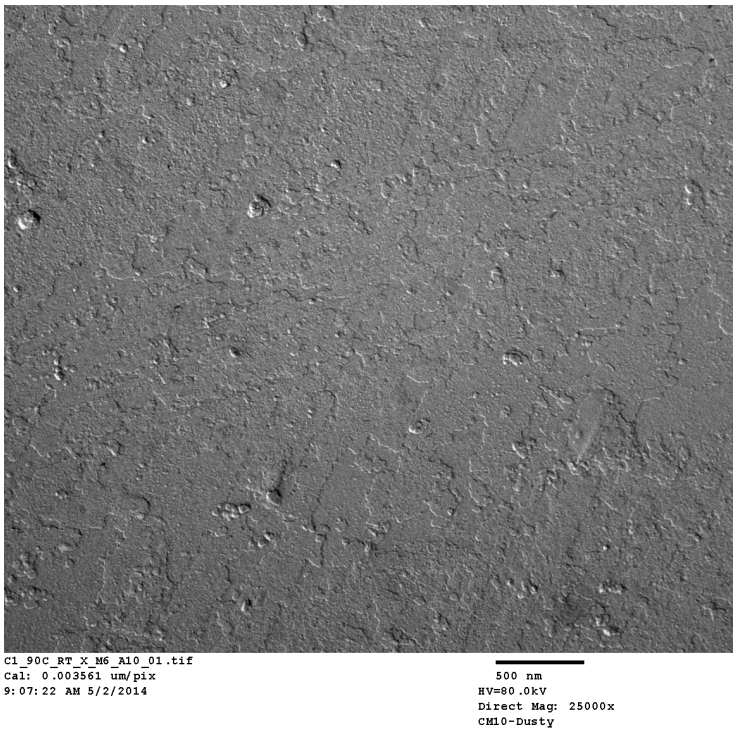

Figure 6-21. TEM image of an unannealed, thin film of 1,2-OBTTT blade-cast at 90°C. Solution concentration = 10 mg/mL. The morphology is highly homogenous and contains very few different domains.

Finally, to further improve morphology, thin films are often annealed at high temperatures for minutes to hours. With liquid crystalline materials, this is especially beneficial since elevated temperatures cause the self-assembly of mesophases. The thin films of 1,2-OBTTT with the best morphologies were obtained by blade-casting a bromoform solution of 10 mg/mL at 90°C (figure 6-22). The film was then annealed at 190°C for 20 minutes, then cooled to room temperature at a rate of 10°C/min. The annealing temperature was chosen to ensure that 1,2-OBTTT would enter the SmA phase. The ideal annealing time was determined by examining changes in the texture of the thin films as a function of temperature by PLM. Annealing was stopped when the texture had become a homogenous monodomain.

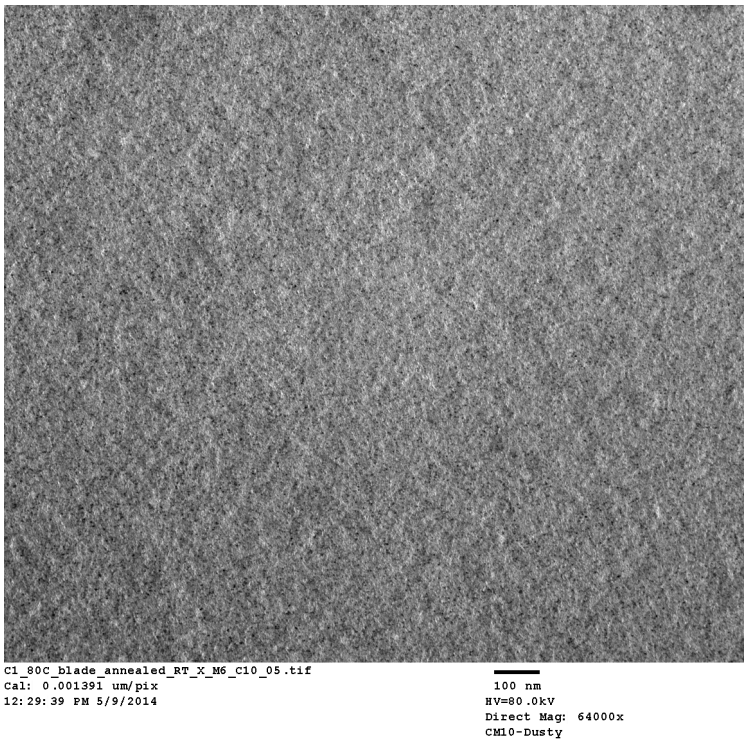

Figure 6-22. TEM image of a thin film of 1,2-OBTTT blade-cast at 90°C. The film was annealed at 190°C for 20 minutes and then cooled to room temperature at a rate of 10°C/min. Solution concentration = 10 mg/mL. A monodomain thin film was achieved.

Although the thin film is not perfectly aligned, no efforts were made to align the thin film beyond the force supplied by blade-casting, so *any* alignment is merely an artifact of the casting and annealing processes. Further, because the director in liquid crystalline domains shifts gently and continuously, not abruptly, it has been found that these morphologies are far more tolerant of slight mis-alignment. What can certainly be said is that there is a huge improvement in morphology from the unannealed spin-cast film (figure 6-18) to the annealed blade-cast film (figure 6-22) and these are films of *the same material*! Future investigations should focus on alignment techniques that can be used to exploit the nature of the liquid crystal phases. Also, mesogens with lower temperature mesophases should be designed. Annealing at temperatures as high as

190°C is not a viable option for many industrial processing techniques. Lastly, deposition of the *neat* liquid crystalline material should be investigated; depositing solutions of liquid crystalline material does not take full advantage of the beneficial properties of the mesophases. Blade-casting allows for a wide-range of deposition temperatures and it would certainly be possible to deposit pure liquid crystalline materials when they have entered a liquid crystal phase.

6.4 Conclusions

The design and synthesis of the n,2-OBTTT series of mesogenic semiconductors has proven to be a successful strategy for the production of highly-ordered, monodomain thin films. The π-π distances observed in the crystal structure of 3,2-OBTTT (d = 3.498 A) are more favorable than pBTTT (d = 3.630 A), the polymer that our series was based on. This is certainly a success. It is unknown what specific features of 3,2-OBTTT caused favorable π-π distances, since no other member of the series exhibited such ideal face-to-face packing. The strategy of utilizing liquid crystalline mesophases for the alignment and ordering of thin film monodomains has proven to be highly successful. More investigations into the specific cause of how chain length affects crystal-smectic phase formation and short π-π distances in crystal structures in warranted. The final demonstration of whether the thin films produced during this project are comparable to the vast array of organic semiconducting materials now available is to measure their charge carrier mobility. Now that promising candidates from the n,2-OBTTT series have been identified by their mesophase behavior and crystal structure (3,2-OBTTT) and the deposition conditions have been optimized, OFET devices should be made and the charge carrier mobility values measured.

Chapter VII: Improving Students' Understanding of Molecular Structure with Computer Models

7.1 Molecular Representation in Chemistry Education

Organic chemistry is a discipline that requires an understanding of a molecule's three-dimensional shape. Until very recently[1], molecules could not been seen directly, so chemists and chemistry students have typically relied on different representations of molecules to understand their shapes and properties.[83] Though all of the images in Figure 7-1 represent the same molecule, the structures appear vastly different. There is more structural information contained in 3-D representations than in 1-D or 2-D representations, like bond angles, relative bond lengths, and the relative size of atoms. Representations of molecular structure differ in their level of detail and physical accuracy. No representation is entirely accurate, not even computer-generated models of molecules.[84] Computer models typically depict nuclei as static, though physicists suggest that they are actually oscillating around some nuclear site; similarly, electrons are usually depicted as solid lines between atoms, though they might be more accurately described as having some probability of being located at a certain distance from the nucleus.[84] Indeed, some authors have suggested that the "electron density" model of molecular structure is easier for students to grasp than the orbital model since orbitals are purely mathematical constructs that have no physical counterpart and electron density is a property that can be experimentally determined.[85-86] What level of accuracy or detail would most effectively teach students about molecular structure?

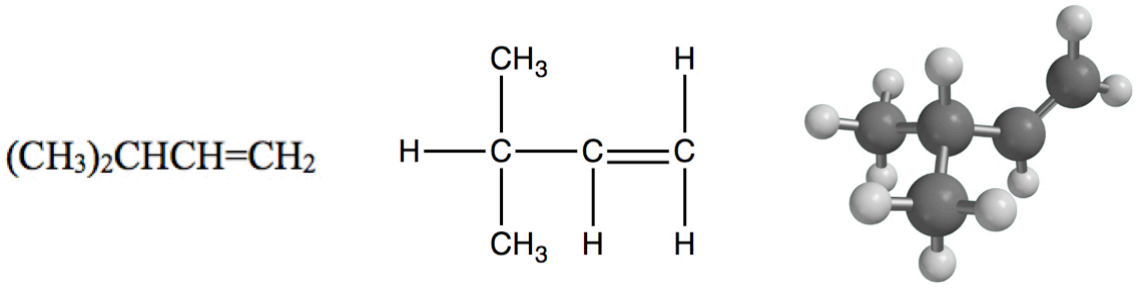

Figure 7-1. Several representations of chemical structure, displaying an evolution from 1-D to 2-D to 3-D representations of *3-methyl-1-butene*.

7.1.1 Physical Accuracy of Computer Models

Computer models are among the most physically accurate representations of molecular structure currently available and several studies have discussed the benefits of including computer models and animations into some part of the chemistry curriculum.[87-103] A study by Ferk et al.[100] concluded that students performed better on tests designed to measure spatial ability and molecular structure when given 3-D models, whether they were physical models, computer models, or photographs of physical models, than if they were given more abstract 2-D images (schematic representations or stereochemical formulas). Several studies have established that students' ability to transfer between 2-D and 3-D representations of a molecule was significantly improved because of their interactions with computer models.[93,99-103] Should educators, then, replace all physically inaccurate representations of molecular structure with physically accurate, computer-generated models?

There are several reasons why providing only one representation of molecular structure may not be desirable, even if the one representation provided is highly accurate and detailed, like computer models. Because chemistry occurs at several different levels of representation (the molecular, the macroscopic, and the symbolic), Kozma and Russell[104] suggest using several *linked* representations of molecular structure to make explicit the connections between these levels. Research by Wu et al.[102] suggests using both physical (plastic) and computer models because different students prefer using different types of models. A study by Copolo and Hounshell[105] has shown that when students are provided with multiple representations of molecular structure, they perform better on tests designed to measure their understanding of isomeric identification, even if they were given exclusively highly accurate computer models. Many tasks in organic chemistry require not only an understanding of molecular structure in three dimensions, but also an understanding of how those 3-D structural relationships are depicted in a 2-D representation of the same molecule. An understanding of how features in one type of representation are related to features in another type of representation is often referred to as *representational translation*.[102,104,106,107] It seems likely that the task of translating between representations would be more difficult if students were only given one representation of molecular structure.

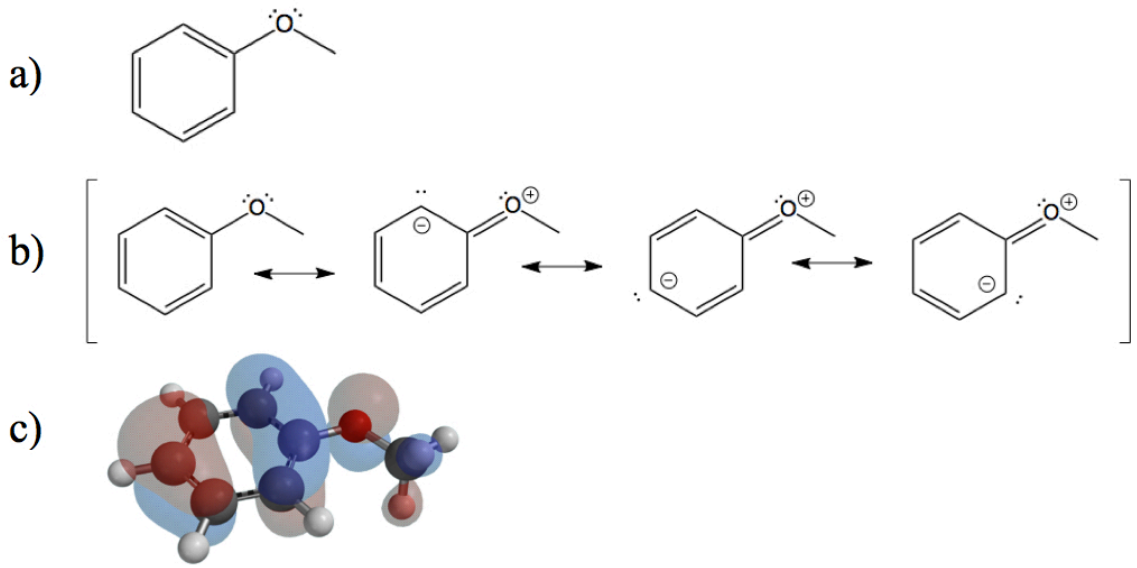

Figure 7-2. Representations of the distribution of electrons within the molecule, *anisole*: a) a 2-D representation of one member of a family of resonance contributors; b) a 2-D representation of the entire family of resonance contributors; c) a 3-D computer-generated representation of the HOMO.

Figure 7-2a is a common representation of the molecule, *anisole*, yet it gives the impression that the oxygen atom has two lone pairs of electrons, that it is sp^3-hybridized, and, thus, has a C-O-C bond angle of about 109.5°. However, calculations show that the oxygen atom in *anisole* is sp^2-hybridized and that the C-O-C bond angle is closer to 120°. This "extra" information about the electron distribution that is missing from the representation in Figure 7-2a is contained within the set of resonance structures in Figure 7-2b. Because of the limitations of 2-D representations of molecules, it is common that bond angles, bond lengths, preferred conformations, etc., are not depicted accurately (or at all) and an experienced chemist must fill-in the missing information from their own understanding of molecular structure. However, computer-generated 3-D models can display physically accurate information about bond angles, bond lengths, and electron distribution in a single structure (Figure 7-2c). Perhaps viewing a physically accurate 3-

D model of a molecule alongside its 2-D representations can direct students' attention to the aspects of the 2-D representations that are misleading or inaccurate, helping to clarify the relationships between the representations and impart a deeper understanding of molecular structure. Making linked referential connections between multiple representations visible has been identified as an important principle for developing effective learning tools for chemistry.[104-105,108]

7.1.2 Making Connections Between Representations

Another reason that computer models should not be the only representation of molecular structure given to students is that some representations may contain *too much* information. Some authors suggest that if an image or animation is too detailed and too much information is presented, students' working memory can be overloaded and effective learning cannot occur.[108-110] The cognitive theory of multimedia learning suggests that human minds contain a finite amount of working memory and that complex learning activities can present too much information to be processed simultaneously.[27] The amount of information presented to the working memory is sometimes called the *cognitive load*.[108-110] It is possible that highly detailed computer models may contain too much information for students to process simultaneously. However, it is also possible that viewing a 3-D computer model could decrease cognitive load by externalizing the transformation from a 2-D representation to a 3-D representation and by performing rotational manipulations of the model in the physical world instead of one's mind.[101-102]

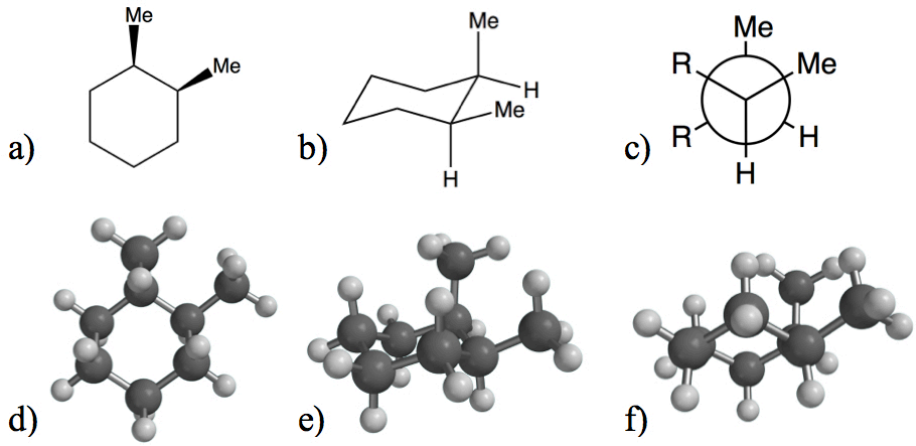

Figure 7-3. Representations of the molecular structure of *cis-1,2-dimethylcyclohexane*: a) a 2-D skeletal structure; b) a 2-D chair-conformation; c) a Newman projection; d), e), and f) are different perspectives of the same 3-D computer model that was rotated to resemble the 2-D representations.

Often, the depiction of 3-D information in 2-D requires several static 2-D images (Figures 7-2 and 7-3). Conformations of cyclohexane are usually explained with at least three 2-D representations of the molecule (Figure 7-3). Further, different representations require different conventions for depicting the 3-D structure of the molecule in the 2 dimensions of the page.[106] Not only must a student understand the 3-D structure of the molecule, they must also understand how all of the representations are related to each other, a task that is not straightforward.[101-102] If these relationships are not understood, a student can develop disjointed knowledge.[106] It is likely that the mental requirements to translate a 2-D representation to a 3-D mental image and to understand the connections between the various 2-D representations place quite a large cognitive load on a student's working memory. Stull et al.[106] suggest that because a computer model is already 3-D, it obviates the need for these conventions to be maintained in working memory. Thus, *simply viewing* a 3-D computer model may be beneficial to learning by reducing the cognitive load on a student's memory. However, these same researchers concluded that

students who simply viewed a 3-D model but did not interact with it performed no better on a test to measure representational translation than students who did not see the models at all.[106] The students that only viewed the model, but did not manipulate it, were still allowed to manipulate it and chose not to; this suggests that perhaps they didn't manipulate the model because they didn't know how the model related to the 2-D representations. Indeed, many researchers have concluded that to fully benefit from model use, students must understand how to correctly interpret them.[91,93,99] Simply viewing a 3-D computer model may not be sufficient to improve performance because many students may not understand what they are seeing.

It has been shown that physical manipulation of a 3-D model can have a beneficial effect on a student's understanding of molecular structure.[102,108] Is it necessary that the manipulations be *performed* by the student or might *simply viewing* the appropriate manipulations being performed achieve similar gains in understanding? Perhaps viewing the appropriate physical manipulations being performed whether the student is actually performing them or not, may impart deeper understanding of molecular structure and the connections among representations by reducing the cognitive load on a student's working memory. Although presenting computer models alongside the current representations of molecular structure during lecture or recitation is actually increasing the amount of information presented to the students, perhaps viewing a 3-D, computer model would improve students' understanding of molecular structure by displaying physically accurate information, like bond angles and bond lengths. Perhaps simply viewing the appropriate rotational manipulations of a 3-D computer generated model being performed by a teacher could help students make connections between 3-D

molecular structure and the various types of 2-D representations, like skeletal structures, chair conformations, and Newman projections (Figure 7-3). Externalizing the transformation from 2-D to 3-D by performing rotational manipulations of the 3-D model in the physical world instead of one's mind could be reducing cognitive load.[101-102] If viewing a computer model helps to make connections between 3-D spatial relationships and 2-D representations, then perhaps it is actually reducing the cognitive load by integrating into a single concept what was before seen as several separate, unrelated images (Figures 7-2 and 7-3).

7.1.3 Research Questions

This study was designed with the following questions in mind:

- Could student understanding of molecular structure be significantly improved by *simply viewing* teacher-performed manipulations of a computer model in recitation or lecture alongside typical 2-D representations?
- What topics, if any, seem to benefit from *simply viewing* computer models?

7.2 Study Design

This study was performed during an introductory organic chemistry course for non-chemistry-major undergraduates at a large research university. The course consisted of two summer semesters of introductory organic chemistry (OCHEM 1 and OCHEM 2). Each semester consisted of a lecture and two recitation sections. Students were required to enroll in both the lecture and 1 of 2 recitation sections. The lecture was given by an assistant professor and was attended by students in both recitation sections, which were led by a teaching assistant (the author). Because this research involved human subjects

and the author was involved in data collection, all aspects of the research design were approved by an institutional review board (IRB) before the study commenced.

7.2.1 Population

The experimental treatment was applied in one of the two recitation sections: one control section and one experimental section. Each recitation section contained roughly 20 students. Demographic data of the research population is presented in Table 7-1.

Table 7-1. Demographic Data of the Student Population

	OCHEM 1		OCHEM 2	
	Control	*Experimental*	*Control*	*Experimental*
Gender				
Female	9	10	11	10
Male	11	9	8	10
Academic Year				
Freshman	1	0	0	0
Sophomore	2	1	1	2
Junior	8	6	10	9
Senior	7	10	5	7
5th Yr. Senior	2	2	3	2
Major				
Soc. Science	2	0	4	3
Nat. Science	5	4	5	4
Pre-Med.	10	11	6	8
Engineering	2	3	3	4
Humanities	0	1	1	1
Non-Degree	1	0	0	0

The students in each recitation section were examined according to major and academic year and it was determined that the groups were randomly distributed according to these two variables. The results of a Shapiro-Wilk test showed the distribution of student majors (OCHEM 1: *control*, $W = 0.85$; *experimental*, $W = 0.81$; OCHEM 2: *control*, $W = 0.96$; *experimental*, $W = 0.94$) and academic year (OCHEM 1: *control*, $W =$

0.82; *experimental*, $W = 0.90$; OCHEM 2: *control*, $W = 0.92$; *experimental*, $W = 0.89$) was normal in all groups at the 95% confidence level. There were roughly equal numbers of males and females in each group. The groups were also subjected to a *t*-test, which found no statistically significant differences with regard to distribution of major (OCHEM 1: $p = 0.94$; OCHEM 2: $p = 0.91$), gender (OCHEM 1: $p = 0.64$; OCHEM2: $p = 0.63$), or academic year (OCHEM 1: $p = 0.93$; OCHEM 2: $p = 0.94$). Because the groups were statistically equivalent with regard to gender, academic year, and major, no further randomization of groups was performed. The students in the second semester study were not necessarily the same students from the first semester study.

7.2.2 Pre/Post-Test Design

An instrument was created to measure student understanding of molecular structure. The pre/post assessment and answers to the pre/post assessment can be found in the supplemental information. Students were given a 2-D representation of a molecule and were asked to determine the magnitude of certain values of the molecule's structure. Test questions required students to either: 1) identify the indicated bond angle; 2) determine which of two bonds is longer or whether they are the same length; 3) determine whether a molecule is chiral, achiral, or meso; 4) determine whether the equilibrium constant (K_{EQ}) for the given reaction is greater than 1, less than 1, or equal to one (as a function of ring strain, steric hindrance, or other structural features of the molecule).

The questions on the instrument were analyzed for content validity by a panel of 10 expert organic chemists (3 university-level professors and 7 chemistry PhD students). The structure and behavior of a molecule is a function of at least three properties: the bond lengths (1-D), the bond angles (2-D), and 3-D properties (like dihedral angle and chirality). These three broad properties are dictated by certain phenomena: steric strain, torsional strain, ring strain, hydrogen-bonding, resonance, conjugation, aromaticity, hybridization, orbital geometry, conformation, and chirality. As all of these topics were included on the instrument and, as such, the measure was considered valid by the panel of chemistry experts.

Table 7-2. Internal Consistency of the Pre/Post Instrument

Cronbach's (α)	OCHEM 1	OCHEM 2
Pre-Test	0.72	0.76
Post-Test	0.69	0.74

The pre/post-test results were analyzed to determine the reliability of the instrument. Table 7-2 reports the values of Cronbach's α for the pre-test and post-test in both semesters. The sample size N for each group is reported in Table 7-3. Cronbach's α is a well-accepted measure of reliability by means of internal consistency. Nunnally[111] suggests that values of α above 0.70 have a moderate level of reliability and can be acceptable for exploratory research, but for applied settings where important decisions are being made as a result of certain test scores (like changes in curriculum), Nunnally[111] suggests seeking α values exceeding 0.90. The obtained values of α (Table 7-2) fall within the range of acceptable reliability (except the post-test of OCHEM 1, which lies

just outside the lower bound of 0.70). These values are acceptable for the present study, since it is exploratory research. As such, the instrument can be considered moderately reliable.

7.2.3 Experimental Treatment

Research done in the classroom can provide external validity and support to more carefully controlled studies, but there are often difficulties in maintaining consistency among groups. For example, Kozma and Russel[107] note that it is difficult to control the specific verbal content, relative to the presentation of visual content during a typical classroom lecture. To avoid this specific problem, the present study employed a "script" that contained both the verbal script and accompanying visual material that was to be employed in each group. The scripts for the control group and experimental group were kept identical, except for the presentation of the experimental treatment to the experimental group, which included both additional verbal and visual material. Examples of the additional visual material can be seen in Figures 7-2 and 7-3 and the additional verbal script contained explanations about how to interpret the computer models and physical manipulations. During a discussion of resonance structures and the distribution of electrons in a molecule, both groups would receive the 2-D representations (Figure 7-2a and 7-2b) as images drawn on the chalkboard by the teaching assistant and the experimental group would also view the 3-D computer model (Figure 7-2c) as well as a verbal explanation of how to interpret the model. During a discussion of conformation and dihedral angles, both groups would be shown the 2-D representations (Figure 7-3a, 3b, and 3c) as images drawn on the chalkboard by the teaching assistant and the

experimental group would also view a projection of the 3-D computer model, rotated by the teaching assistant to resemble the perspectives indicated in the 2-D representations (Figure 7-3d, 3e, and 3f), and accompanied by a verbal explanation of how to interpret the model and manipulations. Presentation of the additional computer models and explanations to the experimental group typically required about 3-5 minutes of additional presentation time per recitation relative to the control group. Scripts were presented as similarly as possible to both groups, except for the experimental treatment. However, even with these precautions, it is highly unlikely that the execution of the two scripts was exactly identical in every case, in terms of timing and other uncontrollable variables. Further, due to ethical concerns, the researcher did not avoid answering student questions when they arose in either group, even if they prompted additional, unscripted discussion of relevant issues. The researcher did not notice significantly greater or fewer questions in either group, but data were not taken.

7.3 Results

The sample size N for each group is reported in Table 7-3. The same value of N is used in all statistical analyses for this study (Tables 7-2, 7-4, and 7-5). The pre/post test results were analyzed using a Shapiro-Wilk test for normality and the results are reported in Table 7-3. Because the calculated values of W were all greater than the value that represents the 95% confidence level, the null hypothesis was accepted. Since all of the data sets were determined to be normally distributed, parametric statistics were used throughout the analysis.

Table 7-3. Statistical Distribution of Student Scores

Shapiro-Wilk Statistic (*W*)	OCHEM 1		OCHEM 2	
	Control	*Experimental*	*Control*	*Experimental*
Sample Size (N)	20	19	19	20
Pre-Test (*W*)	0.965	0.923	0.919	0.961
95% CL	0.905	0.901	0.901	0.905
Post-Test (*W*)	0.948	0.931	0.939	0.946
95% CL	0.905	0.901	0.901	0.905

A paired, two-sample *t*-test for means was performed on student's answers to the pre/post-test and the results are reported in Table 7-4. Because of small sample sizes, the effect size is also reported as measured by Cohen's *d*. No significant differences in pre-test means were found between the control group and the experimental group for either semester at the 95% confidence level. Because there were no statistically significant differences in pre-test means and it was determined that the groups were indeed equivalent with respect to gender, academic major, and academic year, it was concluded that there was no significant class effect and that the groups could be considered equivalent in terms of prior knowledge about molecular structure.

Table 7-4. Statistical Analysis of Pre-Test and Post-Test Results

	OCHEM 1		OCHEM 2	
	Pre	*Post*	*Pre*	*Post*
Exp. Average	3.95	7.11	5.00	8.06
Cont. Average	3.52	5.05	5.20	6.71
***p*-value**	0.42	0.005	0.79	0.035
Effect Size (*d*)	0.23	0.98	0.09	0.75

Students in the experimental group performed much better on the post-test than students in the control group in both semesters (Table 7-4). The results of a *t*-test showed that the difference in post-test means was statistically significant at the 95% confidence level. The values of Cohen's *d* reported in Table 4 show that the effects are medium to large in both semesters.[112] Pre-test results suggested that there was no significant difference between the prior knowledge of the experimental group and control group, so any significant difference in post-test results can be attributed to the experimental treatment.

To examine which broad topics benefited the most from the experimental treatment, results were further analyzed using another paired, two-sample *t*-test for means according to the broad categories of bond angle, bond length, and 3-D properties (like dihedral angle and chirality) to determine where the largest differences in scores occurred (Table 7-5). The greatest gains in the experimental group were achieved in the broad categories of bond angle and 3-D properties in both semesters, while performance on the topic of bond length did not seem to have benefited from the experimental treatment in either semester. In fact, though the difference is not statistically significant, the control group scored higher in bond length in both semesters.

Table 7-5. Statistical Analysis of Post-Test Results by Broad Topic

	OCHEM 1			**OCHEM 2**		
	Bond Angle	*Bond Length*	*3D Properties*	*Bond Angle*	*Bond Length*	*3D Properties*
Exp. Average	2.79	1.42	2.90	2.56	2.56	2.94
Cont. Average	1.47	1.53	2.05	1.65	2.88	2.18
***p*-value**	0.0003	0.76	0.06	0.03	0.43	0.04
Effect Size (*d*)	1.28	0.10	0.64	0.77	0.27	0.72

Student's answers were further analyzed by examining the results of a paired, two-sample *t*-test to the responses to each individual question on the pre/post assessment, since each question was measuring comprehension of a slightly different sub-topic within the larger broad categories. The sub-topics that seem to have benefited the most from the experimental treatment (that is, topics where a statistically significant difference was observed in favor of the experimental group) were ring strain, steric strain, torsional strain, conformation, orbital geometry, and axial chirality. The most significant differences in favor of the experimental group were observed in the topics of steric strain ($p = 0.011$, $d = 0.87$), conformation ($p = 0.020$, $d = 0.66$), and axial chirality ($p = 0.030$, $d = 0.78$). Molecules with axial chirality don't possess a stereogenic center, but rather an *axis* of chirality, like cumulenes and some bi-phenyls. Finally, some sub-topics seem completely unaffected by the experimental treatment. A significant difference was not observed for the sub-topics of hydrogen-bonding, resonance, hybridization, conjugation, aromaticity, and chirality by virtue of asymmetric carbon atoms.

7.4 Discussion

Could student understanding of molecular structure be significantly improved by simply viewing teacher-performed manipulations of a computer model in recitation or lecture alongside typical 2-D representations?

Yes. The results of this study suggest that *simply viewing* computer models and relevant manipulations of computer models with a verbal explanation of how to interpret the models can significantly improve a student's understanding of molecular structure. Students from the experimental group performed significantly better on a post-test designed to measure understanding of molecular structure than those in the control group,

even though there were no significant differences in pre-test scores (Table 7-4); these results suggest that the experimental treatment improved student understanding of molecular structure. The effects were medium to large, as indicated by Cohen's d[112] (Table 7-4 and Table 7-5), and statistically significant at the 95% confidence level. Experimental group students were better able to identify the misleading or incomplete information provided by the 2-D representations on the test and choose the correct values for the indicated spatial relationships.

It is hypothesized that the experimental treatment was effective because viewing the 3-D computer models during recitation decreased the cognitive load on a student's working memory by externalizing the transformation from a 2-D representation to a 3-D representation and by performing rotational manipulations of the model in the physical world instead of the student's mind.[101-102] It is believed that this decrease in cognitive load allowed more meaningful learning and helped students to understand: 1) that 2-D representations of molecules can given incomplete or misleading information and 2) how different 2-D representations of a molecule (i.e., skeletal structures, chair conformations, Newman projections, etc.) are related to the 3-D structure of the molecule and to each other. However, this is only speculation because no data were collected to measure differences in cognitive load between groups; future experiments could be designed with a qualitative aspect to probe what students are thinking as they solve problems and determine whether differences in cognitive load play any significant role.

What topics, if any, seem to benefit most from inclusion of computer models?

Experimental group students performed significantly better in the broad categories of bond angle and 3-D properties in both semesters (Table 7-5). Further, experimental group students performed significantly better on the sub-topics of ring strain, steric strain, torsional strain, conformation, orbital geometry and axial chirality. Experimental group students did not outperform control group students in all categories, though. The broad category of bond length seemed unaffected by the experimental treatment, as did the sub-topics of hydrogen-bonding, resonance, hybridization, conjugation, aromaticity, and chirality by virtue of an asymmetric carbon atom. These preliminary results suggest that 3-D computer models will be more effective at teaching certain topics than others; just as it would be inappropriate to use a Fisher projection to teach about conformation, so, too, it seems less effective to use computer models with certain topics. This trend should be explored further to determine the best, most time-efficient use of computer models in the organic chemistry curriculum.

There seems to be some connection between the topics that were affected by the experimental treatment and those that weren't: namely, the topics that benefitted from the experimental treatment are topics that seem to necessitate some degree of mental visualization and the topics that did not benefit from the experimental treatment may not require mental visualization. For example, to determine whether a compound is chiral, a student can merely look for asymmetric carbons without having to imagine the entire 3-D shape of the molecule and whether its mirror image is superimposable upon itself. This shortcut would only work, however, for chiral compounds that *have* asymmetric carbons. For those that don’t have asymmetric carbons, this shortcut won’t work, and indeed, the post-test results seem to suggest this: for compounds that exhibit axial chirality, there

was a significant difference in performance between the experimental and control groups. Presumably, for students to determine whether a compound displays axial chirality, they would have to mentally visualize the 3-D structure and perform mental rotations and manipulations. Work by Steiff and Raje[113] has shown that students can develop alternative strategies, like learned algorithms and other shortcuts, which obviate the need for mental visualization and allow them to correctly answer questions that seem to require mental visualization. Perhaps some topics did not benefit from the experimental treatment because students were not relying on mental visualization to answer the questions. Although this hypothesis seems consistent with work by Steiff and Raje[113], the current study collected no qualitative data to investigate this question.

7.5 Conclusions

This study suggests a method of displaying 3-D computer models alongside 2-D representations during recitation and demonstrates significant benefits to student understanding of molecular structure. There have been articles published in this journal and elsewhere for more than 20 years appealing for the integration of computer models in the chemistry curriculum[108,114-115], but their use in the undergraduate chemistry curriculum is still limited. A recent survey reported that only 12 of the 71 chemistry graduate students interviewed were involved with computer modeling as part of their introductory or intermediate organic chemistry course work.[91] There are several possible reasons for this limitation and lack of financial resources and/or experience are likely among them. After all, to accommodate student use, a department may need a dedicated computer lab with several software licenses. This can be cost prohibitive for some

departments. However, few resources are required to simply show computer models and simulations during lecture or recitation: most chemical educators have access to a computer, the internet, and a video projector. Further, an educator doesn't have to be an expert in computation to take advantage of the large number of chemical databases online that contain models and simulations for free, like Jmol.[116]

Although experimental group students performed significantly better than control group students on the post-test, it is unclear *why* they benefitted from the experimental treatment. The current experimental design can't explain what students were thinking as they solved the problems, so it can't say anything about *why* the experimental treatment was effective, just *that* it was. It is assumed that the experimental group students performed better on the test because they were better at performing mental representational translations; that they were creating 3-D mental models of the 2-D images on the page. However, without having some qualitative aspect of the study, like a questionnaire or interview, it is impossible to tell what the students were thinking as they solved the problems. A future study could utilize a mixed methods approach and include both a quantitative aspect and a qualitative aspect to understand what students are thinking as they view the computer models and as they solve the problems on the test.

References

1. Blanchet, G.B., et al.; "Large area printing of organic transistors via a high throughput dry process." *MRS Proceedings*. Vol. 736. Cambridge University Press, **2002**.

2. Hendsbee, A.D., et al.; "Electron deficient diketopyrrolopyrrole dyes for organic electronics: synthesis by direct arylation, optoelectronic characterization, and charge carrier mobility." *Journal of Materials Chemistry A,* 2(12), **2014**, 4198-4207.

3. Irimia-Vladu, M., et al.; "Environmentally sustainable organic field effect transistors." *Organic Electronics* 11(12), **2010**, 1974-1990.

4. Humpries, M.; "Rare earth elements: The global supply chain." BiblioGov, **2013**.

5. Klauk, H., ed.; *Organic Electronics: Materials, Manufacturing, and Applications*. John Wiley & Sons, **2006**.

6. Coropceanu, V., et al.; "Charge transport in organic semiconductors." *Chemical reviews,* 107(4), **2007**, 926-952.

7. Thouless, D.J.; "Electrons in disordered systems and the theory of localization." *Physics Reports,* 13(3), **1974**, 93-142.

8. Kreouzis, T., et al.; "Temperature-independent hole mobility in discotic liquid crystals." *The Journal of Chemical Physics,* 114(4), **2001**, 1797-1802.

9. Shiyanovskaya, I., et al.; "Electronic transport in smectic liquid crystals."*Physical Review E,* 65(4), **2002**, 041715.

10. Claverie, P., and G. Jona-Lasinio.; "Instability of tunneling and the concept of molecular structure in quantum mechanics: The case of pyramidal molecules and the enantiomer problem." *Physical Review A,* 33(4), **1986**, 2245-2253.

11. Silinsh, E. A., and Capek, V.; "Organic Molecular Crystals: Interaction."*Localization, and Transport Phenomena, American Institute of Physics, New York,* **1994**, 402.

12. Pope, M.; Swenberg, C. E.; *Electronic Processes in Organic Crystals and Polymers*, 2nd ed.; Oxford University Press: New York, **1999**.

13. Horowitz, G.; "Organic field-effect transistors." *Advanced Materials* 10(5), **1998**, 365-377.

14. Brédas, J.L., et al.; "Charge-transfer and energy-transfer processes in π-conjugated oligomers and polymers: a molecular picture." *Chemical Reviews,* 104(11), **2004**, 4971-5004.

15. Sheraw, C.D., et al.; "Functionalized Pentacene Active Layer Organic Thin‐Film Transistors." *Advanced Materials,* 15(23), **2003**, 2009-2011.

16. Mas-Torrent, M., et al.; "Correlation between crystal structure and mobility in organic field-effect transistors based on single crystals of tetrathiafulvalene derivatives." *Journal of the American Chemical Society,* 126(27), **2004**, 8546-8553.

17. Brédas, J.L., et al.; "Organic semiconductors: A theoretical characterization of the basic parameters governing charge transport. "*Proceedings of the National Academy of Sciences,* 99(9), **2002**, 5804-5809.

18. Weis, M., et al.; "Grain boundary effect on charge transport in pentacene thin films." *Japanese Journal of Applied Physics,* 50.4S, **2011**, 04DK03.

19. Horowitz, G., and Mohsen E. H.; "Mobility in polycrystalline oligothiophene field‐effect transistors dependent on grain size." *Advanced Materials,* 12(14) **2000**: 1046-1050.

20. Bushby, R.J., et al.;. *Liquid Crystalline Semiconductors*. Springer Netherlands, **2010**.

21. Graedel, T.E., et al.; *On the materials basis of modern society,* ONLINE: Proceedings of the National Academy of Sciences of the United States of America. Available: www.pnas.org/cgi/doi/10.1073/pnas.1312752110, December 2, **2013**.

22. 2Committee on Critical Mineral Impacts on the U.S. Economy; *Minerals, Critical Minerals, and the U.S. Economy*, PDF: The National Academies Press, [Available: http://www.nma.org/pdf/101606_nrc_study.pdf, **2008**.]

23. U.S. Energy Information Administration; *How dependent are we on foreign oil?,* ONLINE: U.S. Department of Energy. Available: [http://www.eia.gov/energy_in_brief/article/foreign_oil_dependence.cfm, May 10, **2013**.]

24. Lefton, R., Weiss, D.J.; *Oil Dependence is a Dangerous Habit,* ONLINE: Center for American Progress. [http://americanprogress.org/issues/green/report/2010/01/13/7200/oil-dependence-is-a-dangerous-habit/ January 13, **2010**.]

25. CNA Military Advisory Board; *Powering America's Defense: Energy and the Risks to National Security,* PDF: CNA Corporation: Institute for Public Research. Available: [https://www.cna.org/sites/default/files/Powering%20Americas%20Defense.pdf, May **2009**.]

26. 6- Grasso, V.B.; *Rare Earth Elements in National Defense: Background, Oversight Issues, and Options for Congress*, PDF: Congressional Research Service. [Available: http://fas.org/sgp/crs/natsec/R41744.pdf, December 23, **2013**.]

27. *BP Statistical Review of World Energy 2009,* PDF: BP p.l.c. Available: [http://www.usaee.org/usaee2009/submissions/presentations/Finley.pdf, June **2009**.]

28. Rissman, J., *We Will Not Run Out of Fossil Fuels (Op-Ed),* ONLINE: Live Science. [Available: http://www.livescience.com/37469-fuel-endures.html**,** June 14, **2013**.]

29. PVGIS Solar irridiance data, IES - Institute for Environment and Sustainability. [http://ies.jrc.cec.eu.int/.]

30. *Solar Power Factsheet,* ONLINE: Center for Climate and Energy Solutions. [Available: http://www.c2es.org/technology/factsheet/solar, accessed: June **2014**.]

31. U.S. Energy Information Administration; Annual Energy Outlook 2012, PDF: U.S. Department of Energy. Available: [http://www.eia.gov/forecasts/archive/aeo12/pdf/0383(2012).pdf, June **2012**.]

32. Clifford, M.; China's visible solar power success, ONLINE: Caixin Online. Available: http://english.caixin.com/2012-02-07/100354090.html, February **2012**.

33. Keating, T.; Death to PV Subsidies, ONLINE: RenewableEnergyWorld.com. Available: http://www.renewableenergyworld.com/rea/news/article/2012/02/death-to-pv-subsidies, February **2012**.

34. Olah, G.A., et al.; *Beyond Oil and Gas: The Methanol Economy* (2nd, Updated and Enlarged Edition). Wiley-VCH, December **2009**.

35. Deodhar, P.; Multi-MW Solar PV Plants: More Problem than Solution, ONLINE: RenewableEnergyWorld.com. Available: http://www.renewableenergyworld.com/rea/news/article/2011/07/multi-mw-size-solar-pv-plants-more-problem-than-solution, July **2011**.

36. Whitley, S.; Time to change the game: Fossil fuel subsidies and climate, PDF: Overseas Development Institute. Available: http://www.odi.org/sites/odi.org.uk/files/odi-assets/publications-opinion-files/8668.pdf, November **2013**.

37. Clayton, M.; Budget hawks: Does US need to give gas and oil companies$41 billion a year?, ONLINE: Christian Science Monitor. Available: http://www.csmonitor.com/USA/Politics/2011/0309/Budget-hawks-Does-US-need-to-give-gas-and-oil-companies-41-billion-a-year, March **2011**.

38. Who Pays for Climate Change?, ONLINE: National Resources Defense Council. Available: http://www.nrdc.org/globalwarming/taxpayer-climate-costs.asp, last revised May **2013**.

39. https://bouldercolorado.gov/climate/climate, Visited: April 5, **2014**.

40. http://www.dsireusa.org/, [Visited April 7, **2014**.]

41. Heeter, J., et al.; A Survey of State-Level Cost and Benefit Estimates of Renewable Portfolio Standards, PDF: National Renewable Energy Laboratory. Available: http://emp.lbl.gov/sites/all/files/lbnl-6589e.pdf, May **2014**.

42. Solar Industry Data, ONLINE: Solar Energy Industries Association. Available: http://www.seia.org/research-resources/solar-industry-data, **2014**.

43. Brabec, C., et al.; *Socio-Economic Impact of Low-Cost PV Technologies* Chapter 20: Organic Photovoltaics: Materials, device physics, and manufacturing technologies. Wiley-VCH, Weinheim, **2008**, 531.

44. Gill, R.; "Carbon Nanotube Superconductors"*, International Journal of Engineering and Mathematical Sciences* 1, **2012**, 25-28.

45. Huskinson, B., et al.; "A metal-free organic-inorganic aqueous flow battery." *Nature* 505(7482), **2014**, 195-198.

46. Tamura, M., et al.; "Bulk ferromagnetism in the β-phase crystal of the *p*-nitrophenyl nitronyl nitroxide radical." *Chemical physics letters* 186(4), **1991**, 401-404.

47. Sirringhaus, H.; "25th Anniversary Article: Organic Field‐Effect Transistors: The Path Beyond Amorphous Silicon." *Advanced Materials* 26(9), **2014**, 1319-1335.

48. O'Neill, M., and Kelly, S.M.; "Liquid crystals for organic field-effect transistors." *Liquid Crystalline Semiconductors*. Springer Netherlands, **2013**, 247-268.

49. Pisula, W., et al.; "Liquid crystalline ordering and charge transport in semiconducting materials." *Macromolecular rapid communications* 30(14), **2009**, 1179-1202.

50. Arikainen, E.O., et al.; "Effects of side-chain length on the charge transport properties of discotic liquid crystals and their implications for the transport mechanism." *Journal of Materials Chemistry* 5(12), **1995**, 2161-2165.

51. Iino, H., et al.; "Electronic and ionic carrier transport in discotic liquid crystalline photoconductor." *Physical Review B* 72(19), **2005**, 193203-193206.

52. Dierking, I.; "Soft Crystal Phases and Crystallization." *Textures of Liquid Crystals* **2004**: 141-144.

53. Gray, G. W., Goodby, J.W.; *Smectic Liquid Crystals: Textures And Structures*. Glasgow: Leonard Hill, **1984**.

54. Demus, D., et al., eds.; *Handbook of Liquid Crystals, Low Molecular Weight Liquid Crystals I: Calamitic Liquid Crystals*. John Wiley & Sons, **1998**.

55. Yuan, Y., et al.; "Ultra-high mobility transparent organic thin film transistors grown by an off-centre spin-coating method." *Nature communications* 5, **2014**.

56. Miyazawa, T., et al.; "Revisiting smectic E structure through swollen smectic E phase in binary system of 4-nonyl-4′-isothiocyanatobiphenyl (9TCB) and n-nonane." *The Journal of Physical Chemistry B* 117(27), **2013**, 8293-8299.

57. Adachi, T., et al.; "Universality of molten state of alkyl chain in liquid-crystalline mesophases: smectic E phase of 6-alkyl-2-phenylazulene." *Bulletin of the Chemical Society of Japan* 86(9), **2013**, 1022-1027.

58. Reibel, J.; "Comparison of bulk and thin film structures of the liquid crystal 28OBC: measurements and simulations." *Liquid crystals* 25(6), **1998**, 643-654.

59. Adachi, T., et al.; "Comprehensive characterisation of the E phase of 6-octyl-2-phenylazulene." *Liquid Crystals* 39(11), **2012**, 1340-1344.

60. Yamamura, Y., et al. "Calorimetric and Spectroscopic Evidence of Chain-Melting in Smectic E and Smectic A Phases of 4-Alkyl-4′-isothiocyanatobiphenyl (n TCB)." *The Journal of Physical Chemistry B* 116(30), **2012**, 9255-9260.

61. Newman, C.R., et al.; "Introduction to organic thin film transistors and design of n-channel organic semiconductors." *Chemistry of materials* 16(23), **2004**, 4436-4451.

62. McCulloch, I., et al.; "Liquid-crystalline semiconducting polymers with high charge-carrier mobility." *Nature materials* 5(4), **2006**, 328-333.

63. Zhao, L., et al.; "Role of borderline solvents to induce pronounced extended-chain lamellar order in π-stackable polymers." *Macromolecules* 44(24), **2011**, 9692-9702.

64. Fuller, L.S., et al.; "Thienothiophenes. Part 2. 1 Synthesis, metallation and bromine→ lithium exchange reactions of thieno [3, 2-b] thiophene and its polybromo derivatives." *Journal of the Chemical Society, Perkin Transactions 1* (22), **1997**, 3465-3470.

65. Prim, D., Kirsch, G.; "Synthesis of new 2-arylthieno [3, 2-b] thiophenes." *Journal of the Chemical Society, Perkin Transactions 1* (18), **1994**, 2603-2606.

66. Tietz, J., et al.; "Preparation of Brominated 2-Alkoxythiophenes via Oxidation and Etherification of 2-Thienyltrifluoroborate Salts." *Organic letters* 14(19), **2012**, 5058-5061.

67. Keegstra, M. A., et al.; "Efficient Procedures for the Cu (I)-Catalyzed Methoxylation of 2-and 3-Bromothiophene." *Synthetic Communications* 20(2), **1990**, 213-216.

68. Vlachos, P., et al.; "Charge-Transport in Crystalline Organic Semiconductors with Liquid Crystalline Order." *Chemical Communications* 23, **2005**, 2921-2923.

69. van Breemen, A. J. J. M, et al.; "Large Area Liquid Crystal Monodomain for Field-Effect Transistors." *Journal of the American Chemical Society* 128, **2006**, 2336-2345.

70. Oikawa, K., et al.; "A Novel Calamitic Mesophase Semiconductor with the Fastest Mobility of Charged Carriers: 1,2-di(5'-octyl-2'-thienyl)benzene." *Chemical Communications* 42, **2005**, 5337-5339.

71. Saito, K., et al.; "Reassessment of Structure of Smectic Phases: Nano-segregation in Smectic E Phse in 4-n-alkyl-4'-isothiocyanato-1,1'-biphenyls." *The Journal of Chemical Physics* 139, **2013**, 114902

72. Reznikov, M., et al.; "Monodomain Alignment of Smectic-A Liquid Crystalline Phase from the Isotropic Phase." *Journal of Applied Physics* 104, **2008**, 044902

73. Dierking, Ingo; *Textures of liquid crystals.* John Wiley & Sons, **2006**.

74. Lemaur, V., et al.; "Charge Transport Properties in Discotic Liquid Crystals: a Quantum-chemical Insight into Structure-Property Relationships." *Journal of the American Chemical Society* 126(10), **2004**, 3271-3279

75. Zhang, L., et al.; "Chalcogenoarene Semiconductors: New Ideas from Old Materials." *Journal of Materials Chemistry* 21, **2011**, 1329-1337

76. Horowitz, G., et al.; "Growth and Characterization of Sexithiophene Single Crystals." *Chemistry of Materials* 7(7), **1995**, 1339

77. Maeda, H., et al.; "Electrical Properties of Domain Boundary in Photoconductive Smectic Mesophases and their Crystal Phases." *Molecular Crystals and Liquid Crystals* 366, **2001**, 2221-2228.

78. Baldwin, R.J., et al.; "A Comprehensive Study of the Effect of Reactive End Groups on the Charge Carrier Transport within Polymerized and Nonpolymerized Liquid Crystals." *Journal of Applied Physics* 101(2), **2007**, 023713

79. Contoret, A.E.A., et al.; "Photopolymerisable Nematic Liquid Crystals for Electroluminescent Devices." *Synthetic Metals* 14(4), **2001**, 1629-1630

80. Ebata, H., et al.; "Highly Soluble [1]benzothieno[3,2-b]benzothiophene (BTBT) Derivatives for High-Performance, Solution-Processed, Organic Field-Effect Transistors." *Journal of the American Chemical Society* 129(51), **2007**, 15732-15733

81. Wurthner, F.; "Perylene Bisimide Dyes as Versatile Building Blocks for Functional Supramolecular Architectures." *Chemical Communications* 14, **2004**, 1564-1579.

82. Kazmaier, P.M., et al.; "A Theoretical Study of Crystallochromy: Quantum Interference Effects in the Spectra of Perylene Pigments." *Journal of the American Chemical Society* 116, **1994**, 9684-9691.

83. Gross, L.; Mohn, F.; Moll, N.; Liljeroth, P.; Meyer, G. The Chemical Structure of a Molecule Resolved by Atomic Force Microscopy. *Science* **2009**, *325* (5944), 1110-1114.

84. Hoffman, R.; Laszlo, P. "Representation in Chemistry." *Angew. Chem. Int. Ed. Engl.***1991**, *30*, 1-16.

85. Shusterman, G. P.; Shusterman, A. J. "Teaching Chemistry with Electron Density Models." *J. Chem. Educ.* **1997**, *74* (7), 771-776.

86. Matta, C. F.; Gillespie, R. J. "Understanding and Interpreting Molecular Electron Density Distributions." *J. Chem. Educ.* **2002**, *79* (9), 1141-1152.

87. Klassen, J. B.; Graham, K. J.; Muldoon, W. P. "Molecular Modeling as an Aid to Understanding Stereoselectivity." *J. Chem. Educ.* **1999**, *76* (7), 985-986.

88. Pfennig, B. W.; Frock, R. L. "The Use of Molecular Modeling and VSEPR Theory in the Undergraduate Curriculum to Predict the Three-Dimensional Structure of Molecules." *J. Chem. Educ.* **1999**, *76* (7), 1018-1022.

89. Jones, M. B. "Molecular Modeling in the Undergraduate Chemistry Curriculum." *J. Chem. Educ.* **2001**, *78* (7), 867-868.

90. Horowitz, G.; Schwartz, G. "Exploring Organic Mechanistic Puzzles with Molecular Modeling." *J. Chem. Educ.* **2004**, *81* (8), 1136-1139.

91. Clauss, A. D.; Nelsen, S. F. "Integrating Computational Molecular Modeling into the Undergraduate Organic Chemistry Curriculum." *J. Chem. Educ.* **2009**, *86* (8),

955-958.

92. Wang, L. "Using Molecular Modeling in Teaching Group Theory Analysis of the Infrared Spectra of Organometallic Compounds." *J. Chem. Educ.* **2012**, *89* (3), 360-364.

93. Dori, Y. J.; Kaberman, Z. "Assessing High School Chemistry Students' Modeling Sub-Skills in a Computerized Molecular Modeling Learning Environment." *Instr. Sci.* **2012**, *40*, 69-91.

94. Burkholder, P. R.; Purser, G. H.; Cole, R. S. "Using Molecular Dynamics Simulation to Reinforce Student Understanding of Intermolecular Forces." *J. Chem. Educ.* **2008**, *85* (8), 1071-1077.

95. Box, V. G. S. "Using Molecular Modeling to Understand Some of the More Subtle Aspects of Aromaticity and Antiaromaticity." *J. Chem. Educ.* **2011**, *88* (7), 898-906.

96. Sanger, M. J.; Phelps, A. J.; Fienhold, J. "Using a Computer Animation to Improve Students' Conceptual Understanding of a Can-Crushing Demonstration." *J. Chem. Educ.* **2000**, *77* (11), 1517-1519.

97. Steiff, M.; Wilensky, U. "Connected Chemistry - Incorporating Interactive Simulations into the Chemistry Classroom." *J. Sci. Educ. Technol.* **2003**, *12* (3), 285-302.

98. Ruddick, K. R.; Parrill, A. L.; Petersen, R. L. "Introductory Molecular Orbital Theory: An Honors General Chemistry Computational Lab as Implemented Using Three-Dimensional Modeling Software." *J. Chem. Educ.* **2012**, *89* (11), 1358-1363.

99. Dori, Y. J.; Barak, M. "Virtual and Physical Molecular Modeling: Fostering Model Perception and Spatial Understanding." *Educ. Technol. Soc.* **2001**, *4* (1), 61-74.

100. Ferk, V.; Vrtacnik, M.; Blejec, A.; Gril, A. "Students' Understanding of Molecular Structure Representations." *Int. J. Sci. Educ.* **2003**, *25* (10), 1227-1245.

101. Abraham, M.; Varghese, V.; Tang, H. "Using Molecular Representations to Aid Student Understanding of Stereochemical Concepts." *J. Chem. Educ.* **2010**, *87* (12), 1425-1429.

102. Wu, H-K.; Krajcik, J. S.; Soloway, E. "Promoting Understanding of Chemical Representations: Students' Use of a Visualization Tool in the Classroom." *J. Res. Sci. Teach.* **2001**, *38* (7), 821-842.

103. Dori, Y. J.; Barack, M.; Adir, N. "A Web-Based Chemistry Course as a Means to Foster Freshman Learning." *J. Chem. Educ.* **2003**, *80* (9), 1084-1092.

104. Kozma, R. B.; Russell, J. "The Use of Multiple, Linked Representations to Facilitate Science Understanding." *International perspectives on the design of technology-supported learning environments,* Jones, T.; Marx, N.; Davis, J.; Vosniadou, S., Ed.; De Corte, E., Ed.; Glaser, R., Ed.; Mandl, H., Ed.; Hillsdale, NJ, England: Lawrence Erlbaum Associates, **1996**, 41-60.

105. Copolo, C. F.; Hounshell, P. B. "Using Three-Dimensional Models to Teach Molecular Structures in High School Chemistry." *J. Sci. Educ. Technol.* **1995**, *4* (4), 295-305.

106. Stull, A. T.; Hegarty, M.; Dixon, B.; Stieff, M. "Representational Translation with Concrete Models in Organic Chemistry." *Cognition Instruct.* **2012**, *30* (4), 404-434.

107. Kozma, R.; Russell, J. Chapter 7: Students Becoming Chemists: Developing Representational Competence. *Visualization in Science Education,* Gilbert, J. K., Ed.; Springer: Netherlands, **2005**, 121-146.

108. Wu, H-K.; Shah, P. "Exploring Visuospatial Thinking in Chemistry Learning." *Sci. Educ.* **2004**, *88*, 465-492.

109. Mayer, R. E. Cognitive Theory of Multimedia Learning. *The Cambridge Handbook of Multimedia Learning*; Cambridge University Press, **2005**, 31-48.

110. Cook, M. P. "Visual Representations in Science Education: The Influence of Prior Knowledge and Cognitive Load Theory on Instructional Design Principles." *Sci. Educ.* **2006**, *90*, 1073-1091.

111. Nunnally, J. C. Chapter 7: The Assessment of Reliability. *Psychometric Theory,* 2nd ed.; McGraw-Hill: New York, **1978**; 248-290.

112. Cohen, J. Chapter 2: The t-Test for Means. *Statistical Power Analysis for the Behavioral Sciences*, 2nd ed.; Routledge: Hillsdale, New Jersey, **1988**; 19-27.

113. Stieff, M.; Raje, S. "Expert Algorithmic and Imagistic Problem Solving Strategies in Advanced Chemistry." *Spat. Cognit. Comput.* **2010**, *10* (1), 53-81.

114. Brooks, D. W. "Technology in Chemistry Education." *J. Chem. Educ.* **1993**, *70* (9), 705-707.

115. Moore, J. W. "Tooling up for the 21st Century." *J. Chem. Educ.* **1989**, *66* (1), 15-19.

116. Jmol: an open-source Java viewer for chemical structures in 3D. http://www.jmol.org/ (accessed [Apr] 2014)